

FT-IR SPECTROSCOPIC STUDY
OF PROTON TRANSPORT AND
TRAPPING IN CUBIC ICE

By

PAUL JOSEPH WOOLDRIDGE

Bachelor of Science

Cameron University

Lawton, Oklahoma

1983


Submitted to the Faculty of the Graduate College
of Oklahoma State University
in partial fulfillment of the requirements
for the Degree of
DOCTOR OF PHILOSOPHY
December, 1987

Thesis
19870
W913f
cop. 2




FT-IR SPECTROSCOPIC STUDY
OF PROTON TRANSPORT AND
TRAPPING IN CUBIC ICE

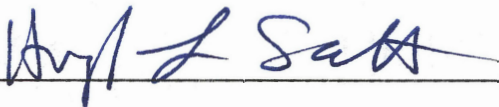
Thesis Approved:

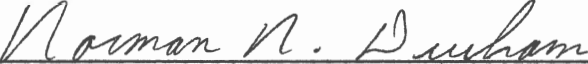


Thesis Adviser









Dean of the Graduate College

PREFACE

The photo-generation of mobile protons in cubic ice has been observed as well as the shallow trapping of these ionic point defects and the kinetics of their thermal release. The observation was based on the infrared spectra from irradiated thin films of H_2O ice which contained small amounts of D_2O .

I wish to express my gratitude to all who assisted me in this work and during my stay at Oklahoma State University. In particular, I am especially indebted to my major advisor, Dr. J. Paul Devlin, for his guidance, concern and help. I am also indebted to the other committee members, Dr. Gilbert J. Mains, Dr. H. Larry Scott and Dr. Donald L. Thompson.

Special thanks are due to the National Science Foundation for the financial support I received during the course of this work.

TABLE OF CONTENTS

Chapter	Page
I. LITERATURE REVIEW	1
Introduction	1
Structure of Ice	2
Proton Positions in Ice	2
Other Low Pressure Forms of Ice	6
Ice Spectra	9
Far Infrared Spectra	10
Mid Infrared Spectra	11
Dynamically Isolated Isotopomers of H ₂ O in Ice	13
Near Infrared	18
Visible	18
Ultraviolet	20
Electron Beam Radiolysis	23
Defects	24
Ion States	24
Orientational Defects	25
Electrical Properties	27
Dielectric Constant	28
Static Conductivity	29
Theoretical Treatment of Ice Conductivity	29
Spectroscopic Studies of Proton Transport	30
The Shallow Trapping of Mobile Protons	35
Presentation of the Problem	40
II. EXPERIMENTAL APPARATUS AND PROCEDURES	41
The Apparatus	41
Cleanliness of the System	45
Sample Preparation	46
Spectra	47
Generation of Mobile Protons in Ice	48
Ultraviolet Irradiated Samples	51
Spectral Stripping	58
Conversion to Concentrations	72
III. MODEL AND DATA FITTING	75
Scrambling Steps	75
Defect Concentrations	82
Low Temperature Analysis	83
High Temperature Data Fitting	96

Chapter	Page
IV. DISCUSSION AND SUMMARY	119
Discussion	119
Summary	125
REFERENCES	127
APPENDIX A - DETERMINATION OF D ₂ O AND (HOD) ₂ ABSORPTIVITIES RELATIVE TO ISOLATED HOD	133
APPENDIX B - PARAMETER FITTING PROGRAM FOR THE 113 K TO 130 K DATA .	141
APPENDIX C - RATE CONSTANT FITTING PROGRAM FOR THE 134 K TO 160 K DATA	145

LIST OF TABLES

Table	Page
I. 110-130 K Data	63
II. 134-160 K Data	68
III. Calculated Molar Absorptivities	73
IV. Best Pseudo-First Order Kinetic Parameters for the First Half-lives of the 113 K to 130 K Data	97
V. Best Constants From Higher Temperature Analysis	109

LIST OF FIGURES

Figure	Page
1. Ice I_h Structure	3
2. Average Deuteron Positions in D_2O Ice	3
3. Ice I_c Lattice	8
4. Water Molecule Normal Modes of Vibration	8
5. Infrared Absorptivity of H_2O Ice	12
6. Frequency of HOD Peak versus Temperature	14
7. FT-IR Spectra of H_2O ice film containing isolated D_2O	16
8. Separate Spectra of HOD, $(HOD)_2$ and D_2O at 90 K	17
9. Absorption of Water and Ice from 15 to 0.9 microns	19
10. Absorption of Ice, 1800 to 2100 Angstroms	21
11. Luminescence of UV Excited Ice	22
12. Possible Formation of Ion-State Pair by Proton Jumping	26
13. Possible Formation of Orientational Defect Pair	26
14. Blocking of a Chain by Motion of One Defect Type	31
15. Resetting of Chain by Other Type of Defect	31
16. Effects of Defect Motion on D_2O isolated in H_2O Ice	34
17. Proton Hopping in Electron Beam Irradiated Ice	36
18. Cold Cell	42
19. Vacuum System	44
20. Ultraviolet Absorption of KBr	52
21. Effects of UV Irradiation on D_2O isolated in H_2O Ice	52
22. Results from Nitrobenzaldehyde Doped Ice	55

Figure	Page
23. Spectra Following Irradiation of Naphthol Doped Ice	56
24. $D_2O \rightleftharpoons (HOD)_2$ Equilibrium System	57
25. $(HOD)_2 \rightarrow 2 HOD$ Kinetics at 145 K	59
26. Derivation of the D_2O Spectrum	60
27. Stripping of a 126 K Spectrum	62
28. Elementary Scrambling Steps of D_2O and $(HOD)_2$	76
29. Elementary Scrambling Steps of $(HOD)_{pc}$	78
30. Elementary Scrambling Steps of $(HOD)_{nn}$	79
31. Reaction Summary	80
32. Simplified Reaction Scheme	81
33-41. Plots of Data in Integrated Rate Form	86-94
42-50. Plots of First Order Fits to First Half-lives	98-106
51. Arrhenius Plot from Low Temperature Initial Rates	107
52-59. Higher Temperature Data Plots with Fitted Curves	110-117
60. Arrhenius Plot for the High Temperature Turning Step	118

CHAPTER I

LITERATURE REVIEW

Introduction

Proton transport in hydrogen bonded solids is of great importance due to its role in the fundamental processes of certain fast-ion conductors (1) and in biological systems including enzymatic reactions, energy transduction and apparently the vision process (2,3). Also of interest is a better understanding of the microscopic processes in ice itself because ice is an important solid here on earth and throughout space, and its mechanical and electrical properties are profoundly influenced by the motions of protons and other defects.

The ability to isolate intact D_2O molecules in H_2O ice in which the D_2O molecules have not exchanged protons with the surrounding H_2O water molecules and then to follow the isotopic scrambling spectroscopically (4,5) makes ice a model system in which to explore the molecular level details of proton transport. This ultrasensitive probe is ideal for studying the phenomenon of shallow trapping of mobile protons in ice, in which protons liberated at low temperatures are quickly trapped and do not cause isotopic scrambling until the crystal is warmed. In this review I will focus on the areas of ice research relating to proton transport and especially the spectroscopic method of detailing proton motions.

Structure of Ice

For an extensive review of the structure and properties of ice see Ice Physics by Peter Hobbs (6). More concise reviews are by Fletcher (7,8). Ice occurs naturally in the form ice I_h (read "one", not "i"), with the subscript h indicating hexagonal symmetry. X-ray diffraction has determined the oxygen atom positions to correspond to the tetrahedrally coordinated wurtzite structure as shown in Figure 1. The oxygen-oxygen distance is 0.276 nm at just below the normal freezing temperature. For D_2O ice the lattice parameters were found to differ by less than 0.1% from those of H_2O ice (9). Unit cell dimensions in ice monotonically contract in going from 273 K to 10 K (10). Dantl's data (11) however shows a negative thermal expansion coefficient below 65 K, not unlike some other tetrahedrally bonded crystals, but there is disagreement as to the thermal expansion curve at low temperatures. The angle between the deuterons (protons) of a water molecule in ice has not been determined exactly, but is thought to lie closer to the tetrahedral angle than to the gas phase value of about 105 degrees, meaning the hydrogen bonds in ice are very nearly linear.

Proton Positions in Ice

The difficulty in determining proton positions by x-ray diffraction allowed much early speculation as to where the hydrogen atoms were. Refuting the notion that the protons were located midway between the oxygen atoms, Bernal and Fowler in 1933 (12) suggested that the water molecules remained intact and that they were linked together so that each proton of one molecule is directed towards a lone-pair electron hybrid orbital of a neighboring molecule. This suggestion was accepted

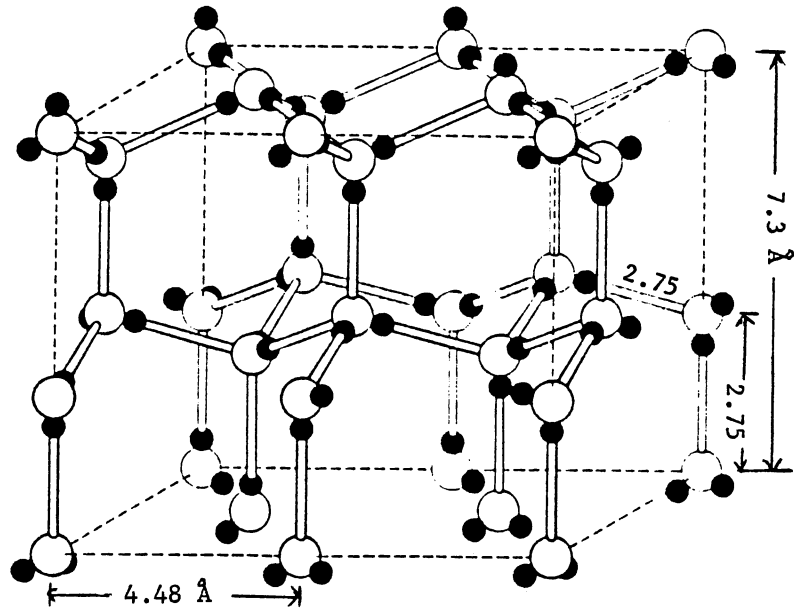


Figure 1. The ice I_h structure, oxygen atoms are represented by open circles and the protons by filled. Dimensions are those for a temperature of 77 K. From reference 7.

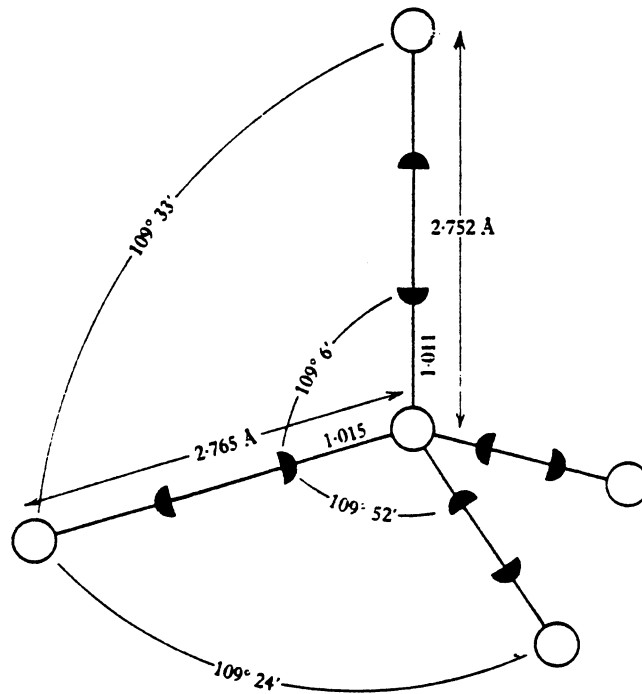


Figure 2. Average environment of a molecule in D_2O ice at $-50\text{ }^\circ\text{C}$ as determined by neutron diffraction. The deuterons appear in symmetrical pairs of half-deuteron positions. From Peterson and Levy, *Acta Cryst.*, 10, 70 (1957).

as reasonable, but it left the problem wide open: it did not specify a particular arrangement of the molecular orientations. Indeed, one could picture many different arrangements that would satisfy Bernal and Fowler's rules. In 1935 Pauling (13) noted that at temperatures above about 200 K the dielectric constant of ice is similar to that of liquid water; showing that the molecules can re-orient themselves with considerable freedom, the crystal changing under the influence of the electric field. On cooling to low temperature the crystal freezes into one of the possible configurations, but does not go to a perfectly ordered one. Pauling calculated the expected residual entropy for ice obeying Bernal and Fowler's rules to be $R \ln W$, where W is the number of configurations accessible to the crystal. An intact water molecule may have 6 possible orientations but the chance that the adjacent molecules will permit a given orientation is $1/4$. Therefore the total number of configurations for N molecules is $W = (6/4)^N = (3/2)^N$. For a mole of ice this gives an entropy $R \ln(3/2) = 0.805 \text{ cal mole}^{-1} \text{ K}^{-1}$, agreeing closely with the experimental value $S_0(\text{expt}) = 0.81 \pm 0.05 \text{ cal mole}^{-1} \text{ K}^{-1}$ of Flubacher and Leadbetter (14). Pauling also noted that although no cubic modification of ice had yet been reported such a configuration would not be distinguishable as far as the residual entropy was concerned. (Interestingly, an x-ray photograph of the cubic form was published in 1935 by Burton and Oliver (15), but they interpreted the simpler diffraction pattern as hexagonal ice building up only upon certain planes, as the crystallization temperature had been held between the formation temperatures of hexagonal and amorphous ices.)

Later calculations by Nagle (16) considered the effects of ice

being closed rings of water molecules which further restrict the configurations available and calculated a value of $S_0(\text{calc})=0.8143 \pm 0.0002 \text{ cal mole}^{-1} \text{ K}^{-1}$, which is about 1% higher than Pauling's value and still in excellent agreement with experiment.

Hence, ice is crystalline only in the positions of its molecules but glass-like in their orientations. Neutron diffraction studies (17,18) found half-deuterons at each of the possible proton positions on each bond (see Figure 2) indicative of a statistical distribution of molecular orientations. Many of ice's interesting properties result from the existence of many very nearly isoenergetic arrangements of water molecule orientations which satisfy the bonding rules of Bernal and Fowler, and the mechanism and dynamics of changing the orientations.

The near equivalence in energy of sets of water molecule orientations is evidenced by the non-zero low temperature entropy of pure ice, which is the same regardless of whether the sample is freshly frozen or well aged. Proton ordering in pure ice at low temperatures occurs with extreme slowness.

In 1982, Suga and coworkers (19) reported the observation of a first-order phase transition in annealed KOH-doped ice at 72 K, which was identified as the order-disorder transition associated with the proton positions. An anomaly in the heat capacity curve was the evidence that about 70% of the residual entropy had been removed. The KOH was added to catalyze the transition to the ordered phase. Earlier studies with HF doped ice showed a similar behavior, but to a much lesser extent (20). A powder neutron diffraction study performed on 0.11 M KOD in D_2O ice (21) gave almost identical scattering properties below and above the calorimetric transition temperature. A model fully

ordered structure which had the same lattice spacings as disordered ice I was applied to the data. By allowing preferred deuteron site occupation to vary between 0.5 (fully disordered) and 1.0 (fully ordered), a best fit was found at an occupancy of 0.63. It was suggested that the site occupation number of 0.63 was due to the sample having ordered domains of less than 4 nm in dimension. Their model had polar domains.

Other Low Pressure Forms of Ice

In addition to ice I_h , two modifications which are metastable with respect to ice I_h are commonly formed at low pressure and temperature. Amorphous, or vitreous, ice (ice I_a , or I_v) is formed by slowly condensing water vapor onto a surface which is kept at about 130 K or lower. Scats and Rice (22) have reviewed the formation of amorphous ice. Ice I_a transforms irreversibly to cubic ice (ice I_c) as the temperature is raised and the transition is fairly rapid above 140 K, being completed in a few minutes (23), releasing about 220 cal/mole. Narten, Venkatesh and Rice (24) reported the existence of two distinguishable forms of amorphous ice. The usual form had a density of $0.94 \text{ gram cm}^{-3}$ while a form produced at 10 K on an oriented single crystal of copper had a density of 1.1 gram cm^{-3} . Handa, Mishima and Whalley (25) produced a high density form of amorphous ice by "melting" ice I at 77 K by applying the extrapolated melting pressure of about 10 kbar. The phase had a density of 1.17 gm cm^{-3} and quickly transformed to a phase having lower density when warmed to 117 K. In 1985 Mayer (26) rapidly cooled an aqueous aerosol on a KBr or sapphire window held at 50-100 K. The infrared spectrum of the sample was compared to that

of vapor deposited amorphous ice and found to have lower OH and OD stretching frequencies than the vapor deposited form. Whether quenched liquid water is the same as vapor deposited amorphous solid water is still unresolved.

Below about 200 K it is possible to produce cubic ice from the vapor or from some high pressure ices (27). This metastable state slowly converts to ice I_h at higher temperatures (6), converting "sluggishly" at 175 K. Ice I_c has been characterized by vapor deposition on an electron diffraction apparatus below 170 K by Honjo and Shamaoka (29). As reviewed by Blackman and Lisgarten (30), ice I_c has essentially the same interatomic distances and angles and the same volume per unit cell as ice I_h . Figure 3 illustrates the cubic ice lattice. Also the mid-infrared spectra of ices I_c and I_h are indistinguishable (27) due to the fact that the nearest neighbors and their distances and angles are identical in the two phases, and the number of nearest neighbors is the same. Sugisaki, Suga and Seki (31) measured the heat capacities of ices I_a , I_h and I_c and found the heat capacities of I_h and I_c to be the same within 1%. The latent heat of transformation from I_c to I_h has been measured recently by Handa, Klug and Whalley (32) using cubic ice made by transforming high pressure phases of ice confined in a soft metal container to prevent the formation of the large surface area which forms when vapor deposited amorphous ice is warmed, which is the common way to produce the cubic form. They measured $-50.5 \pm 2.2 \text{ J mol}^{-1}$ at 200 K for the energy difference between ice I_c and I_h . "The two structures differ only in orientations of second neighbors that are in different layers, and the distances between molecules begin to differ only between some fourth

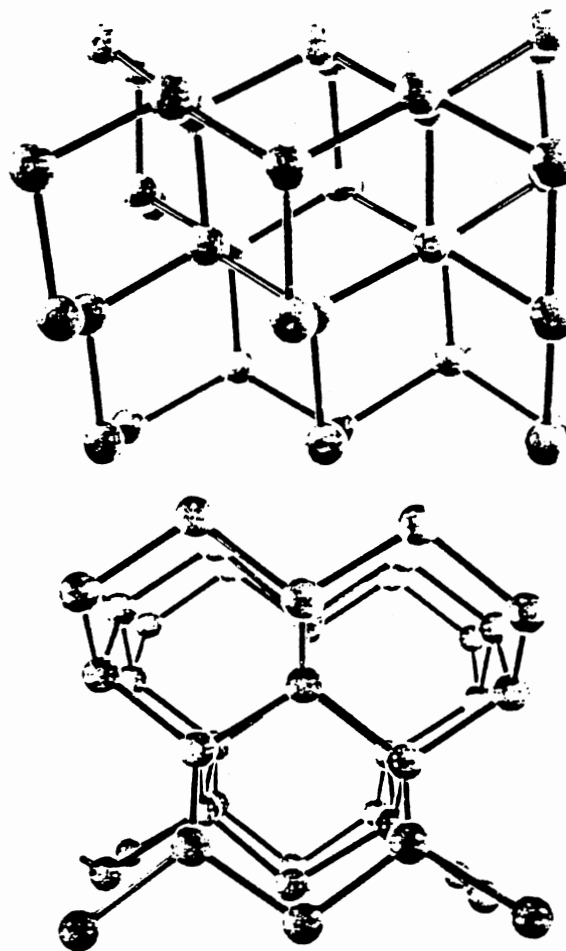


Figure 3. Two views of the ice Ic lattice. Proton positions are not shown, but are randomly distributed. From reference 6.

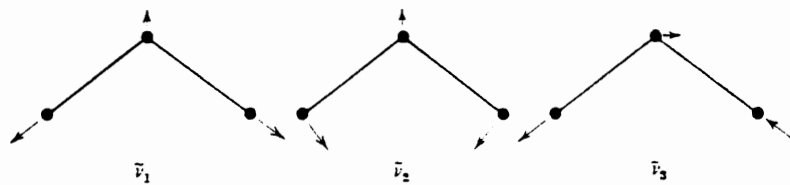


Figure 4. The three normal modes of vibration for the water molecule.

neighbors in different layers. The difference in energy was, therefore, expected to be small."(32)

Honjo and Shimaoko (29) investigated the possible hydrogen atom positions of cubic ice using electron diffraction because hydrogen atoms make a relatively larger contribution in electron diffraction than in x-ray diffraction. They found that the cubic equivalent of Pauling's statistical model of ice I_h still holds. Gough and Davidson (33) measured the dielectric behavior of cubic ice and found it to be almost completely identical to that of hexagonal ice. In light of the equivalence in bond lengths, angles, unit cell dimensions, dielectric behavior, and identical infrared and Raman spectra, it is assumed that other microscopic processes will also be the same in the ices I_c and I_h .

Ice Spectra

The H_2O molecule has $3N-6=3$ degrees of freedom which implies 3 possible normal modes of vibration. These 3 modes obey the symmetry properties of the point group C_{2v} and are shown in Figure 4. The ν_2 bending mode belongs to the irreducible representation A_1 , i.e. the displacements from equilibrium are symmetric under all operations of the point group. The ν_1 vibration belongs to A_1 and is principally an in-phase stretching of the two O-H bonds, a symmetric stretch. The out-of-phase O-H stretch, or antisymmetric stretch, ν_3 belongs to the representation B_1 and is antisymmetric under the rotation C_2 or a reflection operation. From page 14 of ref. 7, the vapor phase frequencies are:

$$\nu_1 = 3651.7, \quad \nu_2 = 1595.0, \quad \nu_3 = 3755.8 \text{ cm}^{-1}$$

In ice, three different type of modes contribute to infrared absorption.

In the first place there are intramolecular modes corresponding principally to combinations of the three fundamental modes of the isolated water molecule, their frequencies being significantly shifted by the effects of hydrogen-bonding. In H_2O ice the ν_1 and ν_3 modes and the ν_2 overtone contribute to the complex peak near 3200 cm^{-1} which is shifted to near 2400 cm^{-1} in D_2O ice, a frequency shift of about $2^{1/2}$.

The other vibrational modes of the crystal may be called intermolecular, since they involve interactions between neighboring molecules. The intermolecular modes may be of two types, either translational, in which case the shift in going from H_2O ice to D_2O ice will be close to $(18/20)^{1/2}$, or rotational, in which case the shift will be about $2^{1/2}$. The rotationally based modes, the librations, contribute to the broad peak extending from 500 to 1050 cm^{-1} in H_2O ice and from 350 to 750 cm^{-1} in D_2O ice. The translational modes give a set of fundamental peaks below 400 cm^{-1} . The interaction of the modes as well as the possible effects of the proton disorder and Fermi resonance make a more detailed assignment of the ice spectra very difficult. As the theory of ice spectra can be found in much more detail elsewhere, I will only cover points of interest to this study.

Far Infrared Spectra

If there is a difference in the spectra of ices I_c and I_h , then it should be most apparent in the lattice mode region in the far infrared. Bertie and Jacobs (34) in 1977 reported for the first time

differences in the spectra of ices I_c and I_h . The range measured was 240 to 20 cm^{-1} and the temperature was 4.3 K where the broadening anharmonic effects are minimized. Overall the spectra were still mostly identical: the major difference found was that a peak at 160 cm^{-1} in ice I_c was somewhat split into a doublet in ice I_h . The spectrum of x-ray-verified cubic ice agreed very well with the spectrum of a sample made by vapor deposition at 173 K (35).

Mid Infrared Spectrum

Figure 5 shows the infrared absorptivity profile for ice as determined by Bertie, Labbe' and Whalley (36). Whalley (37) studied the spectra of ice I_c and I_h and presented a detailed assignment based on the spectrum of the high pressure ice VIII, whose structure consists of two interpenetrating ice I_c lattices in which the protons are in an ordered configuration. The proton disordered form with the same oxygen lattice, ice VII, has a very similar spectra (bandwidths included) as ice VIII. Whalley noted that assignments can be difficult because the vibrations cannot be treated as arising from a single molecule because of the strong intermolecular coupling that exists in ice, the coupled crystalline lattice. Whalley contended that there should be strong similarities in the spectra of ordered and disordered ice I_c , and that the spectra of ices I_c and I_h are identical. He also provided a brief review of previous assignments of the ice I spectrum.

The assignment of the ice spectrum in fullest detail is the subject of much controversy. Rice et al. (38) described the OH stretching spectra of ice I_h , ice I_a and liquid water from a unified point of view. A molecular dynamics simulation was done on a 216 molecule cell

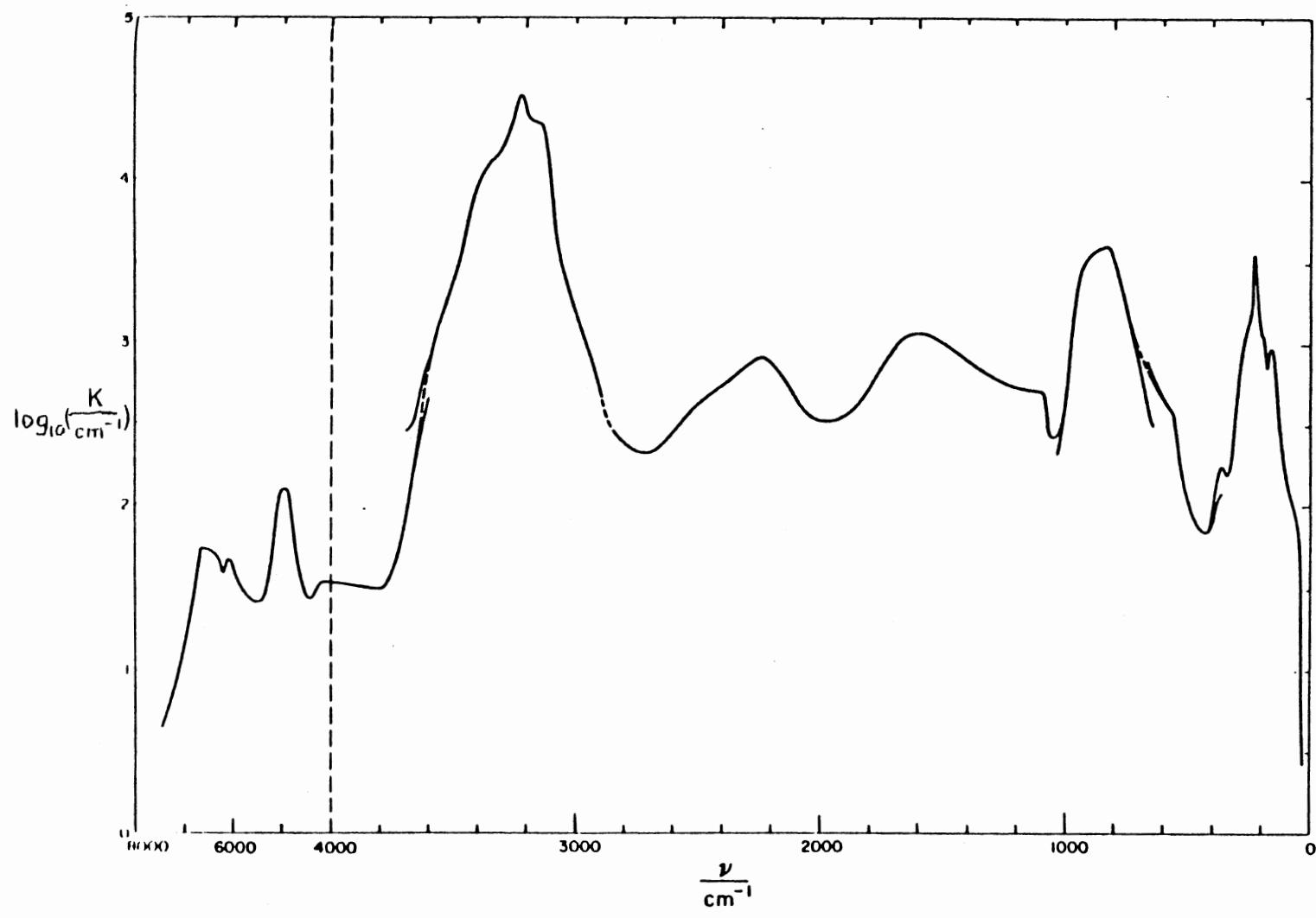


Figure 5. Absorptivity of H₂O ice I in the range 30-7000 cm⁻¹.

J. E Bertie, W. J. Labbe¹ and E. Whalley, J. Chem. Phys., 50, 4507.

using a total Hamiltonian which was the sum of terms for intramolecular harmonic motion, intermolecular anharmonicity, hydrogen bonding to nearest neighbors, and transition dipole-transition dipole coupling to all other neighbors, in that order of importance. They concluded the stretching spectra was dominated by the effects of OH-OH oscillator interaction and much smaller effects were due to Fermi resonance and the proton disorder. Collier provided a review of the experimental work and the theory of ice spectra in his 1983 thesis (39). Important to this study is that the spectra of O-D oscillators isolated in otherwise H₂O ice are relatively clean and simple and have been unambiguously assigned.

Spectra of Dynamically Isolated

Isotopomers of H₂O in Ice

Haas and Hornig (40) studied the 80 K spectra of various mixtures of D₂O and H₂O in the spectral range 700 to 7000 cm⁻¹. For the lowest HOD concentrations a sharp O-D stretch was observed at 2416 cm⁻¹. (The sharpness of the uncoupled O-D stretch makes it a good probe to the structural changes in the crystal, for example Figure 6 shows the shift of the peak to lower frequency as the temperature is lowered and the lattice contracts. The shift is due to increased hydrogen bond strength weakening the O-H stretching force constant.) When the HOD concentration was increased side bands appeared at 2393 and 2442 cm⁻¹. These side bands were assigned to the coupled vibrations of neighboring HOD molecules. For a bond angle of 109 degrees a simple calculation estimated an intensity ratio of 2 to 1 for the in-phase and out-of-phase bands.

In a series of papers Devlin and colleagues (41-43) assigned the

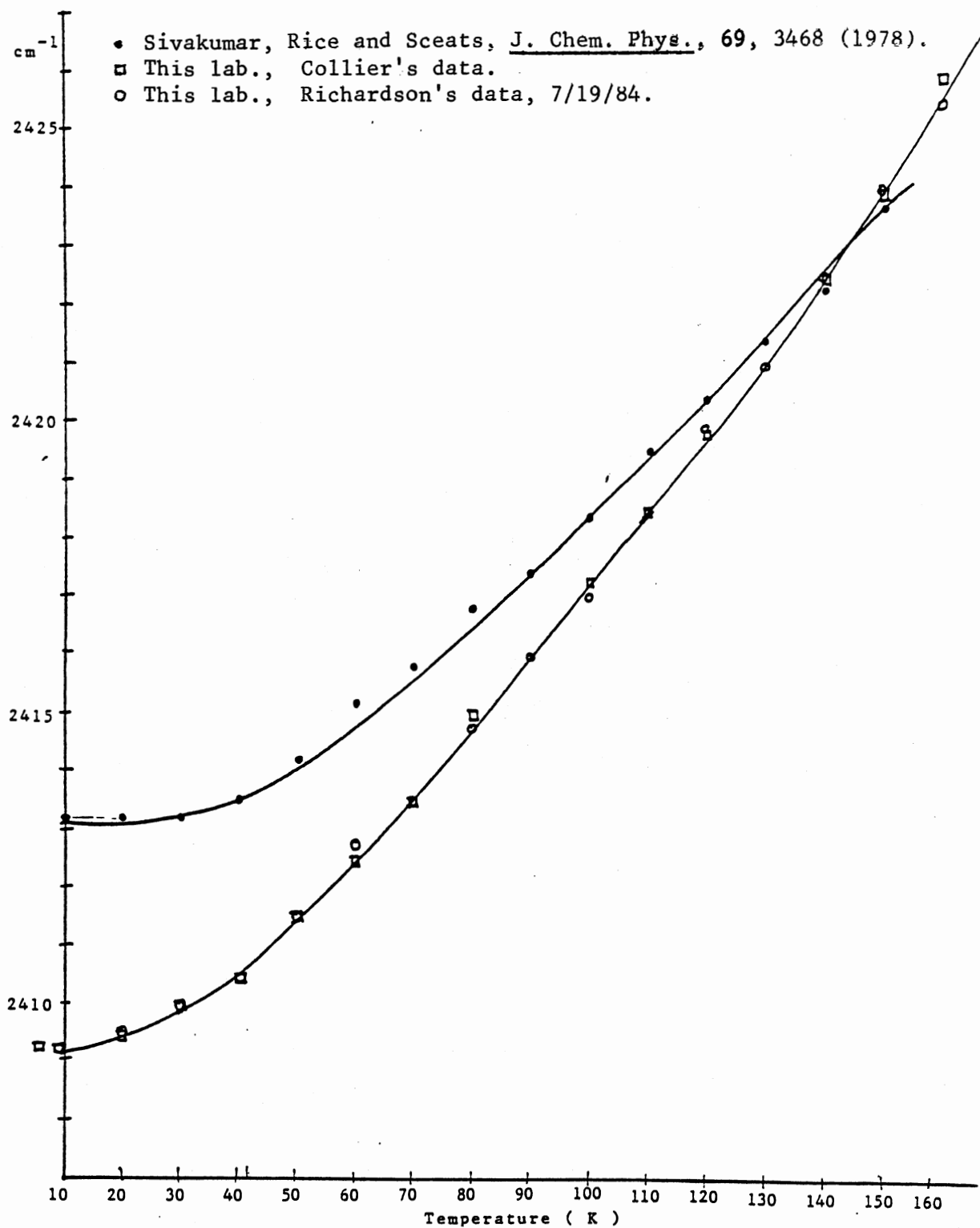


Figure 6. Peak positions of the HOD stretch in H₂O ice I_c.

vibrational frequencies of the isotopic ices. FT-IR and polarized Raman spectra were obtained, and infrared spectral subtractions were performed with the FT-IR computer. With only a small amount of isotopic scrambling, isolated D_2O in H_2O polycrystalline ice can now be routinely made by co-deposition of H_2O and D_2O vapor beams onto a cooled infrared window, with the D_2O beam being about 50 times less dense than the H_2O beam. At <125 K amorphous samples are produced, unless the window has a crystalline ice base layer formed at 145 K or higher, in which case crystalline ice is grown epitaxially. The crystal form produced is probably cubic in view of the 160 cm^{-1} singlet peak in the spectra of Bertie and coworkers for samples formed under the same conditions (27,34,36) though diffraction validation is unavailable for the samples containing isolated D_2O . Figure 7 shows the FT-IR spectrum of a freshly prepared sample with the O-D stretching region boxed in. Spectra of fully scrambled samples, which are of course available, may be scaled and subtracted from initial deposits of D_2O in H_2O to obtain spectra for pure isolated D_2O in H_2O ice with no HOD contaminant. Spectra of "pure" neighbor coupled HOD molecules, $(HOD)_2$, can be obtained from samples treated by ionizing radiation to give a dominant concentration of $(HOD)_2$ by subtracting scaled pure D_2O and HOD spectra. The results at 90 K are shown in Figure 8, each having the background H_2O ice absorption subtracted. The same strategy may be employed to obtain the pure spectra of the O-H stretching modes of H_2O and $(HOD)_2$ isolated in D_2O ice, but is somewhat complicated by the coincidence of the HOD band with one of the H_2O bands. Most recently, Devlin has reviewed the refinements of the experimental data for isolated isotopomers of H_2O in H_2O and D_2O

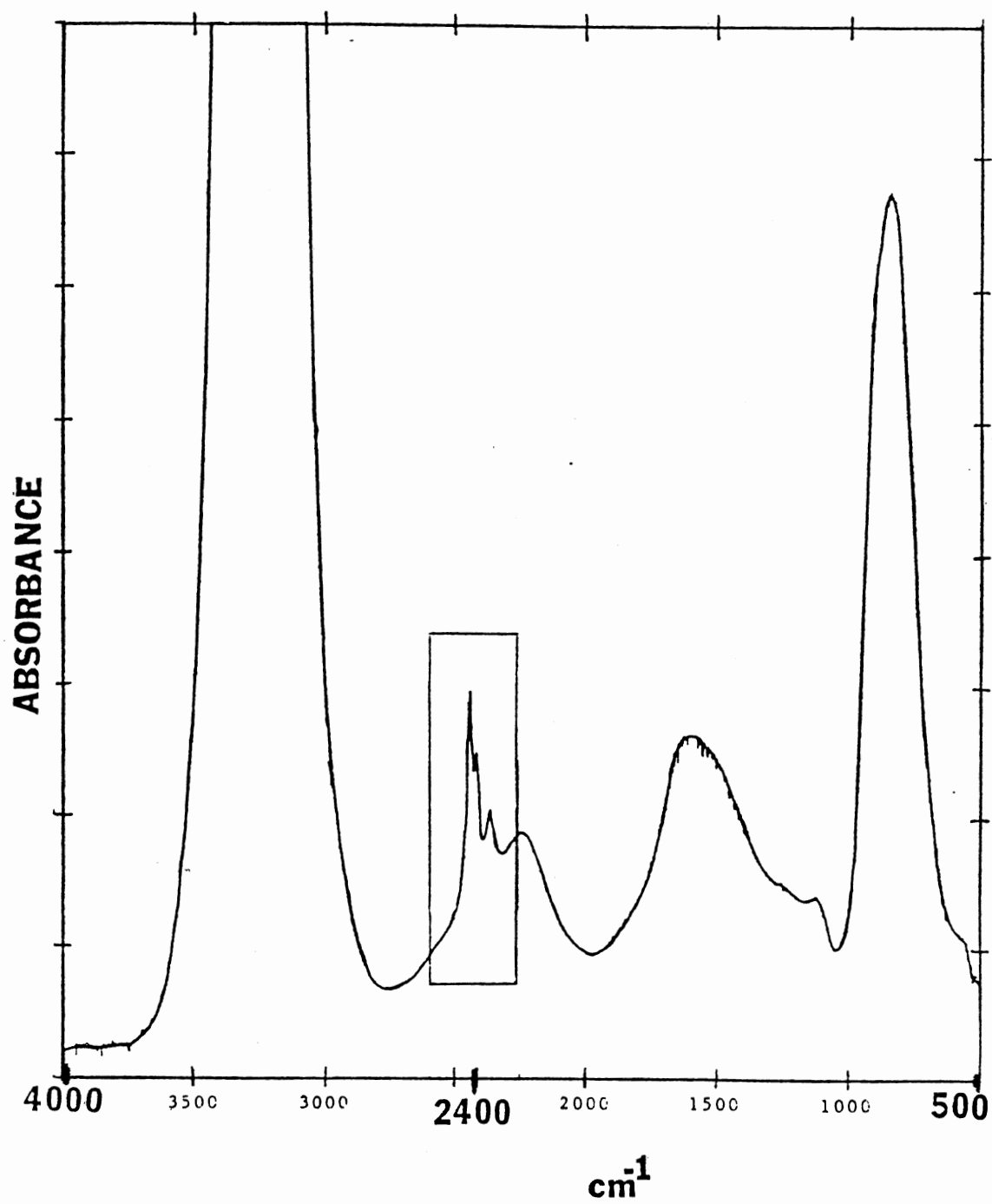


Figure 7. FT-IR spectrum of isolated units in H₂O ice.

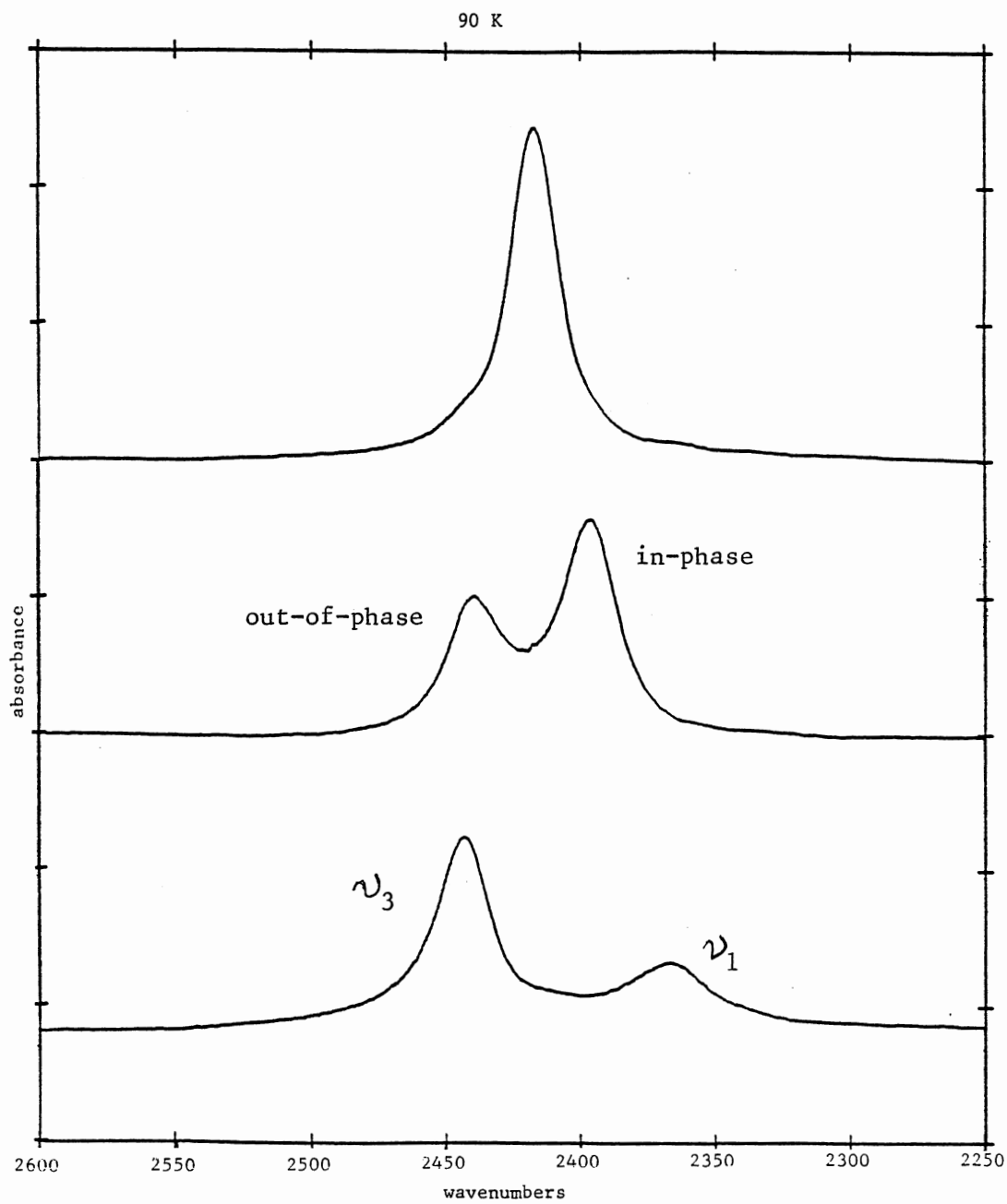


Figure 8. Isolated HOD, coupled HOD neighbors, and isolated D_2O molecules in H_2O ice, all with the H_2O background removed.

ices and the implications towards past assignments and theoretical studies (44). The separability of the O-D multiplet allows the concentrations of D_2O , $(HOD)_2$ and HOD to be followed spectroscopically when isotopic scrambling proceeds as a result of proton mobility.

Near Infrared

The spectra of Haas and Hornig (40) did extend up to 7000 cm^{-1} . The overtone spectra to 7000 cm^{-1} of H_2O and D_2O ices and mixtures were also investigated by Kroh and Ron (45). The absorptions were measured and attributed to various overtones and combinations of fundamentals. From the OH overtone frequency they inferred a lower limit of 18 kcal/mole for proton movement in ice. Sceats and Rice (46) analysed the fundamental and overtone spectra of ice made from H_2O/D_2O mixtures in terms of how the intramolecular potential is altered by hydrogen bonding strength. Bertie, Labbe' and Whalley (36) did include absorbance traces up to 10000 cm^{-1} ; the absorbance was very weak and featureless between 7000 and 10000 cm^{-1} . Figure 9 shows Irvine and Pollack's absorption coefficients vs. wavelength for liquid water from 15 to 0.2 microns and from 15 to 0.9 microns for ice; the absorptivity of ice follows that of the liquid very closely (47).

Visible

This section is exceedingly brief since ice appears to be "totally transparent" throughout the visible spectrum. There appears not to be any reliable data on pure bubble-free ice crystals in this range.

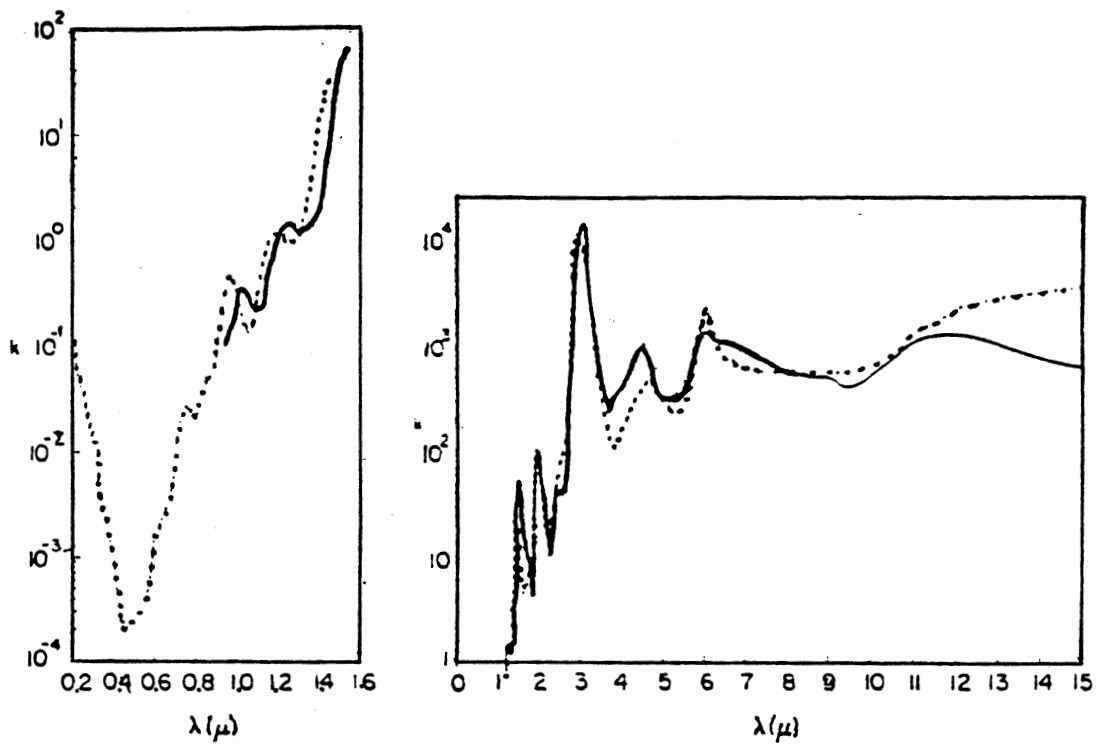


Figure 9. Absorption coefficient in cm^{-1} versus wavelength in microns for water (dashed curve) and for ice (full curve). From reference 47.

Ultraviolet

Cassel (48) studied the vacuum ultraviolet spectra of ice formed from water vapor at liquid air temperature, finding an absorption continuum with a long wavelength limit of 167 nm. Onaka and Takahashi (49) compared the vacuum uv spectra of the vapor, liquid and solid forms of water. They observed absorption beginning at 180 nm in the vapor, shifting to 177 nm for ices I_h and I_a . On top of the gradual rise of absorption of the other ices, cubic ice was found to have a well defined band at 143 nm which could not easily be explained. In no modification was there any noticeable absorption of wavelengths longer than 190 nm. Figure 10 shows the uv absorption of ice and liquid water from 180 to 2100 nm from ref. 50.

Ghormley and Hochanadel (50) have monitored by optical absorption the formation of OH radicals during uv flash photolysis of ice using a Xe flashlamp through suprasil optics (short wavelength cutoff - 160 nm).

They attributed a 265 nm absorption to OH which had been produced by the Xe flash lamp. Quickenden et al. (51), studied the uv excited luminescence from crystalline H_2O ice at 88 K. With excitation using 220 and 255 nm radiation two broad luminescence bands of low intensity around 340 and 420 nm were observed. The spectra exhibited memory effects which were erased by temporary warming to 130 K or higher. The 260 nm absorption and 420 nm emission were attributed to photolytically produced OH radicals which accumulate in the ice lattice. Looking at Figure 11, which reproduces their figures 2 and 4, the 260 nm band is quite apparent, but at the shortest wavelengths the intensity is again rising and it appears from the figures that radiation shorter than 220 nm would be more effective in producing OH.

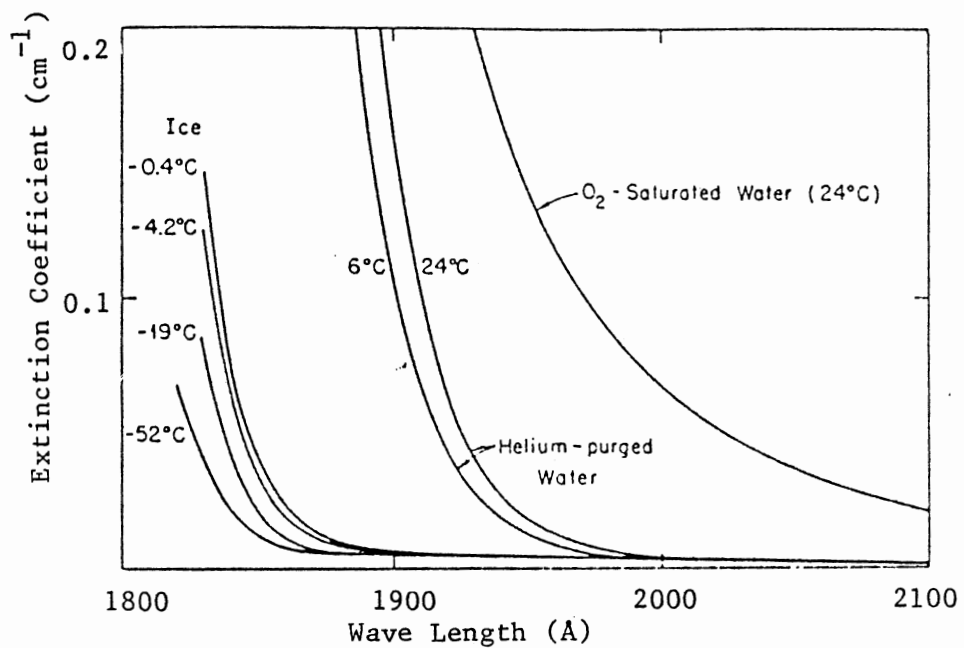


Figure 10. Absorption spectra of ice and water at several temperatures. From reference 50.

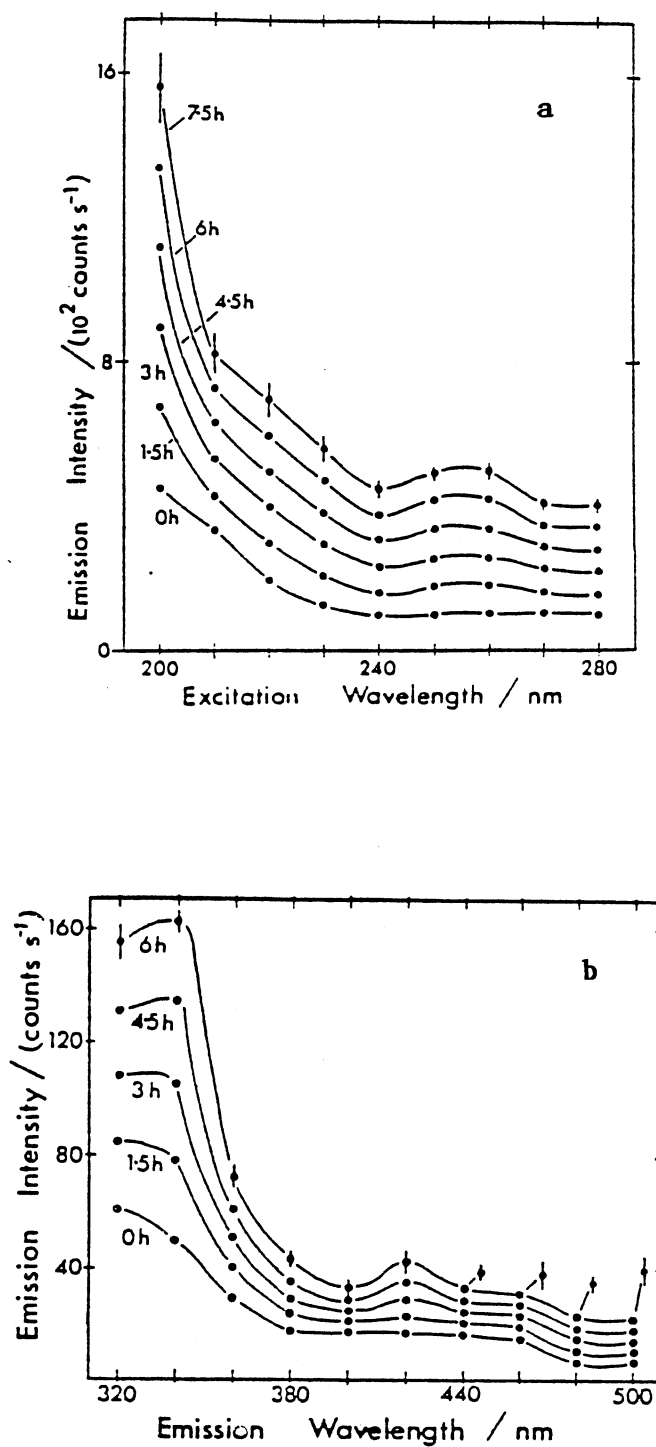


Figure 11. (a) The progressive increase of the luminescence excitation spectrum of purified H₂O ice at 88 K excited by uv light. The emission wavelength was set at 420 nm. (b) Luminescence emission spectra showing the progressive increase of emission intensity during continuous excitation with 220 nm light for a period of 6 hours. From reference 51.

Electron Beam Radiolysis

Quickenden, Trotman and Sangster (52) irradiated ice with a 0.53 MeV electron beam. The ice samples were single crystals and were grown from water which they had taken extreme care to purify and to prevent any probable uv emitters from entering. A broad 385 nm emission was observed and assigned to OH, the product of the bimolecular reaction between H_3O^+ and trapped electrons. Later, thin films of amorphous and polycrystalline ice (vapor deposited onto Cu) were irradiated with 0.53 MeV electrons while at 97 K (53). Luminescence curves had the same general shape as for single crystal ice and had no thickness dependence from 45 nm to 4 microns. Memory effects which had been observed in uv ionized and also in electron beam ionized single crystal ice were, however, diminished in the amorphous and polycrystalline ice films. Also it was noted that amorphous ice gave 4 times more OH emission than the polycrystalline.

An extensive study of the 3 MeV electron beam pulse radiolysis of pure ice at various temperatures was made by Taub and Eiben (54). Below about 200 K they observed optical absorption bands at 670, 280 and 230 nm which they attributed to solvated electrons, OH radicals and HO_2 radicals, respectively. The assignments were supported by ESR spectra. At 260 K the 280 nm band was not observed.

It seems to be generally assumed that when ice is exposed to ionizing radiation, water molecules dissociate but only the hydrogen atom leaves the site of the original water molecule and the OH remains behind, hydrogen bonded to water molecules (50). Indeed, ESR of OH in irradiated ice yielded spectra consistent with the OH remaining at a

lattice site (55). Other ESR studies revealed that, at 4.2 K, H and OH are formed and are stable, but when warmed to 77 K all of the H and only part of the OH disappear (56). The H + H and H + OH combination reactions occur at comparable rates but the OH + OH combination is immeasurably slow (57). With energies less than those of the electron beams, it is still unclear what wavelengths and power levels are necessary to produce observable ion state defects in ice and, in particular, mobile protons.

Defects

Thus far only ice in which all of the molecules strictly obey the rules of Bernal and Fowler have been considered. However there are many imperfections which occur in real crystals: surfaces, impurities, dislocations, point defects and so on.

The structure of a perfect ice crystal is a configuration which satisfies Bernal and Fowler's (BF) rules: (1) each lattice position is occupied by a water molecule tetrahedrally bonded to its four nearest neighbors; (2) water molecules are intact so that there are just two protons near each oxygen; (3) there is just one proton on each bond. Violation of the first rule leads to a vacancy, an impurity or an interstitial. Violation of the second rule leads to ion states.

Ion States

A pair of ion states H_3O^+ and OH^- is formed, at least formally, when a proton jumps from the normal end of a bond to a position near the other end. Calculations disagree as to the existence of a second minimum in the potential curve, but at best the ion states

would be metastable towards recombination. There is, however, a finite possibility that a further proton jump may separate the two ion states. Figure 12, a projection of an ice lattice in two dimensions with oxygens at the intersections and protons marked by dots, illustrates such a formation and separation of an ion-pair. Further proton jumps may then lead to either recombination or a diffusive separation of the two ion states against the attractive electrostatic force between them.

In the lattice the extra proton is expected to have a perturbing influence on the local structure and the excess charge will be distributed over a number of neighboring molecules. Proton hopping does not move an entire proton charge because water molecule dipoles are reoriented at the same time as the positive ion migrates.

In thermal equilibrium the concentrations will be given by $n_+ = n_-$ in pure ice and change with temperature as $\exp(-H_{f+-}/2kT)$ where H_{f+-} is the enthalpy for the formation of a defect pair. The value for H_{f+-} is the sum of two parts, that involved in proton transfer along the bond and a further part arising from the separation of the two ion states against their electrostatic attraction.

The equilibrium ion concentrations are extremely difficult to measure and estimates vary greatly, but are orders of magnitude less than values for liquid water extrapolated to the same temperature. Jaccard (58) postulated that the positive ion states are much more mobile than the negative ions, which was later confirmed by Collier, Ritzhaupt and Devlin (59).

Orientational Defects

Orientational defects exist in violation of the third BF rule.

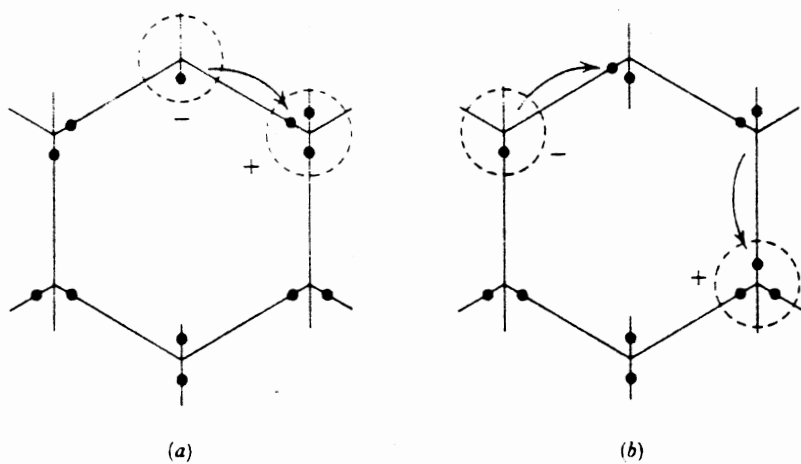


Figure 12. (a) Formation of an ion-state pair, H_3O^+ and OH^- , by a proton jump along a bond. (b) Separation of these two ion states by further proton jumps.

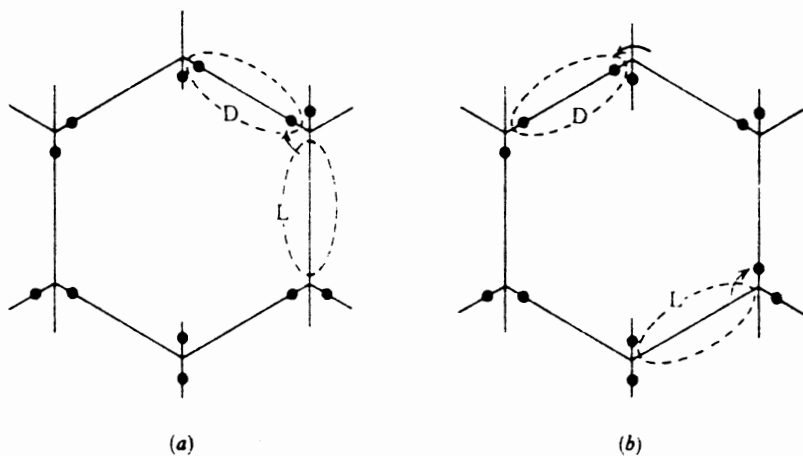


Figure 13. Formation of an orientational defect pair, D and L, by an oblique proton jump or, equivalently, by rotation of a water molecule by $2\pi/3$ about one of its bonds. (b) Separation of these two orientational defects by further oblique proton jumps.

Originally put forth by Bjerrum (60), the defects are produced formally by the rotation of a single molecule through 120 degrees about one of its bond directions, leading to one doubly occupied bond (D-defect) and one unoccupied bond (L-defect) as shown in Figure 13. The two defects can then diffuse apart by successive rotations of neighboring molecules.

The molecular rotations involved can be pictured by an oblique jump of a single proton from one bond to another on the same molecule, the distance in the perfect lattice is about 0.16 nm. Using ab initio molecular orbital methods, Scheiner and Nagle (61) calculated the fraction e_B/e of the full protonic charge carried by Bjerrum defect migration in ice. Their value of 0.36 was found by calculating the change in dipole moment after a defect has been transported down a chain of H_2O molecules. The estimated energy of formation is roughly 15 kcal/mole (7). Motion of point defects has been used to explain many properties of ice, including the mechanical and electrical properties; and, as will be shown in detail later, isotopic scrambling of D_2O in H_2O ice.

Electrical Properties

Of the properties relating to proton transport in ice, historically the electrical properties have received the most attention.

Investigations of the electrical properties have been performed since the beginning of this century. Unfortunately, early measurements of the dielectric spectrum and static conductivity yielded data varying by orders of magnitude which made comparison with theory difficult.

Introducing his theoretical treatment to explain the electrical data in terms of proton transport and orientational defect motion, Jaccard wrote

that (58) "pure ice is altogether a bad conductor and insulator". Similar theories of ice conductivity were put forth by Jaccard (58), Granicher (62,63) and Onsager (64); all requiring the motion of both ionic and orientational defects. In the mid 1960's strides were made in experimental techniques. The effects of surface conductivity were recognized and steps taken to avoid them (6), in particular by the use of guarded three and four terminal electrodes. Another difficulty is that ice conductivity is purely protonic while normal electrodes supply or accept electrons, which leads to the build up of space charge at the electrodes (65). Taking electrode effects into account, totally insulating, or blocking, electrodes have been used (66); or, on the other hand, proton injecting and accepting electrodes made of hydrogen loaded palladium (67) or ion exchange membranes (68) have also been employed. These advances resulted in more consistent agreement between researchers, but there is still disagreement concerning the d.c. conductivity and its activation energy. In his 1974 book, Hobbs (6) reviewed the experimental data and the theories to explain it.

Dielectric Constant

A typical electrical experiment seeks to measure the dielectric constant and conductivity of pure or doped ice as a function of frequency. Steps in the dielectric data curve occur at the characteristic frequencies related to the Maxwell relaxation times of the defect partial conductances. Around 10^{16} Hz the value 1.72 is due to electron polarization, and around 10^{14} Hz the value rises to 3.16 due to ion polarization. The Debye relaxation in ice, with characteristic frequency ω_D , is conditioned by reorientation of water

molecules caused by the motion of defects. Typical values for ω_D are around $3 \times 10^5 \text{ s}^{-1}$ at 0°C with an activation energy of 13.1 kcal/mole (6). The observation of other dispersion steps is dependent upon the electrodes used, as discussed by Petrenko and Ryzhkin (65). The characteristic frequencies depend strongly on the temperature and sample purity.

Static Conductivity

Ice I has a static conductivity whose measured value at 263 K ranges from 10^{-7} S/cm (69) to 10^{-11} S/cm (70). The conductivity increases exponentially with increasing temperature, with an activation energy measured by Durand et. al. (68) to be ~ 9 kcal/mole above 200 K and ~ 13 kcal/mole at lower temperatures. They used ion-exchange electrodes over the range 173 K to 253 K. The conductivity has been shown to be purely protonic without any noticeable contribution from the electrons, the electronic band gap being about 7.3 eV (ref. 7, p212). Careful electrolysis experiments on ice confirmed the current to be totally protonic (71). The conductivity has an extremely critical dependence on the sample purity; for example doping with HF increases the DC conductivity by several orders of magnitude and decreases the activation energy.

Theoretical Treatment of Ice Conductivity

The Jaccard theory of protonic conductivity in ice breaks the conduction into two steps, one involving the transfer of a proton from a H_3O^+ ion to the next water molecule and the other a rotation of the molecule, not unlike the theory of protonic conduction in liquid water of Conway, Bockris and Linton (72).

If at some temperature one type of defect is the majority carrier, then the high frequency conductivity is determined by the majority carrier and the static conductivity is governed by the less effective carrier, that is the one whose product of concentration times mobility is much less.

To explain the static conductivity, motion of both ionic and orientational defects must be considered. If a single type of defect moves along a chain of bonds, the chain becomes polarized so that it is impossible for another defect of the same type to transverse in the same direction, as shown in Figure 14. The passage of a defect of the opposite type will reset the chain and is necessary for sustained current, Figure 15 (58). The total charge transported is the proton charge and is divided between the types of defects necessary for its transduction. The effective charges are

$$e_{+} + e_{DL} = e , \quad e_{+} = 0.62e ,$$

as given by Hubmann (73) who reviewed and commented on Jaccard's theory in a 1979 paper. From studies of pure and acid doped ice, the majority carrier in pure ice at 263 K was determined to be the orientational defects (6). Below 200 K both positive ion and Bjerrum defects were comparably effective in proton transport in the samples of Collier, Ritzhaupt and Devlin (59).

Spectroscopic Studies of Proton Transport

As mentioned before Devlin and coworkers developed the technique for isolating D_2O in H_2O thin-layer ice samples for infrared studies at 130 K, and they definitively assigned the spectra of the isotopomers of H_2O isolated in H_2O ice(4,42,43). Upon warming such a sample to

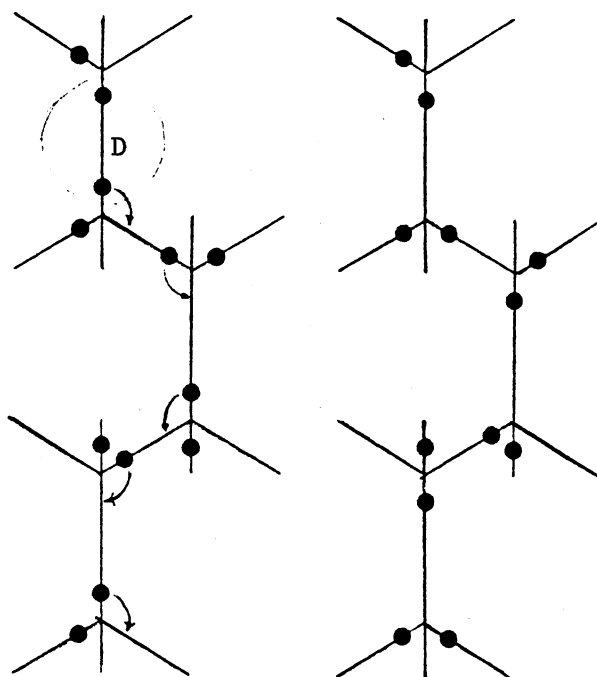


Figure 14. Blocking of a chain parallel to the c -axis by a D-defect. While the protons shift according to the arrows, the D-defect moves downward. The chain then offers no possibility of downward motion to another D-defect.

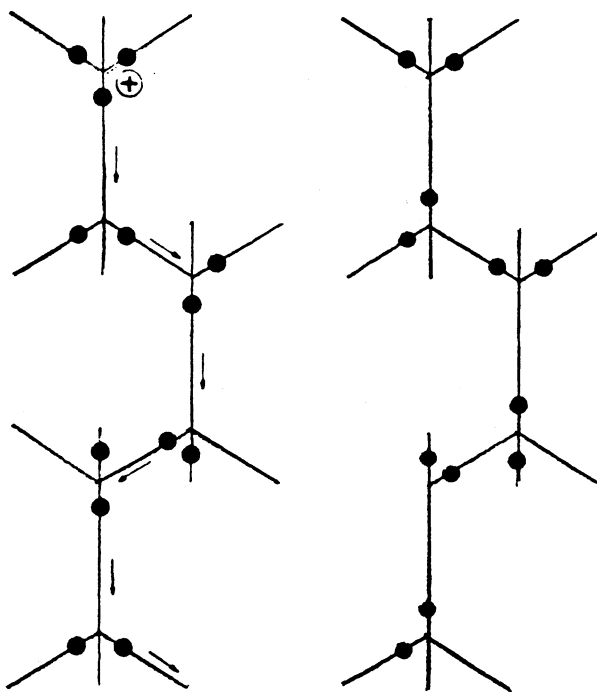
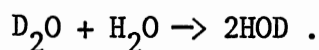


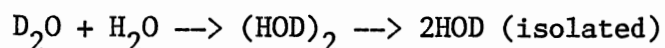
Figure 15. Reactivation of a blocked chain by a positive ion. The shifting protons move the ion downward, and this brings the chain back to its original state, as it was in the figure above.

165–180 K the D_2O bands at 2444 cm^{-1} and 2367 cm^{-1} lost intensity and the isolated HOD band at 2418 cm^{-1} gained intensity. This was due to the thermal proton–deuteron scrambling reaction:



By sampling the spectra at several time intervals and subtractively separating the spectra into its D_2O and HOD components, the rate of exchange could be followed at a particular temperature. Over the temperature range of 165 to 181 K the activation energy was found to be 9.3 kcal/mole (4), close to half the formation energy of a pair of ionic defects (17.6 ± 1.3 kcal/mole) found by Bullemer et al. (74).

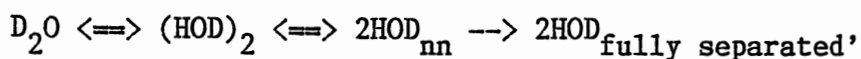
The samples mentioned above were, however, made in a cell that had small quantities of aromatic bases from an earlier pursuit adsorbed on its walls, which impurity molecules slowly desorbed and contaminated the ice with deep traps for thermally generated protons (5). As the contaminate slowly cleared equivalent amounts of exchange per minute occurred at lower temperatures. After a time the rates did become constant and reproducible. The temperature range where exchange in "pure" ice I_c could (and still can) be followed is 135–160 K. At these lower temperatures the peaks now attributed to $(HOD)_2$ became apparent (the absorbance of $(HOD)_2$ was discussed before and shown in Figure 8). The exchange reaction:



can account for the 135–160 K data and the earlier doped 165–181 K data if the second step was much faster at the higher temperature as expected for base-doped samples.

The first step was reasoned to be a proton transfer which would produce next-neighbor HOD molecules, $(HOD)_2$, from an isolated D_2O

molecule, but proton transfer alone cannot separate the deuterons by more than hydrogen-bonding distance from the initial oxygen to which they were attached. In the second step a Bjerrum defect migrates through the site, rotating the molecules and further separating the two deuteriums. Figure 16 illustrates the two steps. The first structure contains an isolated D_2O unit, the deuterons of which cannot be separated by rotating the molecule but only by the migration of a plus ion defect through the D_2O site, resulting in $(HOD)_2$ as shown in the middle structure. Further proton transfer cannot place another oxygen between the deuterons but the passage of a Bjerrum L-defect will, as shown. The deuterons in the resulting third structure can now be further separated by successive transfer and turning-steps. Collier, Ritzhaupt and Devlin (59) reported the detailed study of the thermal reaction with an analysis based on the two step process above. The rates were fit to the differential equations describing the process:



where $2HOD_{nn}$ refers to $(HOD)_2$ uncoupled by the passage of an L-defect but not yet affected by another proton transfer step. The rate constants for the first step relate to proton transfer and the rate constants for the second step are related to the turning step. The ion-pair defects and the Bjerrum orientational defects were found to be comparatively mobile in cubic ice at temperatures around 150 K. From the analysis they obtained an activation energy of 9.5 kcal/mole for the proton transfer step and 12 kcal/mole for the rotational step.

In this work the effects of proton hopping in the absence of orientational L-defect mobility will be studied. Below 130 K extensive proton hopping in an H_2O crystal which initially contains isolated

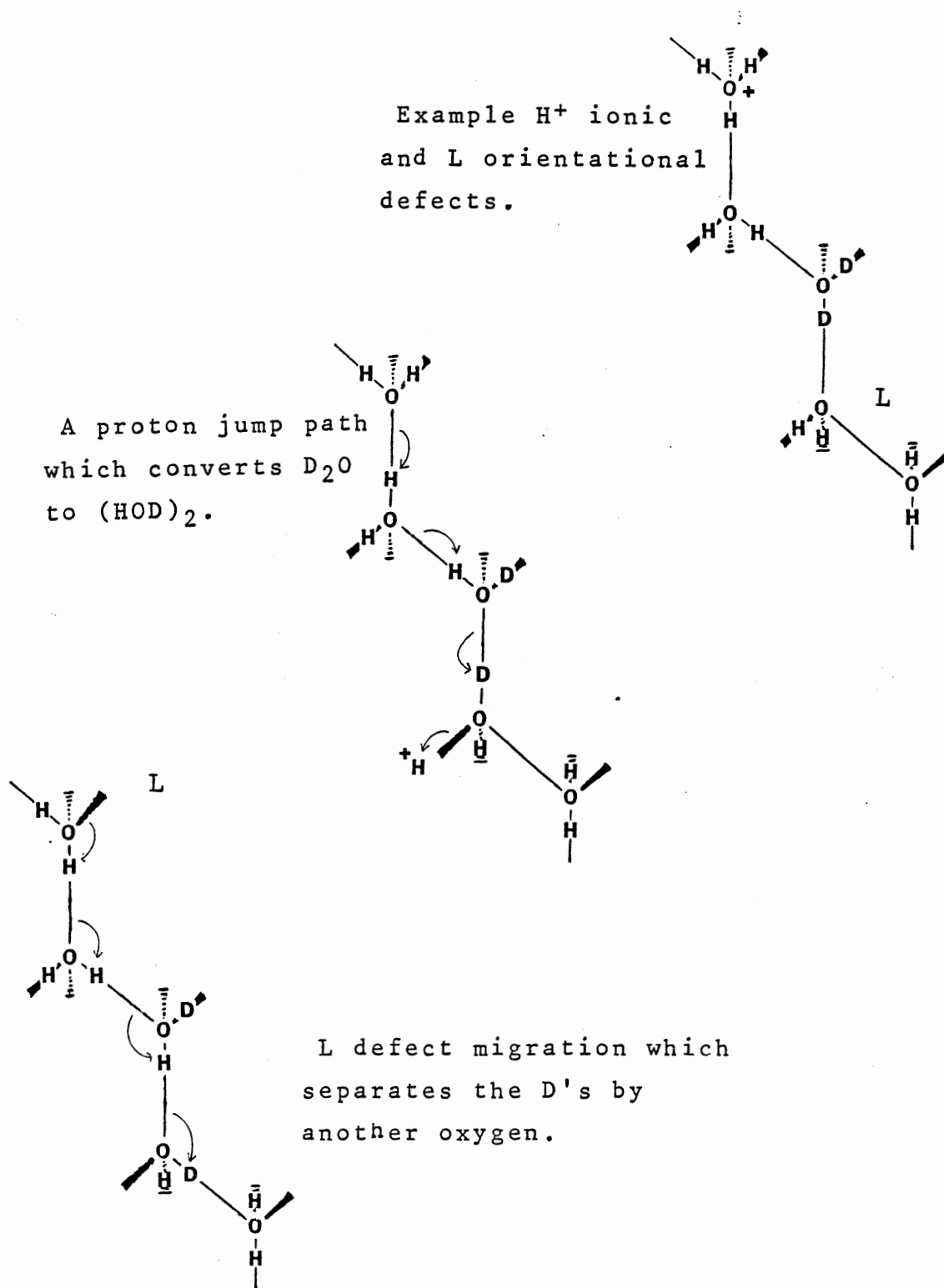


Figure 16. Point defects and proton conduction.

D_2O molecules will lead only to $(HOD)_2$ and D_2O existing in an pseudo-equilibrium. From statistical considerations the $(HOD)_2:D_2O$ ratio should tend to 4:1. In untreated pure ice below 130 K the mobile proton concentration is effectively zero, but at these low temperatures mobile protons may be generated by other than thermal means. If protons are liberated at temperatures below 110 K they quickly become associated with shallow traps.

The Shallow Trapping of Mobile Protons

The bulk properties of ice such as the electrical and mechanical relaxations are usually interpreted in terms of theories considering the motion of noninteracting equilibrium concentrations of ionic and orientational defects. However the equilibrium concentrations of positive ion defects have been shown to be affected by shallow traps, both at relatively high temperatures (75) and at low temperatures (76).

Kunst and Warman (75) observed the microwave conductivity jump and decay rates of ice samples subjected to ionizing pulsed-electron beam radiolysis at 230 K to near the melting temperature. Their model for the decay kinetics of localized solvated electrons involved the presence of a pseudo-equilibrium between mobile protons and protons immobilized by association with shallow traps. They believed these shallow traps to be the orientational Bjerrum L-defects.

Devlin and Richardson (76) subjected samples of cubic ice containing isolated D_2O molecules to a 1.7 MeV electron beam at 90 K. The spectra indicated proton-deuteron scrambling progressed at 90 K but ceased when the irradiation was stopped, as shown in Figure 17. Subsequent warming to 120 K resulted in rapid (minutes) conversion of

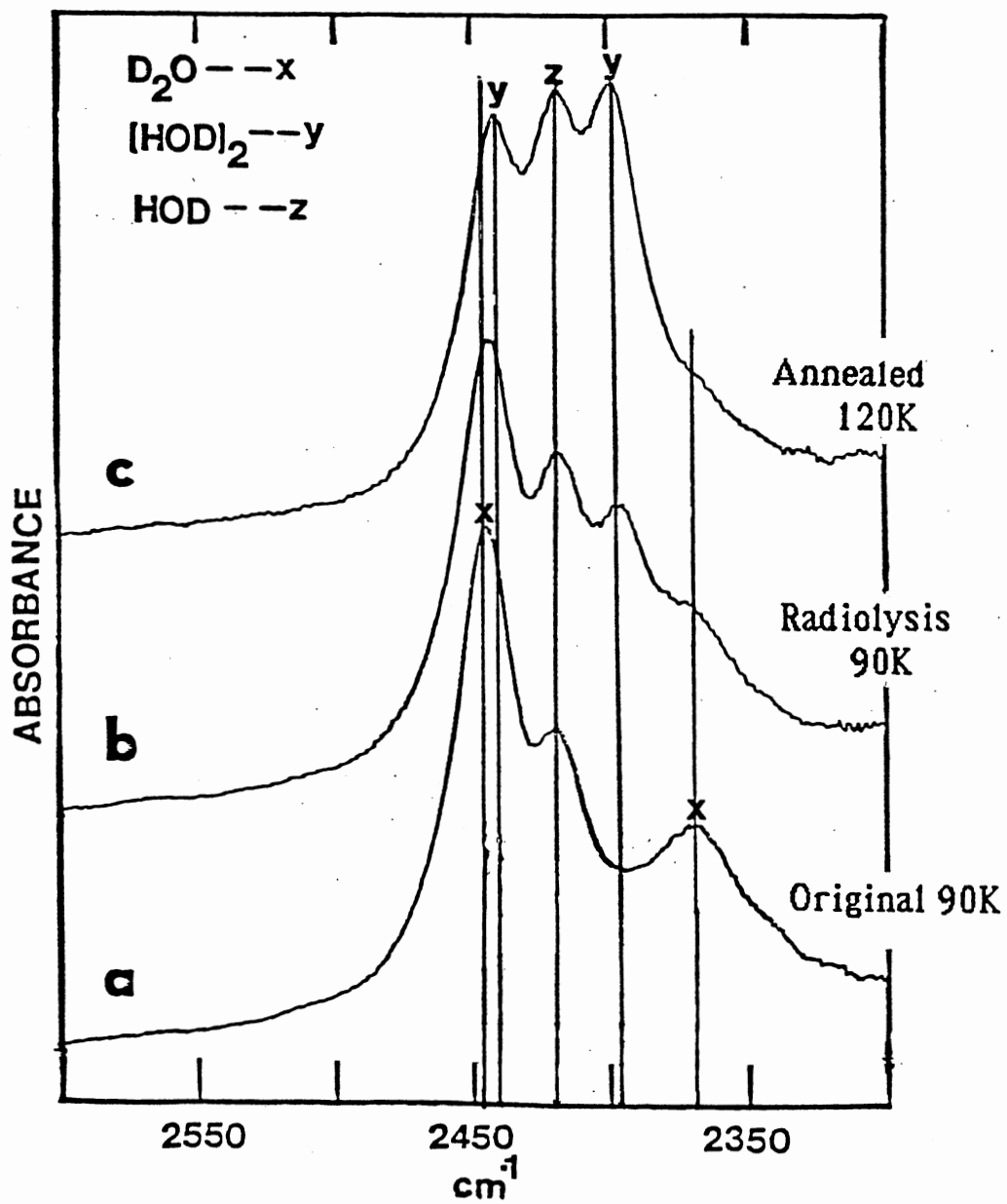


Figure 17. 1.7 MeV irradiated ice.

D_2O to the spectroscopically unique neighbor-coupled HOD molecules, $(HOD)_2$. At 120 K the thermal generation of mobile protons would be insufficient to cause comparable conversion of the D_2O even after several months. Therefore the scrambling at 120 K must have been due to mobile protons which were generated during the 90 K radiolysis, rapidly immobilized by shallow traps, and, finally, thermally liberated at 125 K. The inclusion of the organic base, 7-azaindole, in the ice reduced the effects of the irradiation by at least an order of magnitude. 7-Azaindole had previously been employed as a deep proton trap in ice by Collier, Ritzhaupt and Devlin (59).

Electron beam radiolysis is, however, rough treatment as prolonged exposure may ultimately convert crystalline ice to amorphous ice. The intermediate doses used may possibly have generated many vacancies, interstitials, grain boundaries and other defects. The possibility of these other defects suggest applying caution to the interpretation of the electron beam radiolysis data. There is a need to ensure that the trapping is an intrinsic property of ice, one that would have considerable consequences for the analysis of the kinetic and thermal properties of ion defects in ice.

There are a number of conceivable ways to introduce mobile protons into ice at low temperatures. One would be again to ionize ice itself, using photons rather than electron beams, and with lower energies to reduce the possibility of crystal damage. The excitation of an OH stretching overtone in the near infrared may be sufficient to emulate a step of the thermal process of generation of ionic defects. The dissociative ionization of liquid water induced by single photon vibrational excitation has been pursued in some detail by Goodall and

coworkers. Knight, Goodall and Greenhow (77) provided a detailed account of the experimental apparatus and techniques used, providing substantial evidence for the single photon nature of the ionization and that steps were taken to account for sample heating effects. The quantum yields were measured as a function of laser wavelength in the vibrational overtone and combination range 7605 to 18140 cm^{-1} in a later study by Natzle, Moore, Goodall, Frisch and Holzwarth (78). They claimed that the pattern of the quantum yield correlated with the absorption spectrum, rising rapidly on the low frequency side of a band and remaining relatively constant throughout the peak and high frequency wing. Photoionization of ice with wavelengths ranging from near infrared to ultraviolet will be pursued here.

Another means of creating an enhanced proton concentration in ice is by doping the ice with an acid. Producing crystalline ice requires temperatures of 145 K or greater to nucleate on a clean surface and temperatures of at least 125 K to continue the growth epitaxially. Under these conditions the acid could easily outnumber the intrinsic trapping ability of pure ice at a temperature where the orientational defects are active enough to enable considerable scrambling of the D_2O and H_2O into HOD during the deposit, meaning the loss of the spectroscopic probe. Deposits of acid doped $\text{H}_2\text{O}/\text{D}_2\text{O}$ vapor do show an enhanced $(\text{HOD})_2$ concentration, but provide little information about the trapping process. The informative experiment would be to produce mobile protons in ice at a lower temperature than necessary for crystal formation.

Mobile protons may also be introduced by doping with a "delayed" acid. That is by doping with a neutral compound that can be triggered

into becoming acidic after the crystal has been produced and the temperature lowered. 1- and 2-naphthols, o-nitrobenzaldehyde and 8-hydroxypyrene-1,3,6-trisulfonate are such compounds.

2-Naphthol has a phenolic OH whose pK_a changes from 9.5 to about 2.5 upon absorption of an ultraviolet photon (79). Ice doped with 2-naphthol will be studied.

An o-nitrobenzaldehyde molecule and a water molecule combine irreversibly to form o-nitrobenzoic acid under uv illumination. The photoconductivity of such doped ice crystals has been studied by Petrenko and coworkers (80). They noted an increase in both high and low frequency conductivities of the doped as compared to a pure ice sample. The spectroscopic study of similarly doped ice crystals containing isolated D_2O may provide interesting data. Petrenko also noted that no attempts to observe protonic photoconductivity in pure ice had generated enough charge carriers to be detected by electrical measuring apparatus.

The kinetics of proton diffusion in polycrystalline ice were studied by Pines and Huppert (81) using this pH jump method. Their dopant molecule was 8-hydroxypyrene-1,3,6-trisulfonate. In the first electronically excited singlet state the hydroxyl group is acidic and may form a hydrated proton as with the naphthols. The pH jump involved using intense short laser pulses to increase the proton concentration of a neutral or basic solution by several orders of magnitude. They did not measure the conductivity but rather the optical absorption of the HPTS molecule, whose absorption maxima is unique from its deprotonated form. The proton mobilities deduced were lower than those from conductivity experiments and well below those expected for supercooled

water at the same temperature.

Presentation of the Problem

The goal of this study is to employ the molecular level probe of proton transduction detailed by Collier, Ritzhaupt and Devlin in the study of ice irradiated at temperatures where the thermal processes cause no noticeable effects. The electron beam radiolysis work of Devlin and Richardson has shown that a concentration of shallow trapped protons is generated in ice at 90 K, and it was speculated that the traps were Bjerrum L-defects. The goal is to study the release of the protons from the traps, which can be populated by the photolysis of special dopant molecules or possibly by the photoionization of ice itself at energies lower than that of the electron beams and which can be followed spectroscopically, and to determine the activation energy for the process. The test of photoionization will involve irradiating ice films containing isolated D_2O with wavelengths ranging from the near infrared stretching overtone region to the ultraviolet region.

CHAPTER II

EXPERIMENTAL APPARATUS and PROCEDURES

The Apparatus

The problem of isolating D_2O in H_2O ice without extensive isotopic scrambling is quite similar to that of isolating reactive species in a matrix for study, hence the techniques used here were essentially the same as used in matrix isolation spectroscopy. The low temperature cell is based on an Air Products CSA-202 closed cycle helium cryogenic refrigerator which can cool its cold station down to about 12 K in about an hour. The refrigerator consists of a bulky helium compressor which is connected by hoses to a smaller expander module where high pressure helium expands, does "external" work, and cools the cold station. The two piece arrangement allows the expander to be carried from the vacuum rack to the FT-IR instrument.

The cell is diagramed in Figure 18. The expander unit may assume any orientation and has a copper block attached to the end of its cold station for mounting a cesium iodide window for infrared transmission studies. Indium wire gaskets provided good thermal contacts between the copper mount, the backing plate and the CsI substrate. The brass shroud could be rotated with the cell under vacuum to give a straight through path for the infrared beam. The temperature of the sample was measured by a thermocouple (chromel vs. gold with 0.07% atomic iron) in direct contact with the substrate where the sample was deposited. The actual

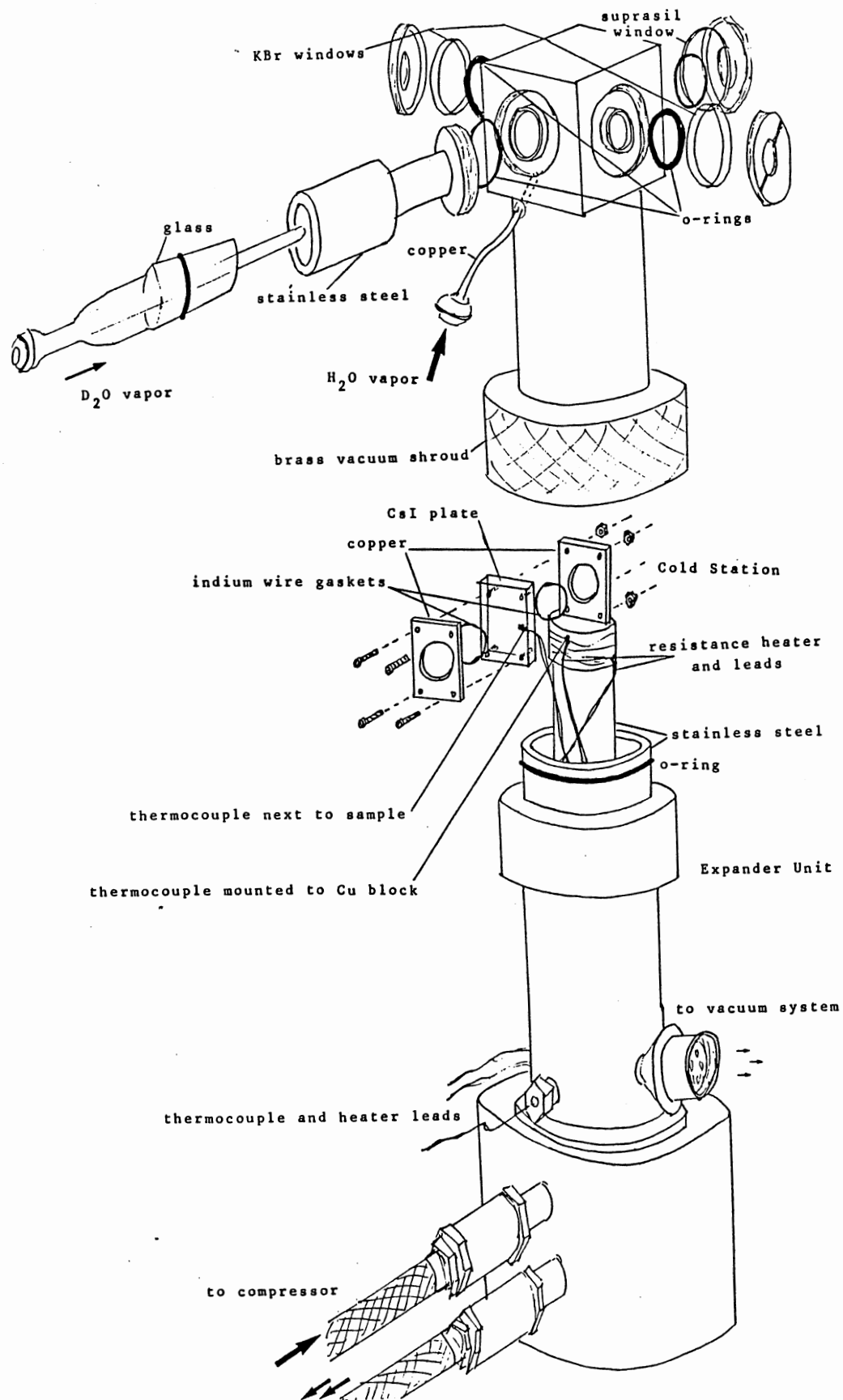


Figure 18. The cell.

readings were taken from a temperature vs. voltage table and a Honeywell 2745 potentiometer with built in manual reference junction compensator. The output of a second thermocouple was fed into an Air Products APD-B temperature controller which provided heat to the cold station via a small resistance heater. The controller kept the substrate temperature constant to within ± 1 K. No independent measurements were made as to the accuracy of the measured temperature but the measured infrared band positions, the crystallization temperature of the amorphous, and the sublimation temperature of ice in vacuum all corresponded well with values reported from other labs.

A single vacuum rack provided the vacuum necessary for the cold cell as well as facilities for handling (and mixing if necessary) gases with pressures ranging from 10^{-5} torr to atmospheric and also for controlling the flow rates into the cold cell. The vacuum system is shown in Figure 19. Rough vacuum was provided by a mechanical pump (Welch Duo-Seal model 1402) and working vacuum by further pumping with an oil diffusion pump to about 10^{-5} torr. Pressure was measured by three gauges: a capacitance type (Validyne model CD223, range--0 to 1000 torr), a thermocouple type (Hastings LV-1, range--0 to 100 millitorr), and a Bayard-Alpert ionization gauge (Veeco RG-1000, range-- 10^{-3} to 10^{-10} torr). The cell was connected to the vacuum system by glass tubes bent appropriately and having viton o-ring sealed ball and socket joints.

Supplies of liquid H_2O and D_2O were kept in small reservoirs mounted to the rack, from which the large bulbs could be easily filled with the vapors. The combination of vapor bulbs with needle valves provided very steady and repeatable streams of H_2O and D_2O .

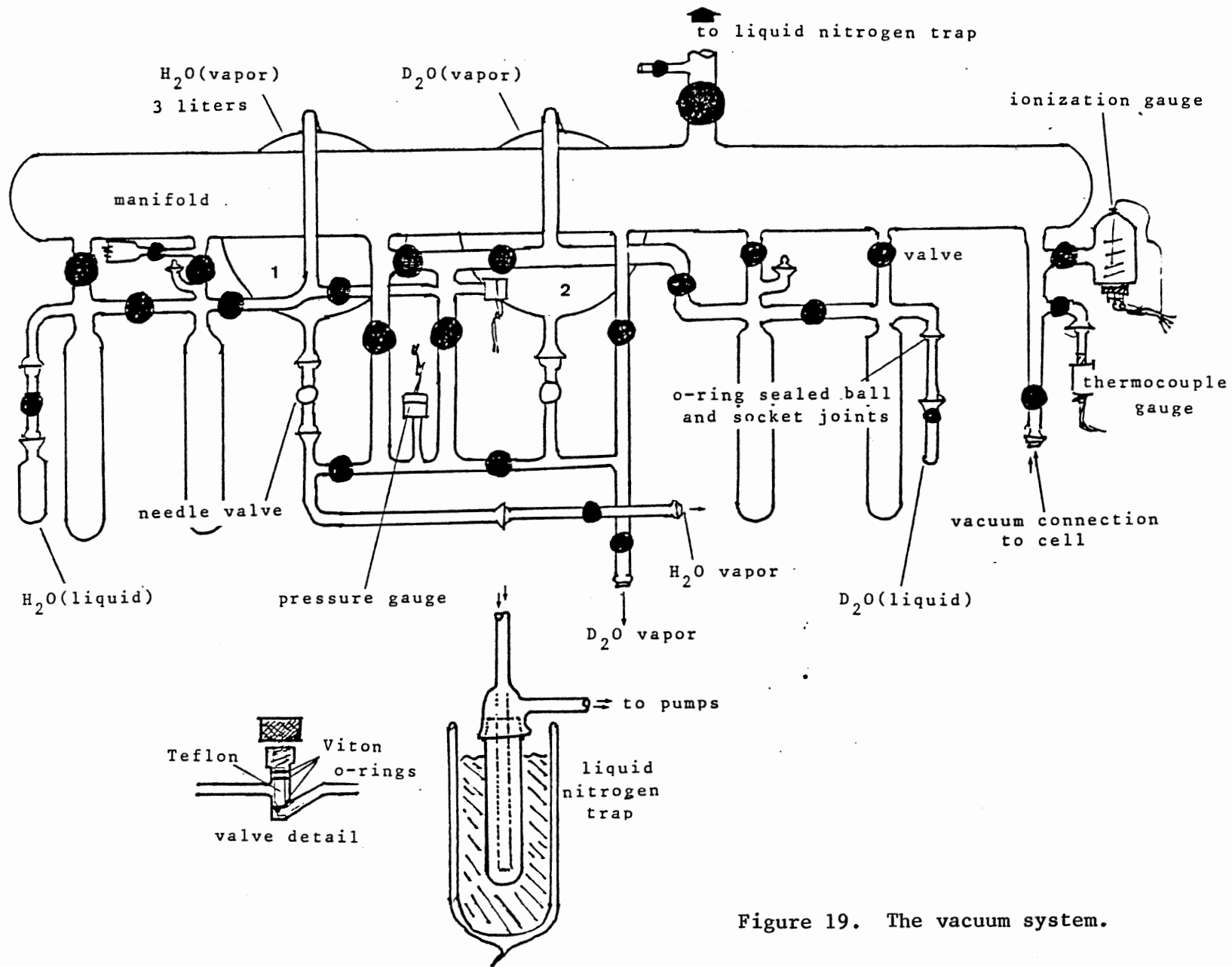


Figure 19. The vacuum system.

Cleanliness of the System

In the study of proton transduction in ice, very minute concentrations of impurities may cause drastic changes in the measured properties as evidenced by the vastly different electrical data from ice samples prepared in different labs or even consecutive samples in the same lab. The water used here was multiply distilled and the D_2O was used as purchased; both were degassed under vacuum by several freeze-thaw cycles. Water obtained from different labs gave the same results.

Perhaps more important than the initial purity of the water is the cleanliness of the vacuum system and especially the cold cell. The vacuum system was constructed as to be nearly grease free—once past the liquid nitrogen trap only teflon valves were used rather than the ground glass type which requires grease. The vacuum system was kept at less than 10^{-4} torr at essentially all times, sometimes going for months without being opened to the atmosphere.

The metal cold cell presented problems as to impurities. The helium expander and sample mount necessarily have a large metal surface area which may provide a sink for many sorbable contaminants. Also the cell has relatively large o-rings which were lubricated by either Apiezon (hydrocarbon based) or Dow high vacuum silicone grease for sealing and because the vacuum shroud needed to be rotated between the deposition and taking spectra. No difference in sample behavior was noted when the different greases were used.

Because such small amounts of impurities can sharply alter the rates, it was questioned whether the rates claimed for pure ice were

correct or were significantly off due to impurities. The long term behavior of the system following acid or base doped samples support the correctness of the rates. After a base doped sample the next sample may contain some base molecules which had adsorbed onto the cell walls and the next sample should have less and so on. The suppressed exchange rates indicate this behaviour. Following an acid sample the next would have enhanced rates and the next would have less enhanced rates. (The system being kept under vacuum all the while.) Eventually the rates settle on a constant value which is the same regardless of whether the system has been subjected to base or acid, or has been uncontaminated for an extended time. Additionally, when the system appears to be base contaminated a very slight amount of acid doping does not enhance the rates; but a sample made with more acid doping begins to show enhancement. Base doping of an acid contaminated system was not examined.

Sample Preparation

For a typical sample, the cell and its connecting lines would be put in place and evacuated at least overnight. System pressure during sample preparation was usually about 2×10^{-5} torr. A few hours before a run the liquid nitrogen trap would be filled. With the substrate cooled to about 170 K, a small burst of H_2O is sprayed onto the plate to form a thin layer of crystalline ice onto which the main sample is to be grown epitaxially. The salt plate is then cooled to 125–130 K and the needle valves set for the desired H_2O and D_2O flow rates for typically 20 minutes to build up a sample thickness of 5 to 10 microns. The thickness of a sample can be estimated by comparing the measured

absorbance intensity of the ice bands to those reported by Bertie, Labbe and Whalley (36). From their absorptivity curve (Figure 5), the absorptivity of ice at 850 cm^{-1} is approximately $10^{3.25}\text{ cm}^{-1}$. Accordingly, a typical sample from this study with an absorbance of 1.2 for the 850 cm^{-1} band should have a thickness of about $1.2/10^{3.5}\text{ cm}$ or 7 microns. This compares well with an extrapolation of the rate of formation of about the first ten interference fringes to the full deposition time. (For example, a red interference fringe is visible when the thickness of the ice is a multiple of one-half the wavelength so that approximately 3 red fringes appear as the sample grows by one micron. The fringes, however, are no longer visible after the first few microns, perhaps due to slightly uneven growth of the sample.) That the crystalline samples grow epitaxially at 125-130 K and not homogeneously was proven by deliberately depositing a layer of amorphous ice at 90 K and then warming to 130 K for an otherwise typical sample deposition. The resulting sample had the spectral properties of amorphous ice (from the positions and shapes of the spectral bands it is obvious whether a sample is crystalline). Also of note is that when contaminants were present it was difficult to grow samples epitaxially, i.e., at 130 K amorphous ice would grow on a crystalline base layer.

Spectra

All samples were characterized by their infrared spectra, taken on a DigiLab FTS-20C Fourier Transform-Infrared Spectrometer (FT-IR). This is a single beam instrument which collects digitized interferograms from a Michelson interferometer and Fourier transforms the data into the frequency domain infrared spectrum. Many interferograms can be

collected and averaged before the transform to obtain better signal to noise. Actual background corrected transmission or absorbance plots are made by ratioing the single beam sample spectrum to a reference spectrum of the cell containing no sample, which was taken at a different time. The cell was suspended in the beam path of the FT-IR spectrometer so that the interferometer was isolated from the vibrations of the cryogenic refrigerator. The spectra were taken in transmission configuration and plotted as absorbance, $\log_{10}(I_{\text{reference}}/I_{\text{sample}})$, so that spectral subtractions could be performed. The FT-IR operational parameters were typically set for triangular apodization, zero gain-ranging, normal sensitivity, real Fourier transform, double precision computation, the normal undersampling ratio and zero filling, and for spectral resolution of 2 cm^{-1} (one output point per wavenumber). Reference spectra were computed from the average of 200 scans, and 20 scans were typically collected for a sample spectrum. With this spectrometer 20 scans at 2 cm^{-1} resolution takes almost one minute to collect and about four minutes to compute. The instrument can perform interactive graphic manipulation of spectra, especially including the subtraction of one spectrum from another using user entered coefficients which the machine can continuously increment or decrement while displaying the results. More complicated procedures can be programmed in FORTRAN IV, which has access to the spectral data files.

Generation of Mobile Protons in Ice at Low Temperatures

As mentioned in Chapter I, the ionization of pure liquid water by laser pumping of the O-H stretching overtones has been demonstrated by

Goodall and co-workers (78), who watched the conductivity of water jump in response to laser shots. Considering their results, it seemed probable that laser ionization would also occur in ice as the ice overtone spectrum parallels that of liquid water, and also that it would be observable by the methods used in this study--by watching D_2O convert to coupled HOD in response to proton hopping. Here the effects are cumulative as longer irradiation should lead to more extensive conversion toward an ultimate $(HOD)_2:D_2O$ pseudoequilibrium ratio of 4:1.

Samples were deposited at 125-130 K and then cooled to 90 K for laser irradiation. The samples were irradiated by directing the laser beam into the cell through the suprasil window. A compromise between restricting the sample area for higher laser power and for increasing the sample area for better signal to noise with the FT-IR was made by installing an aluminum sheet with a 2 mm diameter aperture against the substrate. This was the approximate size of the argon ion laser beam and usable FT-IR spectra could be obtained with about 40 minutes of scanning.

The longest laser wavelength tried was the neodymium/YAG fundamental at about 1 micron, which was one of the same wavelengths used in the liquid water ionization. The results after four hours of irradiation (125 mW average power, similar to the liquid water work) however showed no indication at all that mobile protons had been generated at 90 K: spectra from before and after irradiation overlapped perfectly and there was also no change in the spectra after the sample had been held at 125 K overnight. 125 K is warm enough that trapped protons should have been released.

Samples were also subjected to visible wavelengths at higher power levels. The wavelengths included the 514.5 and 488.0 nm lines of an Argon ion laser (Laser Ionics model 556A) at 2 to 3 watts and also 700-620 nm using an Argon ion pumped dye laser (Spectra Physics model 375 using Rhodamine 6G, Rhodamine B and Exciton LDS698 dyes) at a few hundred milliwatts. Again the results showed no signs of proton motion when irradiated at 90 K or even at 120 K.

The shortest laser wavelength tried was 337 nm from a Molelectron UV-400 nitrogen laser at an estimated 50-100 mW. Three and one-half hours of irradiation caused no observable change in the sample.

The YAG laser experiment in particular should have given positive results; but, although Goodall and coworkers found single-photon dissociative-ionization quantum yields which correlated with the absorption spectrum of water, having a yield of about $10^{-6.2}$ at 1 micron, ice samples here gave no evidence for generation of mobile protons whatsoever. The average laser powers were comparable and also the absorption of liquid water and ice are nearly equal at 1 micron; therefore the experiments should be directly comparable. A possible hindrance to the comparison is that, although average power levels were similar, the peak power from the 5 picosecond pulsed YAG laser used here was much higher than the 10 ns YAG they used: the peak power may have exceeded the dielectric breakdown threshold for ice. If dielectric breakdown did occur it resulted in no mobile protons being liberated in the irradiated sample. Also only one ice sample was irradiated with the YAG laser.

Ultraviolet Irradiated Samples

Samples were deposited at 125–130 K and then cooled to 90 K and irradiated for two hours with a mercury resonance lamp with a quartz envelope. It was estimated that the power reaching the sample was ≤ 5 watts. The uv light passed a short distance through air as the surface of the lamp envelope was about 4 mm away from the cell's suprasil window. Low pressure mercury lamps are generally used for the 253.7 nm resonance line which is the major output of the lamps, but substantial amounts of the strong 184.9 nm line of mercury are also emitted (82). When the 184.9 nm line of the Hg lamp was to be eliminated a KBr window was substituted for the suprasil as KBr absorbs wavelengths shorter than 195 nm as shown in Figure 20 (83). The results of the irradiation of "pure" ice at 90 K are shown in Figure 21. With 184.9 nm blocked out and primarily 253.7 nm reaching the sample, no effects were noticed after irradiation at 90 K or when held at 125 K after irradiation, and the sample behaved as pure, unionized ice when later warmed to 145 K; but after irradiation through suprasil rather than through KBr, the 90 K spectra revealed a slight forward progress of the reaction: $D_2O \rightleftharpoons (HOD)_2$. At 125 K this reaction progressed slowly. When irradiated at 12 K the post-irradiated spectrum was identical to the pre-irradiated one, but the reaction progressed when warmed to around 125 K. The reaction of pure irradiated ice proceeded too slowly to study the temperature dependent kinetics on our laboratory time scale. (Actually the 184.9 nm line of the Hg lamp coincided with the tail of the ice absorption spectrum and it was supposed that shorter wavelengths would have had more extensive effects, but no lamp was available nor could the short wavelength radiation have been transmitted into the cell.) To

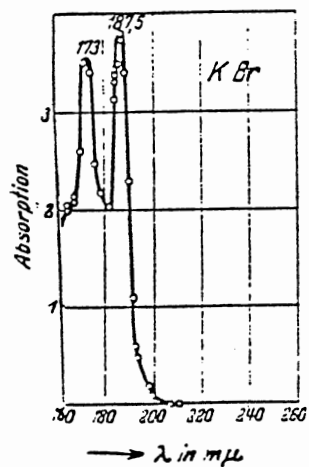


Fig. 20. Ultraviolet absorption of KBr (78).

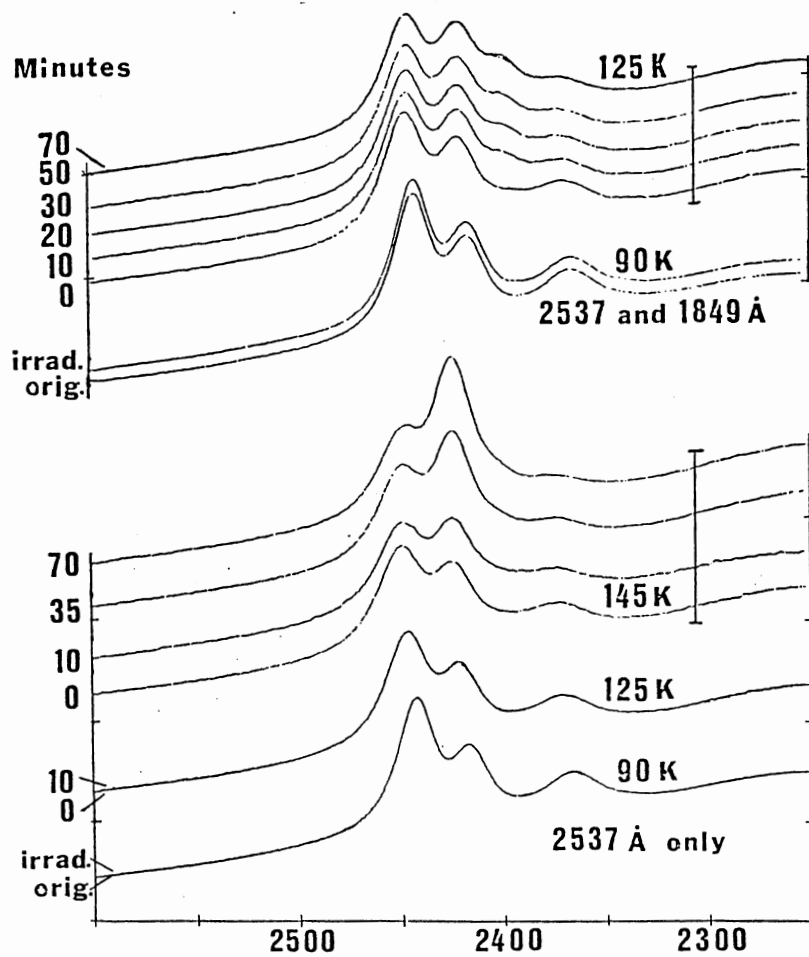


Fig. 21. Hg Lamp irradiated pure ice

characterize the kinetics of D_2O converting to $(HOD)_2$ caused by the release of mobile protons from traps, greater numbers of mobile protons needed to be generated at 90 K.

To generate excess mobile protons in ice at 90 K one dopant chosen was o-nitrobenzaldehyde (NBald) which photoisomerizes under mercury lamp illumination to become o-nitrobenzioc acid, which has a pH of 2.16 at 18 °C. Konstantinov et. al. (84) rapidly froze solutions of NBald containing pH buffers and indicators, and subjected them to mercury lamp irradiation at 77 K. The indicator did not change at 77 K, but irreversibly changed to acid color within a few seconds when warmed to 140-145 K. The conditions in most of those ice samples were probably different from pure ice in that most of the samples contained higher concentrations of NBald, buffers and indicators than would be soluble in ice, which would lead to clusters, aggregation along grain boundaries, and other inhomogeneities. Their results, however, were consistent using concentrations down to 10^{-5} M.

Petrenko, Ebimma and Maeno measured the electrical properties of ice containing 6.6×10^{-3} M NBald (80). After irradiation with a Xenon lamp at -10 °C or -25 °C, they found that both the conductivity and the capacitance of the sample had increased significantly, indicating that the mobile proton concentration had been increased.

In this lab NBald doped samples were prepared by placing a few small crystals (from Aldrich) along the H_2O vapor flow path and then preparing samples as described previously. Two crystalline samples were made containing NBald. The first, which was very lightly doped, showed no noticeable sign of change at 90 K after 253.7 nm irradiation at 90 K, and very slight proton exchange when warmed to 125 K. The second sample

was made three days later and with more dopant. The results are shown in Figure 22. Again no change was seen immediately after the two hour 90 K uv irradiation, but upon warming to 130 K for 100 minutes the conversion of D_2O into $(HOD)_2$ had proceeded nearly to the pseudoequilibrium. Some conversion into HOD was also seen during that time at 130 K.

Pines and Huppert (81) produced excess protons in ice by laser excitation of 8-hydroxypyrene-1,3,6-trisulfonate (HPTS), which is acidic in its excited state. They measured the time decay of the HPTS anion absorption following its production by the laser pulse and they related the decay to the rate of the diffusion controlled back protonation reaction. From their data they estimated a value for the proton mobility at $-10^\circ C$ which falls within the lowest values obtained by conductivity measurements. However HPTS is a large molecule which may disturb the local ice structure. Smaller molecules which exhibit similar pH jumps include 1- and 2-naphthol.

Naphthol containing sample preparation and characterization was achieved in the same way as for NBAld containing samples. 1- and 2-naphthols were obtained locally and their infrared spectra compared to library entries for the compounds. Samples doped with 1-naphthol showed more proton exchange than pure ice and 2-naphthol doped samples showed even more, probably due to higher volatility. Figure 23 shows spectra from a 2-naphthol doped sample warmed to 126 K following 2 hours of uv irradiation at 90 K. With this doped ice the D_2O to coupled HOD reaction could be followed to its equilibrium within a day (Figure 24), where the amount of isolated HOD remained nearly the same throughout and the final $(HOD)_2:D_2O$ ratio approached 4:1. Several of these samples

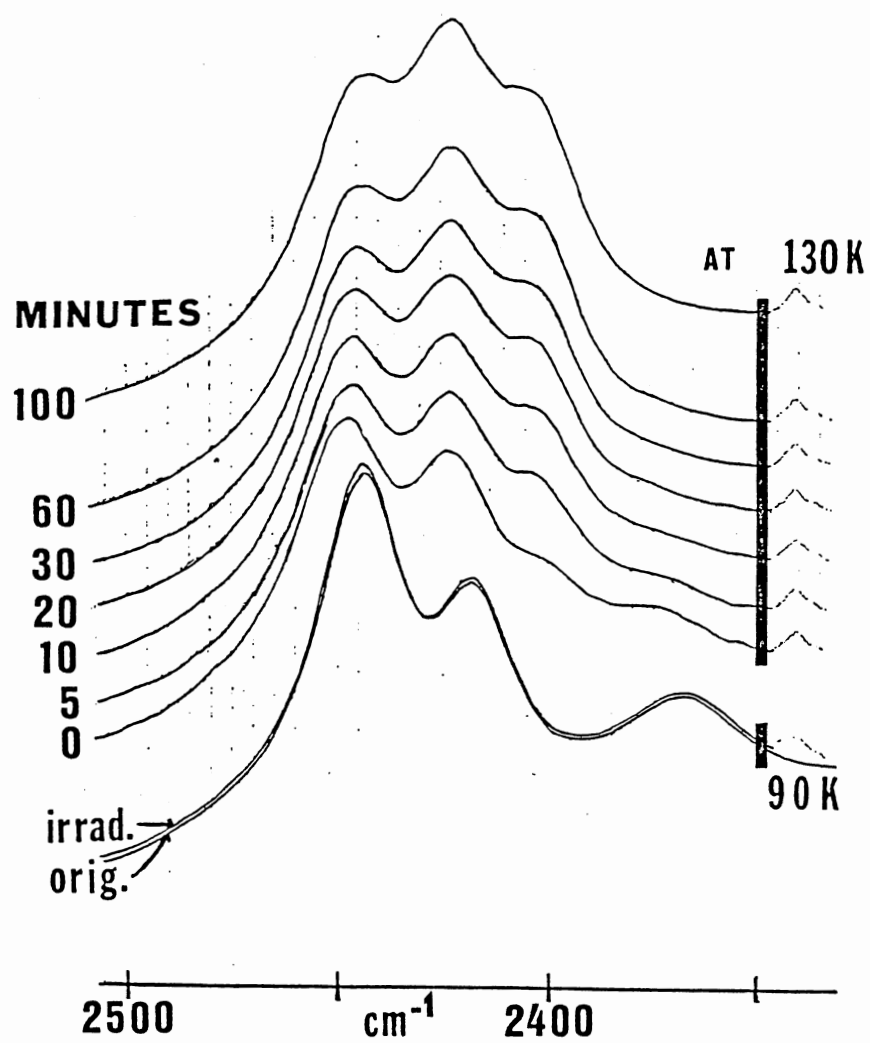


Figure 22. UV irradiated nitrobenzaldehyde doped ice.

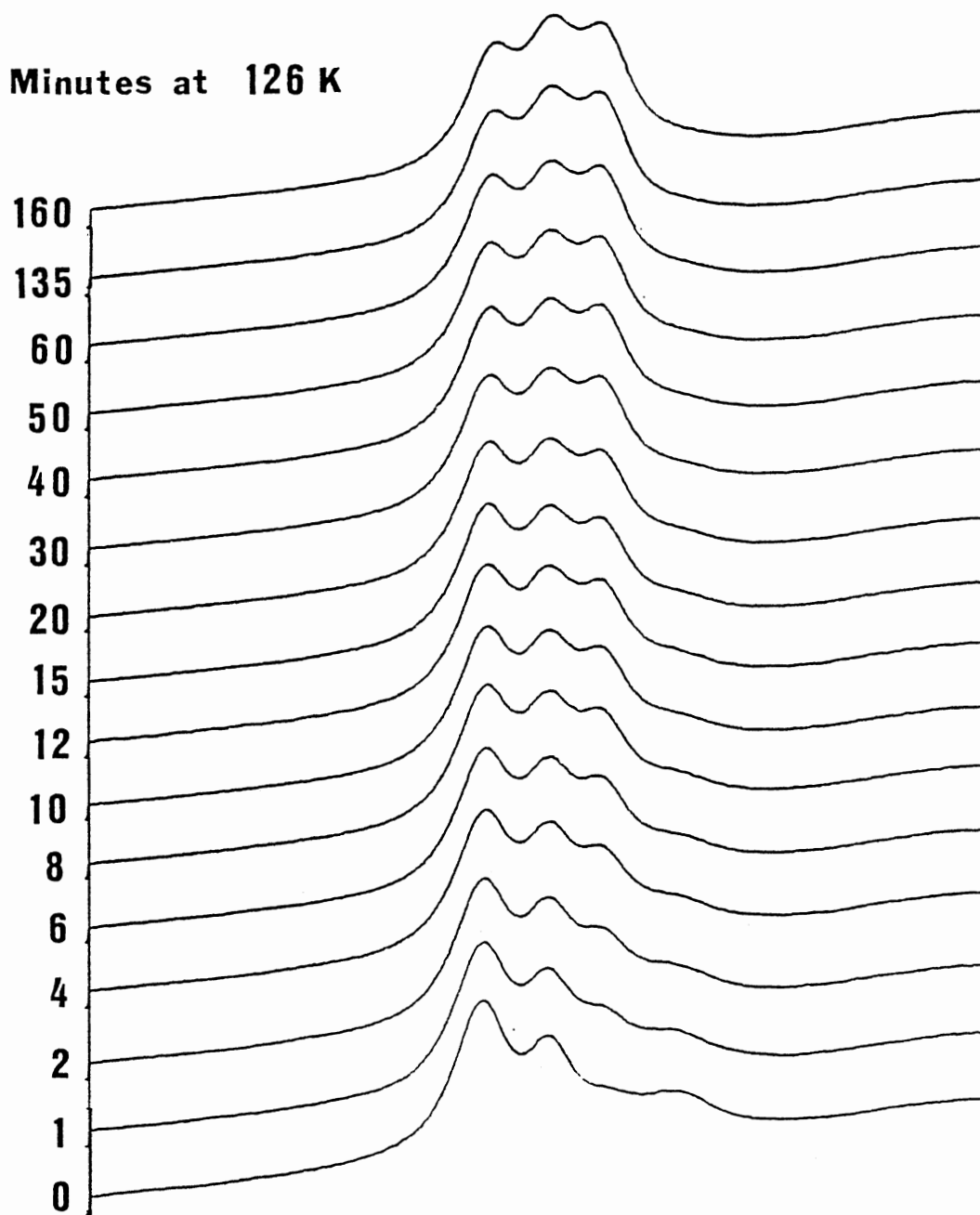


Figure 23. UV-irradiated 2-naphthol doped ice at 126 K.

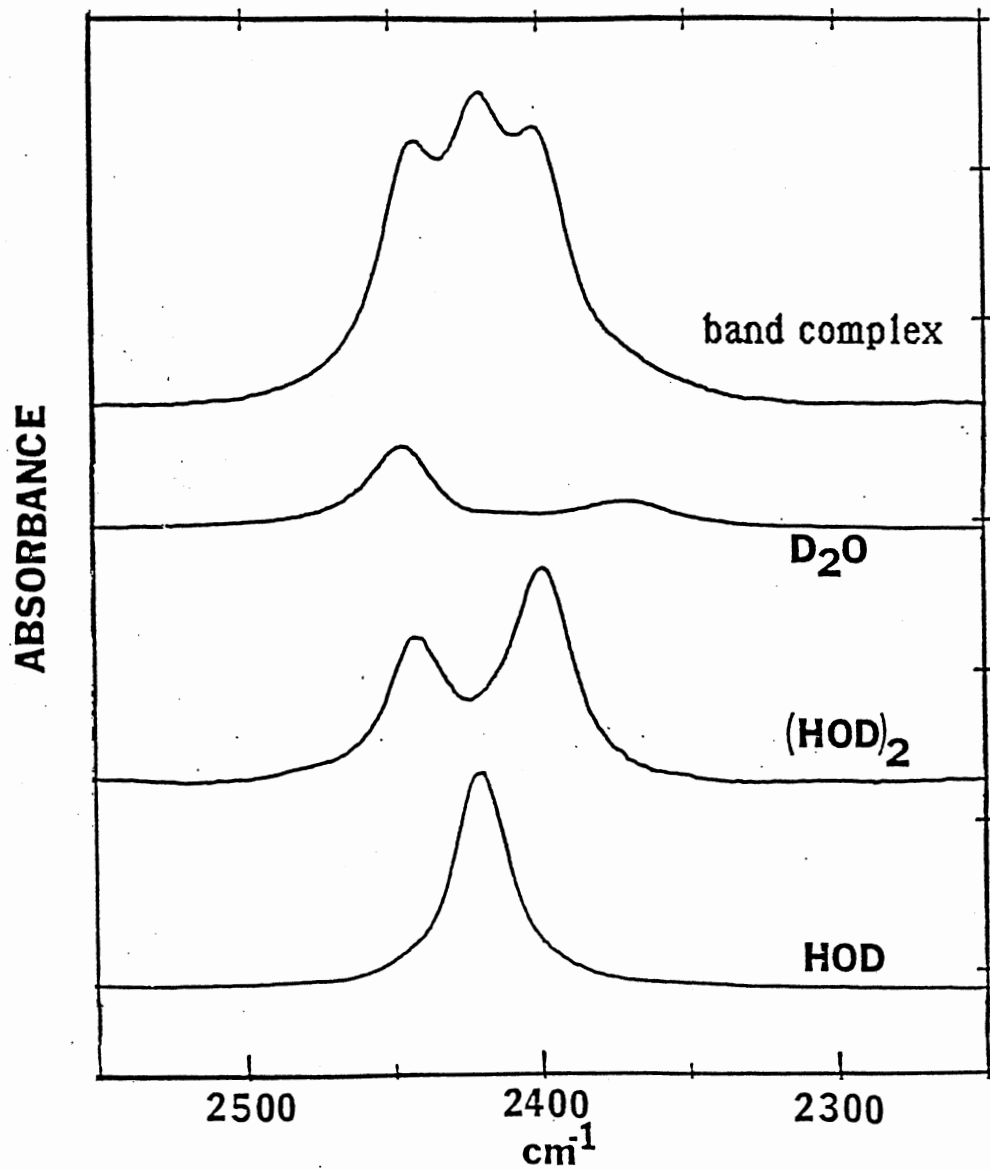


Figure 24. $D_2O \leftrightarrow (HOD)_2$ equilibrium system (115 K).

were prepared and the kinetics of the D_2O to coupled-HOD reaction were observed from 110 to 130 K.

Having samples with the major deuterated species being $(HOD)_2$ provided an opportunity to take another, perhaps more accurate, look at the second step of the thermal scrambling reaction in which coupled HOD pairs have their deuterons separated by the passage of L-defects. Figure 25 shows spectra taken after warming an irradiated sample from 126 K to 145 K, illustrating the kinetics of the turning step.

Spectral Stripping

The raw data are the FT-IR spectra of D_2O isolated in H_2O ices taken at various stages during the isotopic scrambling of the D_2O into $(HOD)_2$ and finally into HOD. The deuterated species each have different spectra, but the application of Beer's law to determine concentration changes was complicated by the overlap of the component spectra. The usual methods of determining concentrations require that the spectra of the pure components be available, but in the present case only spectra for the fully scrambled HOD is available. By using the subtraction capabilities of the FT-IR data system the contributions of the other two pure components can be deduced with little error.

Figure 26 illustrates the derivation of the spectrum for just D_2O at a particular temperature. The procedure begins with the subtraction of the background 2250 cm^{-1} H_2O ice band (from a sample containing no deuterium). A spectrum representing pure isolated HOD was obtained by subtracting the H_2O ice background from a fully scrambled sample (D_2O and $(HOD)_2$ are negligible compared to isolated HOD at the dilution used). A pure D_2O spectrum could then be obtained by

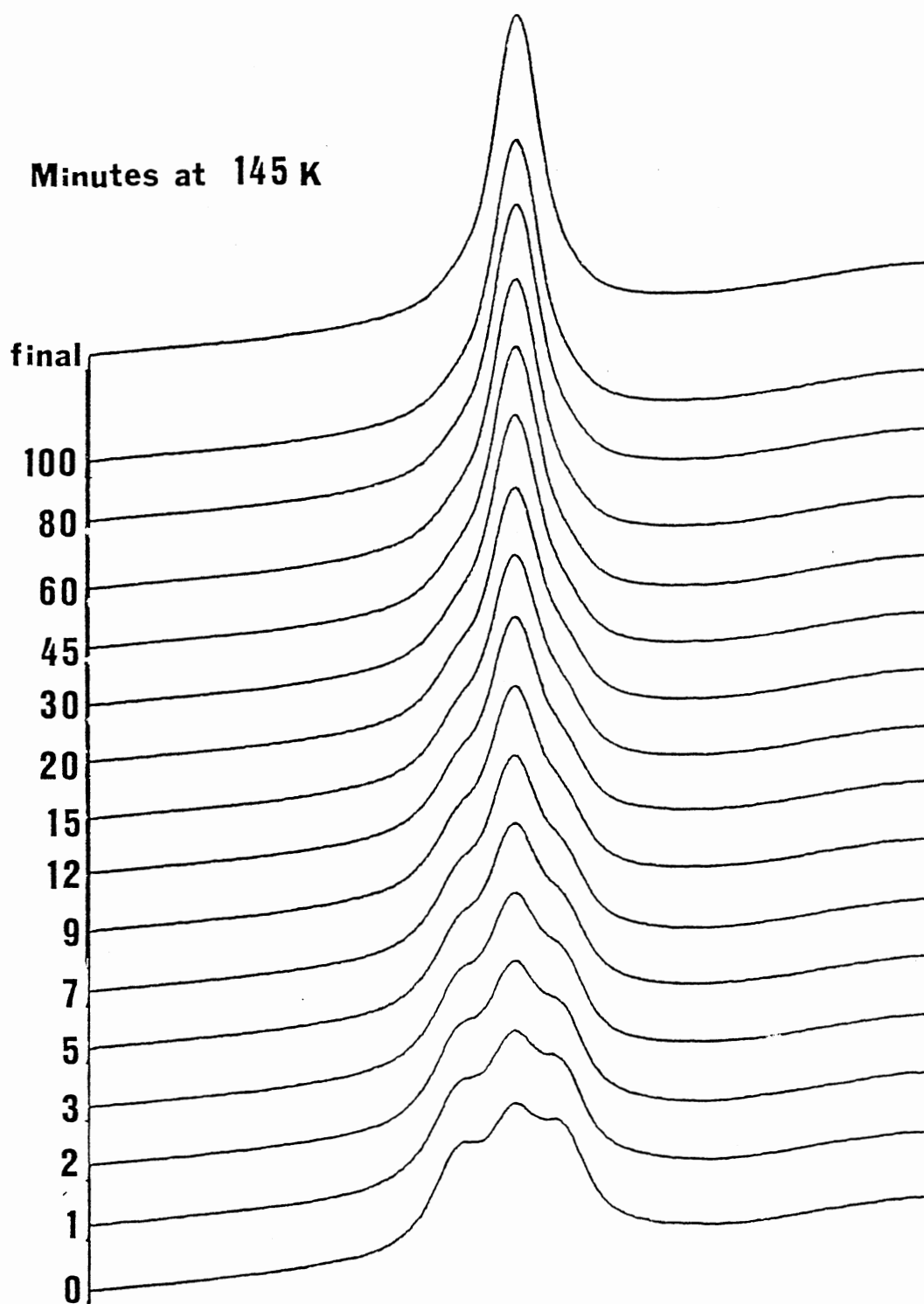


Figure 25. UV-irradiated 2-naphthol doped ice at 145 K.

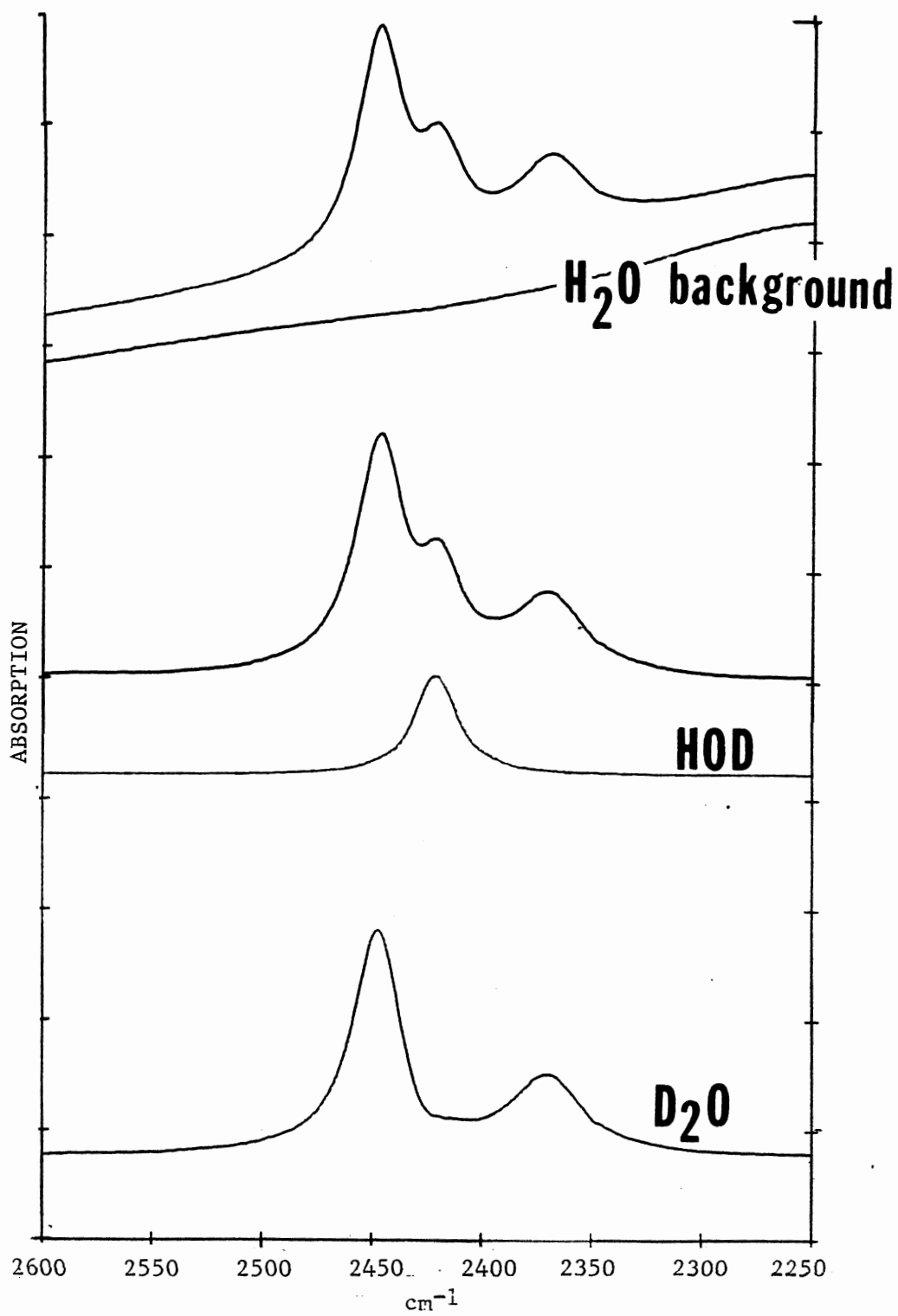


Figure 26. Derivation of a D_2O spectrum.

subtracting both ice background and HOD spectra from an initial spectrum of a fresh deposit because D_2O and HOD, but no noticeable amounts of $(HOD)_2$, are present. Finally pure $(HOD)_2$ spectra were obtained by subtracting ice, D_2O and HOD spectra from $(HOD)_2$ rich spectra taken during the course of the reaction. The stripping of one of the 126 K spectra from Figure 23 is shown in Figure 27. Analysis of $(HOD)_2$ rich samples resulted in superior spectra for that component. Subtraction scaling coefficients were chosen for the best visual result, seeking to completely remove the subtrahend peaks without leaving dips in the minuend spectrum.

This separation into components needed to be done at each reaction temperature because the bandwidths and positions were slightly temperature dependent (the dependence of the HOD peak position was shown in Figure 6). As the warming was not instantaneous, above 140 K initial spectra of undoped samples would contain some $(HOD)_2$, but pure D_2O spectra were available from earlier base-doped samples which did not react until higher temperatures (39).

Finally, the pure D_2O , $(HOD)_2$ and HOD spectra (such as those in Figure 8) were least-squares fit to each spectrum in a reaction series. Subtraction coefficients were output by a least-squares spectral fitting program (85) with the peak absorbance of each component being the coefficient times the peak height of the pure spectrum. The results of the decompositions of the spectra of the low and higher temperature samples are given in Tables I and II. The percent absorbances needed to be converted into concentrations for use in the kinetic data treatment.

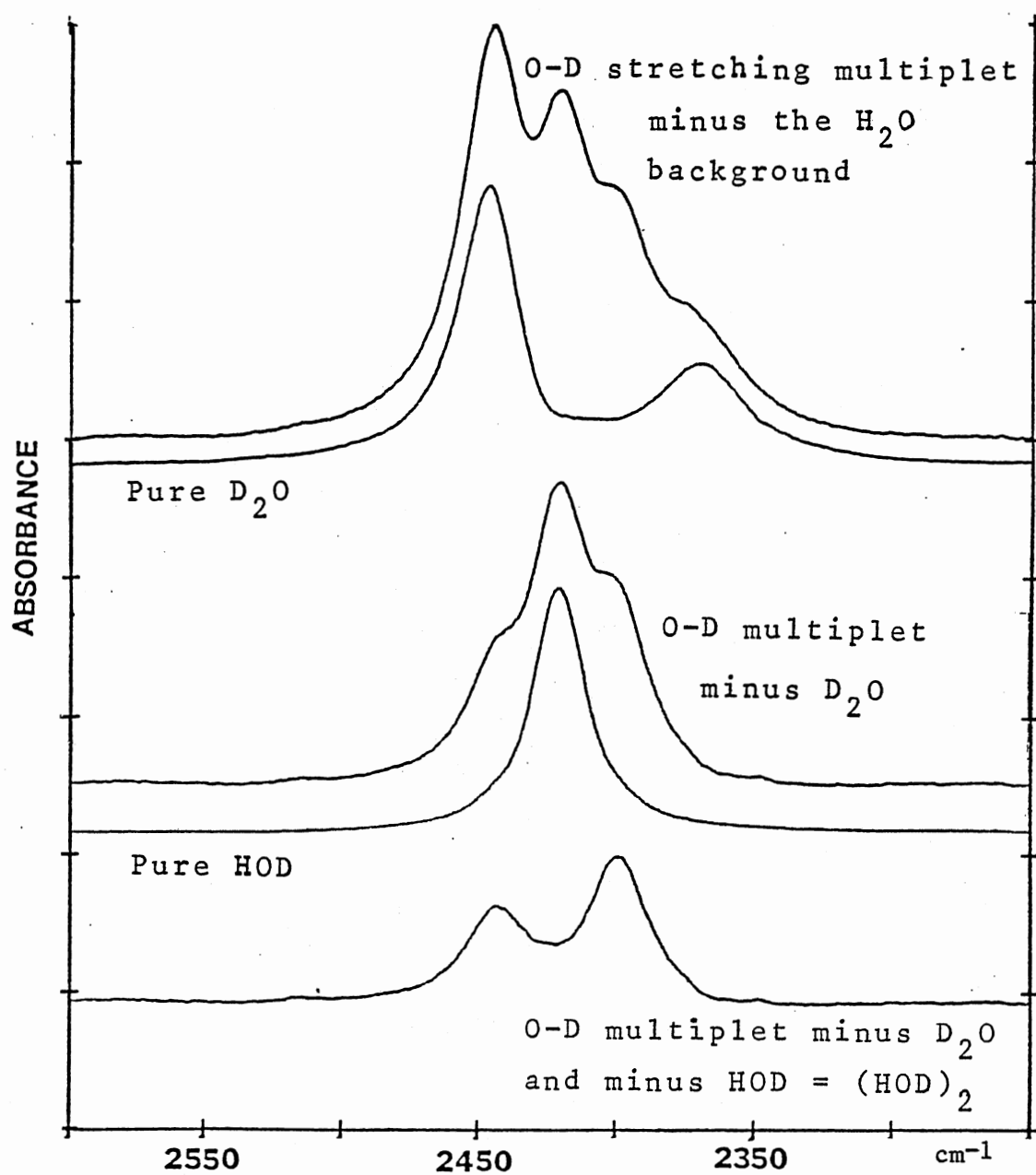


Figure 27. Typical decomposition of the O-D stretching multiplet.

TABLE I
110-130 K Data

Temperature = 110 K Date: 2/8/85

Minutes	%Absorbance of Strongest Peak		
	D ₂ O	(HOD) ₂	HOD
orig.	30.03	0.00	18.85
0	24.00	5.81	18.59
6	23.42	6.48	18.41
20	25.12	5.99	19.47
33	24.83	6.39	19.54
+ 5 more hours uv at 110 K			
20	13.32	8.10	20.17
880	11.15	20.42	20.94

H₂O 2250 cm⁻¹ peak = 20%

Temperature = 113 K Date: 1/28/85

Minutes	%Absorbance of Strongest Peak		
	D ₂ O	(HOD) ₂	HOD
0	29.61	4.34	15.68
6	28.98	4.93	15.58
18	28.61	5.46	15.66
50	27.71	6.63	15.40
72	27.26	6.98	15.56
90	26.87	7.36	15.57
110	26.58	7.84	15.31
130	25.96	8.02	15.70
150	25.92	8.36	15.41
180	25.44	8.75	15.39
205	25.11	8.95	15.42
1080	22.28	12.45	15.48

H₂O 2250 cm⁻¹ peak = 24%

Table I (Continued)

Temperature = 115 K Date: 2/11/85

Minutes	%Absorbance of Strongest Peak		
	D ₂ O	(HOD) ₂	HOD
orig.	33.72	0.00	16.36
0	29.96	2.96	15.67
5	29.91	3.83	15.68
15	28.50	5.34	15.47
25	27.98	5.86	15.70
40	27.00	6.90	15.39
60	25.81	7.92	15.51
90	24.89	8.83	15.65
125	23.78	9.69	15.80
160	22.87	10.71	15.10
1110	16.52	16.36	15.41

$$\text{H}_2\text{O } 2250 \text{ cm}^{-1} \text{ peak} = 22.4\%$$

Temperature = 117 K Date: 2/26/85

Minutes	%Absorbance of Strongest Peak		
	D ₂ O	(HOD) ₂	HOD
orig.	32.48	0.00	14.14
0	30.81	2.62	14.20
2	29.66	3.83	14.23
4	28.89	4.79	14.25
6	28.20	5.57	14.25
8	27.98	5.92	14.36
10	27.63	6.39	14.30
15	26.90	7.10	14.47
26	26.27	7.16	14.51
32	25.18	9.09	14.59
41	24.35	9.83	14.72
55	23.43	10.81	14.74
70	22.64	11.82	14.72
90	21.92	12.69	15.19
120	21.05	13.48	15.38
160	20.08	14.60	15.50
200	19.37	15.35	15.57
240	18.74	15.97	15.85
1290	13.63	21.25	17.42

$$\text{H}_2\text{O } 2250 \text{ cm}^{-1} \text{ peak} = 21.6\%$$

Table I (Continued)

Temperature = 120 K Date: 2/15/85

Minutes	%Absorbance of Strongest Peak		
	D ₂ O	(HOD) ₂	HOD
orig.	34.71	0.00	16.74
0.0	31.52	3.29	15.92
1.5	29.41	5.18	15.45
3.0	27.77	7.08	17.02
5.0	27.17	8.47	14.52
7.0	26.04	9.56	14.23
9.0	25.22	9.97	14.71
11.0	24.57	10.65	14.44
14.0	22.82	11.92	13.89
17.0	22.00	12.35	14.11
20.0	21.77	12.87	13.97
25.0	21.05	13.66	13.84
30.0	20.37	14.27	13.75
42.0	19.19	15.32	13.81
55.0	18.34	16.47	13.39
75.0	16.24	17.38	12.84
100.0	16.06	18.30	13.67
130.0	15.02	19.32	13.65
1070.0	8.33	25.65	16.89

H₂O 2250 cm⁻¹ peak = 20%

Temperature = 120 K Date: 3/18/85

Minutes	%Absorbance of Strongest Peak		
	D ₂ O	(HOD) ₂	HOD
orig.	28.92	0.00	16.36
0	24.79	4.01	15.44
2	23.02	5.78	15.65
4	21.28	7.08	15.78
6	20.79	8.17	15.04
10	19.30	9.41	15.46
15	18.16	10.35	15.57
20	17.65	11.00	15.61
30	16.55	12.16	15.53
50	14.99	13.69	15.59
80	13.76	15.01	15.58
110	12.84	15.45	16.20
140	12.15	16.38	15.86
1200	7.67	18.98	19.12

H₂O 2250 cm⁻¹ peak = 26%

TABLE I (Continued)

Temperature = 123 K Date: 2/5/85

Minutes	%Absorbance of Strongest Peak		
	D ₂ O	(HOD) ₂	HOD
orig.	42.43	0.00	16.35
0	37.51	5.14	16.89
2	33.25	9.44	17.02
4	30.57	11.98	17.39
7	28.75	13.58	18.11
10	27.45	14.91	18.09
14	26.28	15.99	18.38
18	25.31	16.85	18.63
23	24.33	17.83	18.75
28	23.31	18.71	18.88
37	22.07	19.76	19.42
46	20.92	20.94	19.38
58	19.88	21.32	20.37
78	18.92	22.78	19.95
103	16.91	23.84	21.35
140	15.58	24.86	22.01
190	14.43	25.75	22.55
1320	9.43	26.67	28.68

H₂O 2250 cm⁻¹ peak = 19:2%

Temperature = 126 K Date: 2/19/85

Minutes	%Absorbance of Strongest Peak		
	D ₂ O	(HOD) ₂	HOD
orig.	31.68	0.00	18.38
0.0	26.68	4.88	17.98
1.0	23.06	8.31	17.73
2.0	20.71	10.50	17.78
4.0	18.27	12.69	17.97
6.0	16.77	14.14	18.07
8.0	15.81	14.93	18.27
10.0	15.11	15.57	18.34
12.5	14.45	16.17	18.40
15.0	13.92	16.77	18.32
20.0	12.97	17.36	18.74
30.0	11.65	18.47	18.96
40.0	10.83	19.26	19.04
50.0	10.15	19.59	19.50
60.0	9.59	20.01	19.65
135.0	7.42	21.17	21.23
160.0	6.97	21.35	21.62

H₂O 2250 cm⁻¹ peak = 20%

TABLE I (Continued)

Temperature = 126 K Date: 3/8/85

Minutes	%Absorbance of Strongest Peak		
	D ₂ O	(HOD) ₂	HOD
orig.	26.52	0.00	16.06
0	22.47	5.20	16.23
1	19.59	8.77	16.54
2	17.82	10.86	16.70
4	15.27	12.94	16.78
6	14.69	14.59	17.48
8	13.96	15.56	17.44
10	13.48	16.18	17.81
15	12.50	17.17	18.14
20	11.73	17.91	18.48
30	10.93	19.08	18.91
40	10.13	19.76	19.24
60	9.18	20.21	19.45
100	8.28	21.49	21.06
150	7.69	21.79	22.08

H₂O 2250 cm⁻¹ peak = 26%

Temperature = 130 K Date: 2/28/85

Minutes	%Absorbance of Strongest Peak		
	D ₂ O	(HOD) ₂	HOD
orig.	29.98	0.00	13.83
0	19.79	8.28	13.49
1	15.95	11.32	13.69
2	14.19	12.72	14.14
3	12.98	14.24	13.73
12	9.59	16.53	14.85
16	9.10	16.86	15.13
25	8.08	17.59	15.46
55	6.85	17.92	16.80
1320	3.34	10.05	32.90

H₂O 2250 cm⁻¹ peak = 22%

TABLE II
134-160 K Data

Temperature = 134 K Date: 2/6/85

Minutes	%Absorbance of Strongest Peak		
	D ₂ O	(HOD) ₂	HOD
0	7.83	26.70	23.41
3	7.89	26.27	23.95
6	7.66	26.17	24.48
12	7.37	25.90	25.30
31	6.98	24.56	28.16
45	6.32	24.05	29.90
63	6.06	22.84	32.32
81	5.67	21.97	34.27
102	5.67	21.15	35.53
132	5.32	19.92	38.11
162	5.07	18.81	40.05
195	4.60	17.84	42.24

H₂O 2250 cm⁻¹ peak = 19.2%

Temperature = 160 K Date: 2/9/85

Minutes	%Absorbance of Strongest Peak		
	D ₂ O	(HOD) ₂	HOD
0	4.70	19.30	19.62
2	.78	4.21	50.75
4	1.80	2.56	42.71
6	2.14	2.41	42.59
8	.31	.69	57.19
10	-.25	.78	58.23
13	.02	.44	58.42
43	0.00	0.00	59.47

H₂O 2250 cm⁻¹ peak = 20%

TABLE II (Continued)

Temperature = 137 K Date: 2/12/85

Minutes	%Absorbance of Strongest Peak		
	D ₂ O	(HOD) ₂	HOD
0	13.50	15.85	15.24
1	11.92	17.53	15.60
2	10.54	17.41	16.62
4	8.63	17.95	18.33
6	7.73	18.65	18.43
8	7.18	18.01	19.51
10	6.83	18.46	20.04
15	5.70	18.39	21.38
20	5.30	17.80	23.13
30	5.23	17.08	24.77
48	4.54	15.50	28.50
64	4.22	14.47	30.63
92	3.50	12.25	35.60
120	3.62	10.81	37.92
165	2.79	9.22	41.68
205	2.29	7.89	44.55
307	1.85	6.54	47.73
final	0.00	0.00	61.46

$$\text{H}_2\text{O } 2250 \text{ cm}^{-1} \text{ peak} = 22.4\%$$

Temperature = 150 K Date: 2/16/85

Minutes	%Absorbance of Strongest Peak		
	D ₂ O	(HOD) ₂	HOD
0.0	2.87	20.15	25.90
2.0	1.50	13.65	39.80
4.0	1.10	9.37	48.07
6.0	.86	7.16	52.81
8.0	.58	5.99	55.32
10.0	-.18	5.54	57.62
12.5	-.52	4.60	59.79
15.0	-.51	3.64	61.17
20.0	-.43	3.18	62.46
40.0	.00	1.09	65.41
70.0	-.26	.42	66.89

$$\text{H}_2\text{O } 2250 \text{ cm}^{-1} \text{ peak} = 20\%$$

TABLE II (Continued)

Temperature = 140 K Date: 2/27/85

Minutes	%Absorbance of Strongest Peak		
	D ₂ O	(HOD) ₂	HOD
0.0	12.48	18.90	18.23
2.0	10.31	19.00	21.24
4.0	9.02	18.63	23.60
6.0	8.66	18.16	25.01
8.0	8.25	17.44	26.62
10.0	8.00	17.04	18.89
12.5	7.25	16.57	29.54
15.0	6.94	15.92	30.49
20.0	6.74	15.01	32.93
25.0	6.06	13.99	34.96
35.0	6.24	12.51	36.36
55.0	4.42	9.83	43.81
75.0	3.95	8.02	47.44
100.0	3.23	6.60	50.41
130.0	2.58	5.53	53.36
145.0	2.89	4.56	54.70

$$\text{H}_2\text{O } 2250 \text{ cm}^{-1} \text{ peak} = 21.6\%$$

Temperature = 140 K Date: 3/19/85

Minutes	%Absorbance of Strongest Peak		
	D ₂ O	(HOD) ₂	HOD
0	6.45	18.48	19.44
2	5.57	17.90	21.44
4	5.66	16.84	23.53
6	5.41	16.34	24.53
10	5.04	15.24	26.86
15	4.05	14.06	30.23
20	3.92	12.88	32.20
32	3.03	10.94	36.63
50	2.12	8.60	41.75
80	1.64	5.86	46.45
110	2.10	4.62	47.51
150	1.58	3.21	50.61

$$\text{H}_2\text{O } 2250 \text{ cm}^{-1} \text{ peak} = 26\%$$

TABLE II (Continued)

Temperature = 145 K Date: 2/19/85

Minutes	%Absorbance of Strongest Peak		
	D ₂ O	(HOD) ₂	HOD
0	7.28	18.93	23.71
1	7.38	17.58	25.95
2	6.67	16.48	28.86
3	5.15	15.69	31.21
5	5.27	14.08	34.40
7	4.82	12.74	37.10
9	4.08	11.79	39.37
12	3.65	10.51	42.08
15	3.24	9.64	43.90
20	2.85	8.24	46.63
30	2.07	6.19	50.90
45	1.56	4.50	54.09
60	1.46	3.22	56.27
80	1.13	2.24	58.17
100	1.00	1.66	59.36

H₂O 2250 cm⁻¹ peak = 20%

Temperature = 145 K Date: 3/8/85

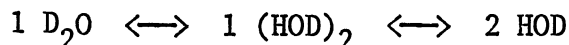
Minutes	%Absorbance of Strongest Peak		
	D ₂ O	(HOD) ₂	HOD
0	7.07	19.24	22.84
1	6.41	18.15	25.69
2	5.92	16.98	28.20
4	5.26	14.93	30.95
6	4.65	13.97	34.93
8	4.29	12.92	36.91
10	3.84	11.86	39.11
15	3.36	10.10	42.66
20	2.86	8.73	45.42
30	2.27	6.71	49.30
50	1.56	4.49	53.77
80	1.14	2.77	56.83
100	.95	2.10	58.19

H₂O 2250 cm⁻¹ peak = 26%

Conversion to Concentrations

The data were measured as the overlapping absorbance bands of D_2O , $(HOD)_2$, and HOD in H_2O ice, and were separated into the individual component bands as just described. The peak height of the strongest band of a component was the value recorded for each species at each time as it varies linearly with the concentration of the absorber, being related by the relative molar absorptivities (Beer's law is obeyed at the D_2O dilutions used here).

Absorptivities of D_2O and $(HOD)_2$ can be determined relative to that of HOD as the concentration changes follow the relation:



At the conclusion of the reaction essentially all of the deuterium exist as isolated HOD, so that at any time during the reaction the material balance is

$$[D_2O] + [(HOD)_2] + 0.5[HOD] = 0.5[HOD]_{\text{infinite time}}$$

According to Beer's law

$$\frac{2A_{D_2O}}{e_{D_2O}} + \frac{2A_{(HOD)_2}}{e_{(HOD)_2}} + \frac{A_{HOD}}{e_{HOD}} = \frac{A_{HOD}}{e_{HOD}}$$

where A_{D_2O} is the observed absorbance of D_2O and e_{D_2O} its absorptivity. These absorptivity factors could be determined at this stage by least squares or they could be included as adjustable parameters when the model is fit to the data. From a least squares analysis using the program described and listed in Appendix A the absorptivity values given in Table III were calculated. At the lower temperatures only the ratio between e_{D_2O} and $e_{(HOD)_2}$ is important as $[HOD]$ does not change significantly. At higher temperatures the ratios to e_{HOD} could be calculated and are given.

TABLE III

Calculated Molar Absorptivities
and Absolute HOD Concentrations

Date	T(K)	$\frac{e_{D_2O}}{e_{(HOD)_2}}$	$\frac{e_{(HOD)_2}}{e_{HOD}}$	final A_{HOD}	approx. $[HOD]_{\infty}$
2/ 9/85	160	0.94	1.22	59.0	3.25
2/16/85	150	0.78	1.14	67.4	3.71
3/18/85	145	0.95	1.06	62.9	2.66
2/19/85	145	0.98	1.31	63.0	3.47
2/27/85	140	1.08	1.26	66.5	3.39
3/19/85	140	0.94	1.35	58.0	2.45
2/12/85	137	1.23	1.17	61.8	3.03
2/ 5/85	134	0.95	1.29	77.5	4.44
2/28/85	130	1.19	1.36	52.2	2.61
3/ 8/85	126	1.60	1.83	66.9	2.83
2/19/85	126	1.22	1.12	71.0	3.91
2/ 5/85	123	1.14	13.24	83.0	4.75
2/15/85	120	1.21	8.32	73.4	4.04
3/18/85	120	1.02	1.13	65.0	2.75
2/26/85	117	1.26	3.18	70.7	3.60
2/11/85	115	1.23	8.94	67.6	3.32
1/28/85	113	1.02	6.90	66.6	3.05
2/ 8/85	110	1.06	-2.44	69.8	3.84

Collier's average values for e_{D_2O}/e_{HOD} and $e_{D_2O}/e_{(HOD)_2}$ were 1.31 ± 0.03 and 1.1 ± 0.1 , respectively (39). Also in Table III are estimates of the absolute HOD concentrations after complete scrambling.

Absolute values for the concentrations could be roughly estimated by comparison of the sample spectra to the spectrum of a sample made from a mixture containing a known amount of HOD. Ice samples containing a known amount of HOD have been prepared in this lab. Such a sample (in particular, the one made by Gary Ritzhaupt on 7-10-84) which contained 2% HOD had a HOD band absorbance of 0.462 units above the H_2O ice background, while a background band at around 2250 cm^{-1} had 0.255 absorbance. The percentage of HOD in any ice sample therefore is approximately

$$\%HOD = \frac{\text{absorbance of HOD}}{\text{absorbance of } H_2O} \times \frac{0.255 \times 2\%}{0.462} = \frac{\text{absorbance of HOD}}{\text{absorbance of } H_2O} \times 1.1\%$$

for up to a few percent HOD. Larger amounts of HOD would exist in equilibrium with appreciable amounts of D_2O and $(HOD)_2$ which are not accounted for in the above equation. Typical samples had HOD absorbances of 0.6 and H_2O 2250 cm^{-1} band absorbances of 0.25 and hence had about 2.6% HOD upon complete isotopic scrambling.

CHAPTER III

MODEL AND DATA FITTING

Scrambling Steps

To describe isotopic scrambling in ice one begins by considering D_2O isolated in the H_2O lattice, as depicted in Figure 16 and again in Figure 28, and what becomes of the deuterons as the result of the net forward motions of point defects. Figure 28 has columns for the species in the lattice, depicted by formula and schematically; the bond number through which a defect may effectively visit, again depicted schematically; the resulting species in the lattice and also columns to sum up the number of effective approach channels, the number of possible outcomes resulting from approach through those channels, and the number of outcomes in which a deuteron had been moved rather than just protons; and, finally, columns with the equation for that elementary step along with the rate constant nomenclature. The first scrambling step will be the migration of a proton through the D_2O site resulting in the formation of vibrationally coupled HOD neighbors, H-O-D..HOD, denoted as $(HOD)_2$. (An OH^- ion, if mobile, would cause the same result but it is generally agreed to be orders of magnitude less mobile than the positive ion.) A proton moving through an $(HOD)_2$ may change it back to D_2O or to a configuration, H-O-D.. H_2O ..D-O-H, denoted as $(HOD)_{pc}$ for pseudo-coupled. The $(HOD)_2$ may be changed by the passage of an ion or an L or D type orientational defect, of which the

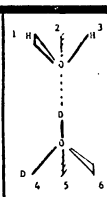
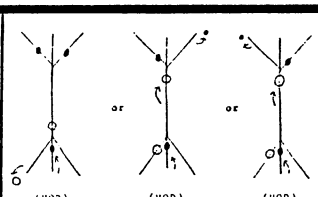
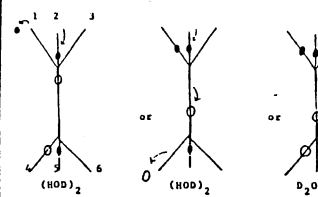
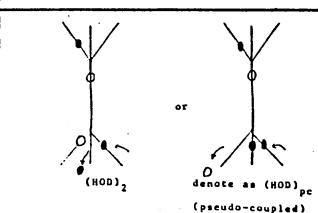
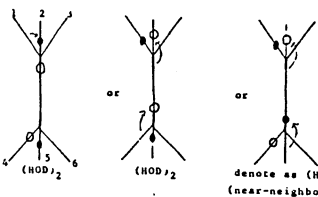
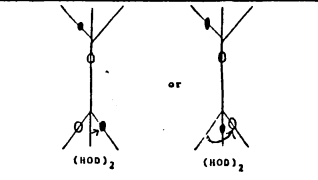
SPECIES IN LATTICE	EFFECTIVE DEFECT APPROACH CHANNELS	RESULTING SPECIES	APPROACH CHANNELS	POSSIBLE OUTCOMES	MOVED A DEUTERON	REACTION	RATE CONSTANT
D_2O	 5 (or) 6 	6 $(HOD)_2$	2	6	6	$D_2O + H^+ \rightarrow H^+ + (HOD)_2$	K_{1d}
$(HOD)_2$	2 (or) 3 	2 D_2O	3	8	2	$(HOD)_2 + H^+ \rightarrow$ $H^+ + \frac{2}{5}(HOD)_2 + \frac{2}{5}D_2O + \frac{1}{5}(HOD)_{pc}$	$\frac{5}{8}K_{2d}$
	6 	5 $(HOD)_2$			2		
$(HOD)_2$	2 (or) 3 	6 $(HOD)_2$	3	8	3	$(HOD)_2 + L \rightarrow L + \frac{3}{5}(HOD)_2 + \frac{2}{5}(HOD)_{nn}$	$\frac{5}{8}K_{3d}$
	6 	2 $(HOD)_{nn}$			2		

Figure 28. Elementary scrambling steps of D_2O and $(HOD)_2$.

L-defect is considered to be somewhat more mobile. Passage of an L-defect through the $(\text{HOD})_2$ has a chance of separating the deuterons by two oxygen atoms to form D-O-H..HOD , a configuration denoted as $(\text{HOD})_{\text{nn}}$, for near-neighbor.

The effects of defect passage through $(\text{HOD})_{\text{pc}}$ and $(\text{HOD})_{\text{nn}}$ are illustrated in Figures 29 and 30. When the deuterons of a D_2O become separated by an $\text{H-O-D..H}_2\text{O..HOD}$ linkage they are considered to belong to a pair of isolated HOD molecules with a negligible chance of recombining. The reactions describing the individual steps are summarized in Figure 31. Those which involve moving a deuteron carry the "D" subscript while those where only protons are moved carry an "H" subscript. The denominators in the rate equations and rate constants are the number of possible outcomes of the reaction; the numerators are the number of outcomes that result in that particular species.

Because there should be no difference between any of the K's involved in the same elementary step such as moving a deuteron along a hydrogen bond, the following equalities should hold

$$K_{\text{H}} = K_{1\text{D}} = K_{2\text{D}} = K_{4\text{D}} = K_{6\text{D}} ; \text{ deuteron hop,}$$

$$K_{\text{H}_\text{H}} = K_{2\text{H}} = K_{4\text{H}} = K_{6\text{H}} ; \text{ only protons hop,}$$

$$K_{\text{L}} = K_{3\text{D}} = K_{5\text{D}} = K_{7\text{D}} ; \text{ deuteron turn,}$$

$$K_{\text{L}_\text{H}} = K_{3\text{H}} = K_{5\text{H}} = K_{7\text{H}} ; \text{ turn involving no deuterons.}$$

With these considerations the equations of Figure 31 can be simplified to those shown in Figure 32.

SPECIES IN LATTICE	EFFECTIVE DEFECT APPROACH CHANNELS	RESULTING SPECIES	APPROACH CHANNELS	POSSIBLE OUTCOMES	MOVED A DEUTERON	REACTION	RATE CONSTANT
$(\text{HOD})_{\text{pc}}$	1	$8 (\text{HOD})_2$	4	12	8	$(\text{HOD})_{\text{pc}} + \text{H}^+ \rightarrow \text{H}^+ + (\text{HOD})_2$	$\frac{8}{12} K_{4d}$
	2						
	3						
	4						
5	1	$4 (\text{HOD})_{\text{pc}}$	4	12	8	$(\text{HOD})_{\text{pc}} + \text{L} \rightarrow \text{L} + 2 \text{HOD}_{\text{isolated}}$	$\frac{8}{12} K_{5d}$
	2						
	3						
	4						
$(\text{HOD})_{\text{pc}}$	1	$8 (\text{HOD})_{\text{isolated}}$	4	12	8	$(\text{HOD})_{\text{pc}} + \text{L} \rightarrow \text{L} + (\text{HOD})_{\text{pc}}$	$\frac{4}{12} K_{5h}$
	2						
	3						
	4						

Figure 29. Elementary scrambling steps of $(\text{HOD})_{\text{pc}}$.

SPECIES IN LATTICE	EFFECTIVE DEFECT APPROACH CHANNELS	RESULTING SPECIES	APPROACH CHANNELS	POSSIBLE OUTCOMES	MOVED A DEUTERON	REACTION	RATE CONSTANT
$(\text{HOD})_{nn}$	<p>5 (or 6)</p> <p>2 HOD_{isolated} (HOD)_{nn} 2 HOD_{isolated}</p>	3 $(\text{HOD})_{nn}$	3	8		$(\text{HOD})_{nn} + \text{H}^+ \rightarrow \text{H}^+ + 2\text{HOD}_{\text{isolated}}$	$\frac{5}{8}K_{6d}$
	<p>3</p> <p>HOD (HOD)_{nn}</p>	5 HOD pairs			5	$(\text{HOD})_{nn} + \text{H}^+ \rightarrow \text{H}^+ + (\text{HOD})_{nn}$	$\frac{3}{8}K_{6h}$
$(\text{HOD})_{nn}$	<p>5 (or 6)</p> <p>(HOD)_{nn} (HOD)₂ (HOD)_{nn}</p>	2 $(\text{HOD})_2$	3	8	2	$(\text{HOD})_{nn} + \text{L} \rightarrow \text{L} + \frac{2}{5}(\text{HOD})_2 + \frac{3}{5}(\text{HOD})_{nn}$	$\frac{5}{8}K_{7d}$
	<p>3</p> <p>(HOD)_{nn} (HOD)_{nn}</p>	6 $(\text{HOD})_{nn}$			3	$(\text{HOD})_{nn} + \text{L} \rightarrow \text{L} + (\text{HOD})_{nn}$	$\frac{3}{8}K_{7h}$

Figure 30. Elementary scrambling steps of $(\text{HOD})_{nn}$.

REACTION SUMMARY

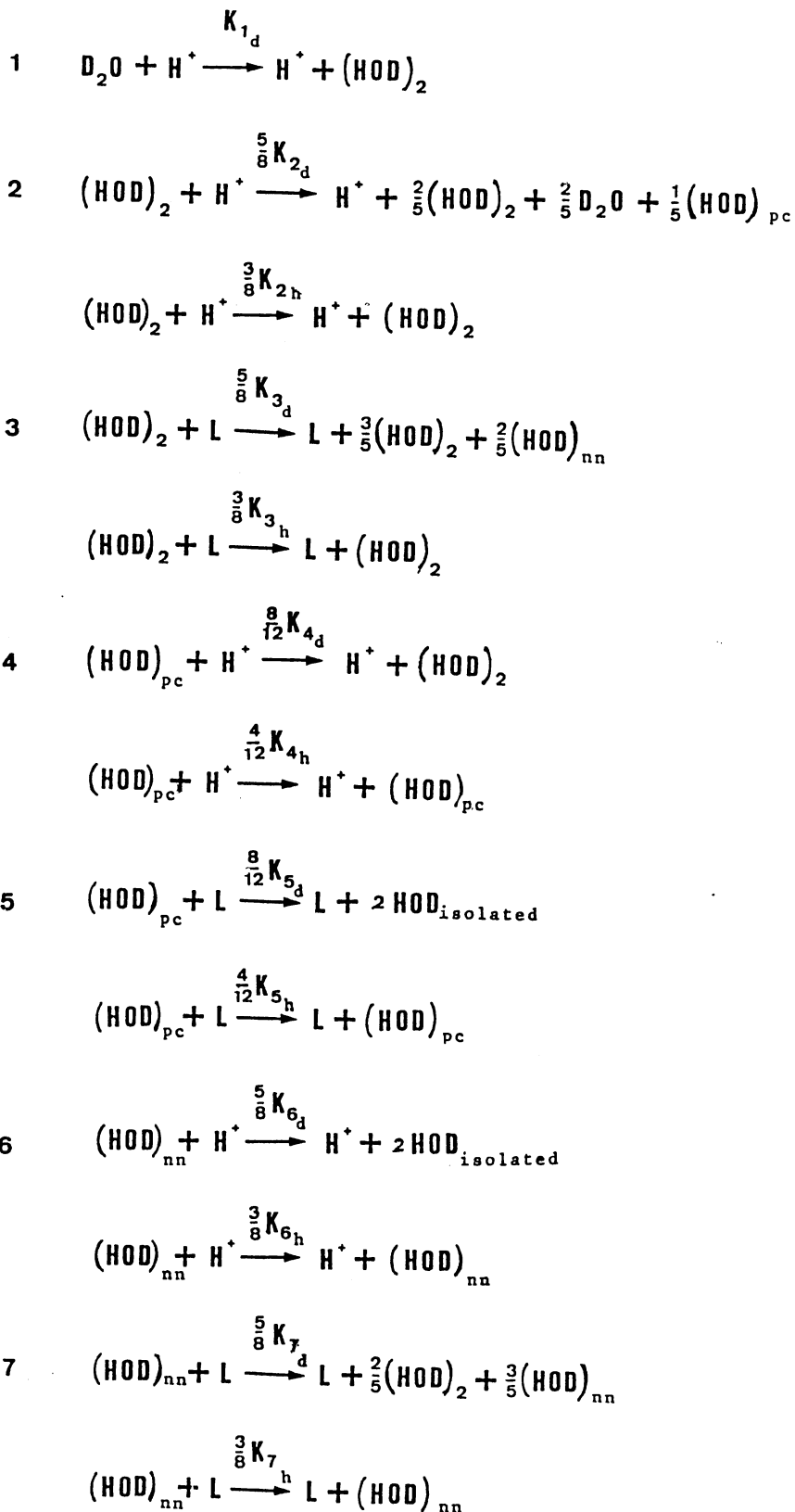
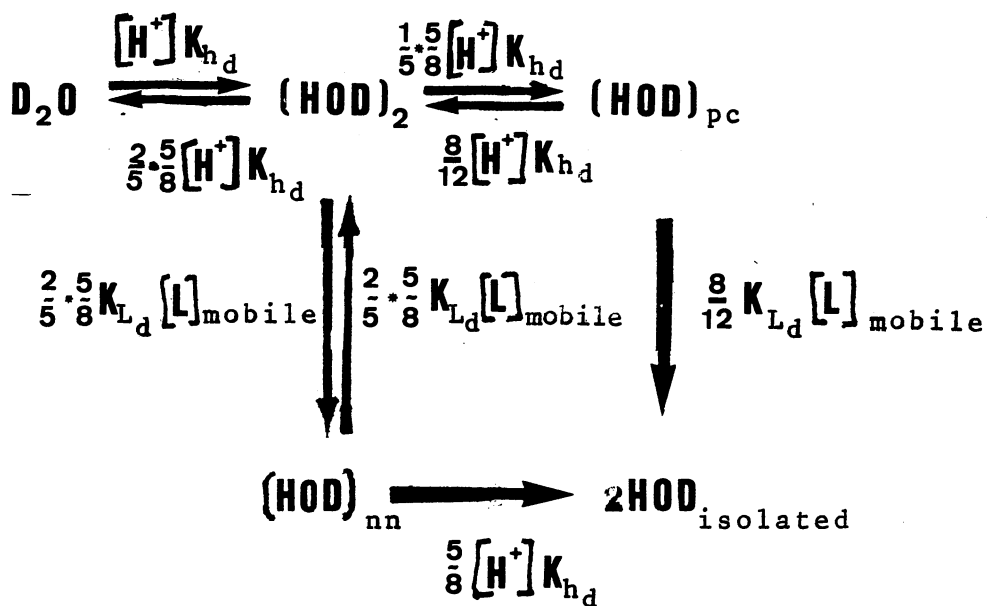


Figure 31.



OR

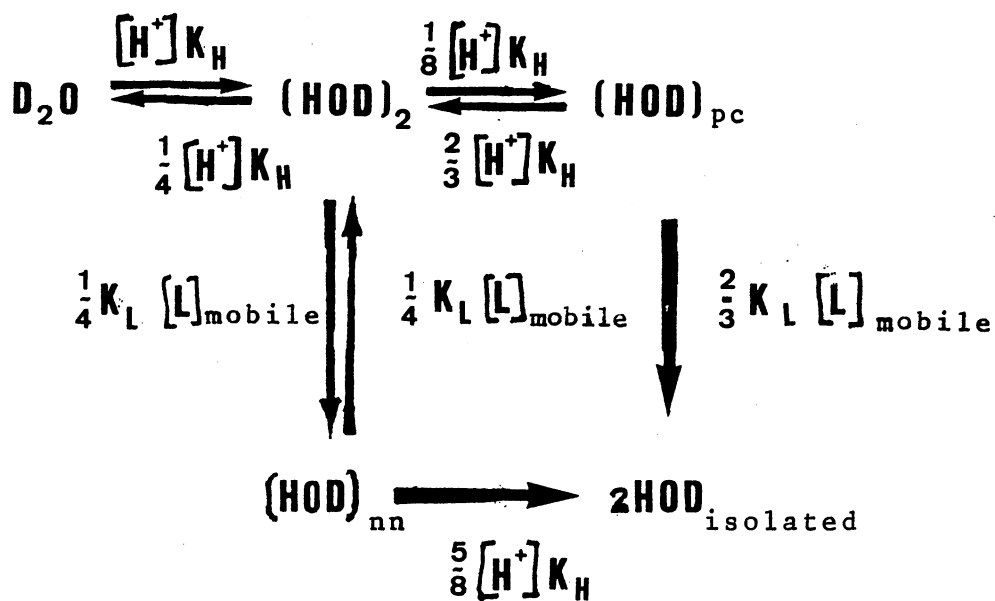


Figure 32.

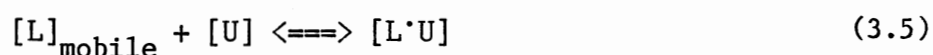
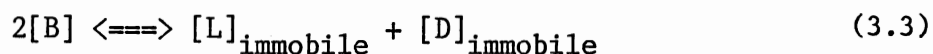
Defect Concentrations

The time dependence of the observed amounts of D_2O , $(HOD)_2$ and HOD reflect the unmeasurable H^+ and L-defect concentrations. The trapping results have shown that the H^+ concentration is not always simply activated but is also subject to shallow trapping. A general model should consider two traps for mobile protons: first, a shallow trap which requires less energy for dissociation than the normal ionization process; and, second, the OH^- ion. The shallow trap has been equated with L-defects by some authors who point out that the L-defect is associated with an effective partial negative charge which may attract and weakly hold a proton. The H^+ and OH^- concentrations are not necessarily equal and in fact appear to be severely disturbed by the presence of minute amounts of impurities such as organic amines, which trap protons quite deeply. The reactions controlling the mobile proton concentration are



where S denotes the shallow trap and the $S \cdot H^+$ complex is immobile.

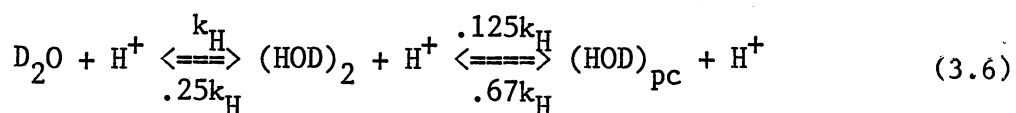
The Bjerrum defects do not move freely through the crystal but have an appreciable activation energy for diffusion. Concerning the mobile L-defect population three reactions need be considered: (1) the formation-recombination of L-D pairs, (2) the mobilization of an L-defect, and (3) an unspecified shallow trap (possibly the combination of a mobile proton with a mobile L-defect to form an immobile complex):



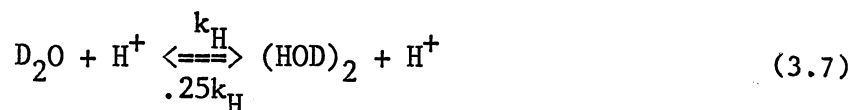
where B are properly oriented ice bonds and U is the unspecified shallow trap for L-defects. D-defects are assumed not to mobilize to any appreciable extent.

Low Temperature Analysis

From the data it is clear that $[L]_{\text{mobile}}$ is approximately zero at $T \leq 130$ K because essentially no $(\text{HOD})_2$ converted to HOD. This leaves



or by ignoring the minor species, $(\text{HOD})_{\text{pc}}$:



which should tend to an equilibrium ratio of 1:4 for $\text{D}_2\text{O}:(\text{HOD})_2$.

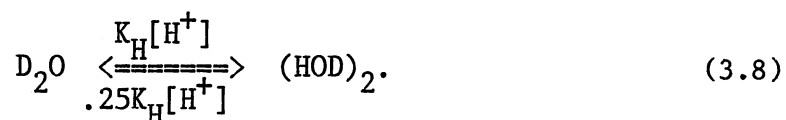
Inclusion of $(\text{HOD})_{\text{pc}}$ would change this ratio only slightly and would complicate the analysis because it is uncertain whether this species appears in the data as part of what is counted as $(\text{HOD})_2$ or as HOD.

The low temperature experiments involved trapping mobile protons generated at 90 K and watching the isotopic conversion caused by their release at 110–130 K; hence while the reaction progresses the H^+ concentration changes according to the defect concentration controlling reactions given in the preceding section. Assumed is that the total number of shallow traps remains constant during the course of the scrambling at a given temperature. This is reasonable if the traps are immobile L-defects because the observed effects of the mobile L-defects were essentially zero.

Ideally, differential equations representing 3.1, 3.2 and 3.7 would

be coded into a program which would integrate the equations and compare the results to the data and adjust the parameters to obtain the best least squares fit. The difficulty lies in the number of parameters involved in integrating the equations. Needed are the initial concentrations of all the species, $[D_2O]_0$, $[(HOD)_2]_0$, $[H^+]_0$, $[S]_0$, $[S \cdot H^+]_0$ and $[OH^-]_0$; as well as the rate constants, K_H , K_{S-1} , K_S , $K_{\text{self-ionization}}$ and $K_{\text{recombination}}$. Of the aforementioned parameters, the only ones for which better than wild guesses could be made were $[D_2O]_0$ and $[(HOD)_2]_0$, the observed data. Some reasonable restrictions could be imposed on a few parameters such as having $[OH^-] = [H^+] + [S \cdot H^+]$, but there remained still too many unknowns to fit to data that is basically of the simple form: $[D_2O]_t$ vs. time.

Assuming that the proton concentration changes slowly compared to the effects of proton hopping allows one to write the integrable scheme



Which by having

$$x = [D_2O]_0 - [D_2O]$$

$$a = [D_2O]_0$$

$$b = [(HOD)_2]_0$$

the rate equation is

$$\begin{aligned} \frac{dx}{dt} &= K_H[H^+](a-x) - 0.25(b+x) \\ &= 1.25K_H[H^+](m-x) \end{aligned} \quad (3.9)$$

where $m = 0.2(4a-b)$.

Now

$$\frac{dx}{m-x} = 1.25K_H[H^+]dt$$

so that

$$\ln\left(\frac{m}{m-x}\right) = 1.25K_H \int_0^t [H^+]dt . \quad (3.10)$$

If $[H^+]$ were constant with time then a plot of $\ln(m/(m-x))$ vs. time would be linear and have a slope equal to $1.25K_H[H^+]$. Figures 33-41 are plots made utilizing data from Tables I & III; the abscissa are the \ln functions, which would have the numerical value of $\ln(2^n)$ at the n^{th} half-life. Clearly the curves are not linear and indeed indicate that the mobile proton concentration tails off with time as the sample is held at a constant temperature after irradiation. This type of treatment magnifies any errors late in the reaction when x nears m in value so the final points at a given temperature may be unreliable. The quickness of the initial rates attests to the validity of the assumption made above, but if it does fail it will be at lower mobile proton concentrations--at the later times during the reaction.

The experiments were performed in a consistent way such that the initial conditions should have been the same throughout this series of samples; having generated approximately the same concentration of trapped protons each time. Because no irradiation gave even the slightest indication of saturating the shallow trap concentration, it may be assumed that the trap concentration was very much greater than the amount of photoliberated mobile protons:

$$([S] \approx [S]_0) \gg ([H^+ \cdot S] \approx [OH^-])$$

As the initial rates were always the fastest at a particular temperature, reaction 3.2 establishes a pseudoequilibrium during the rapid warming to the reaction temperature, and the decay of the rates of

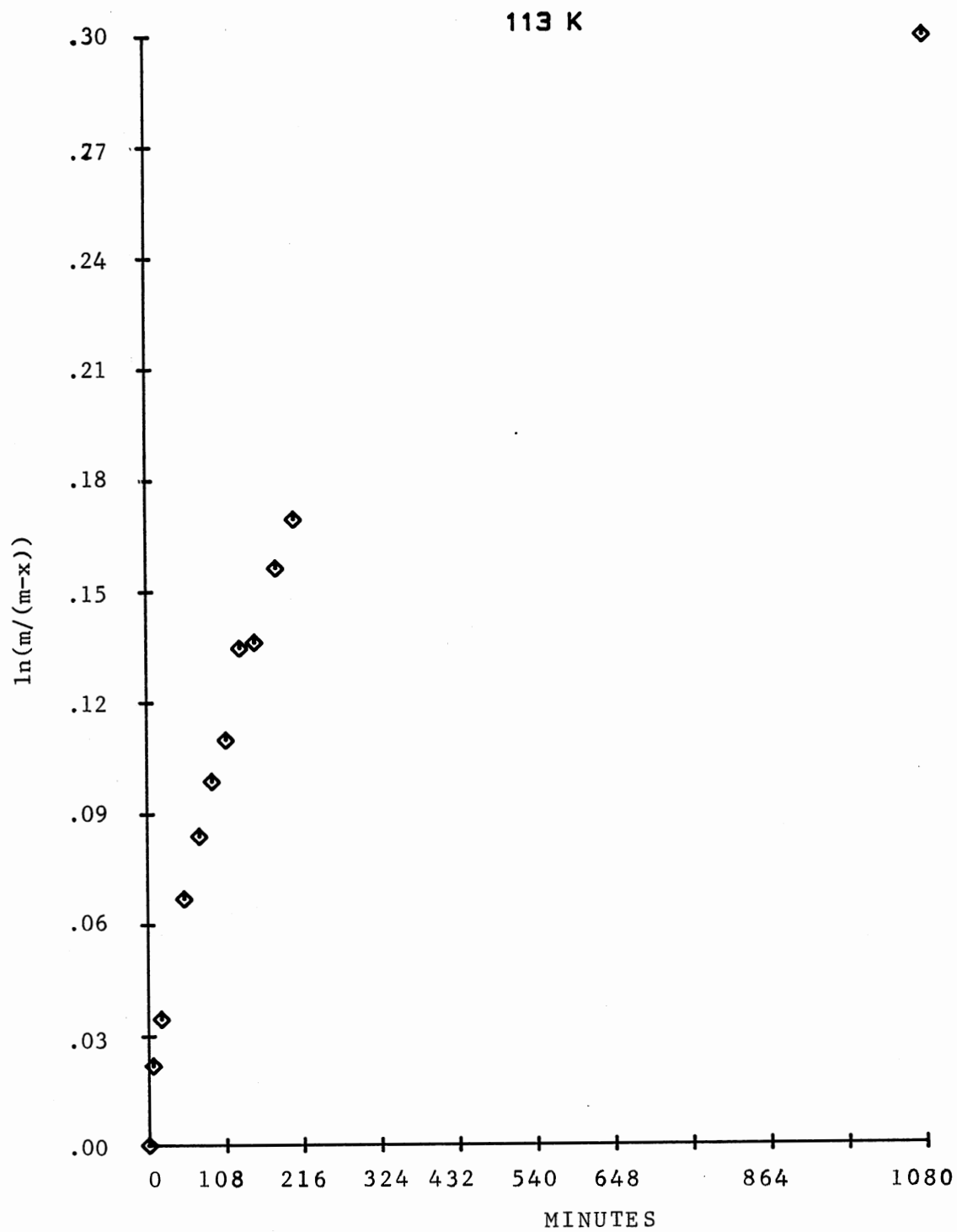


Figure 33. Integral of rate from 113 K data.

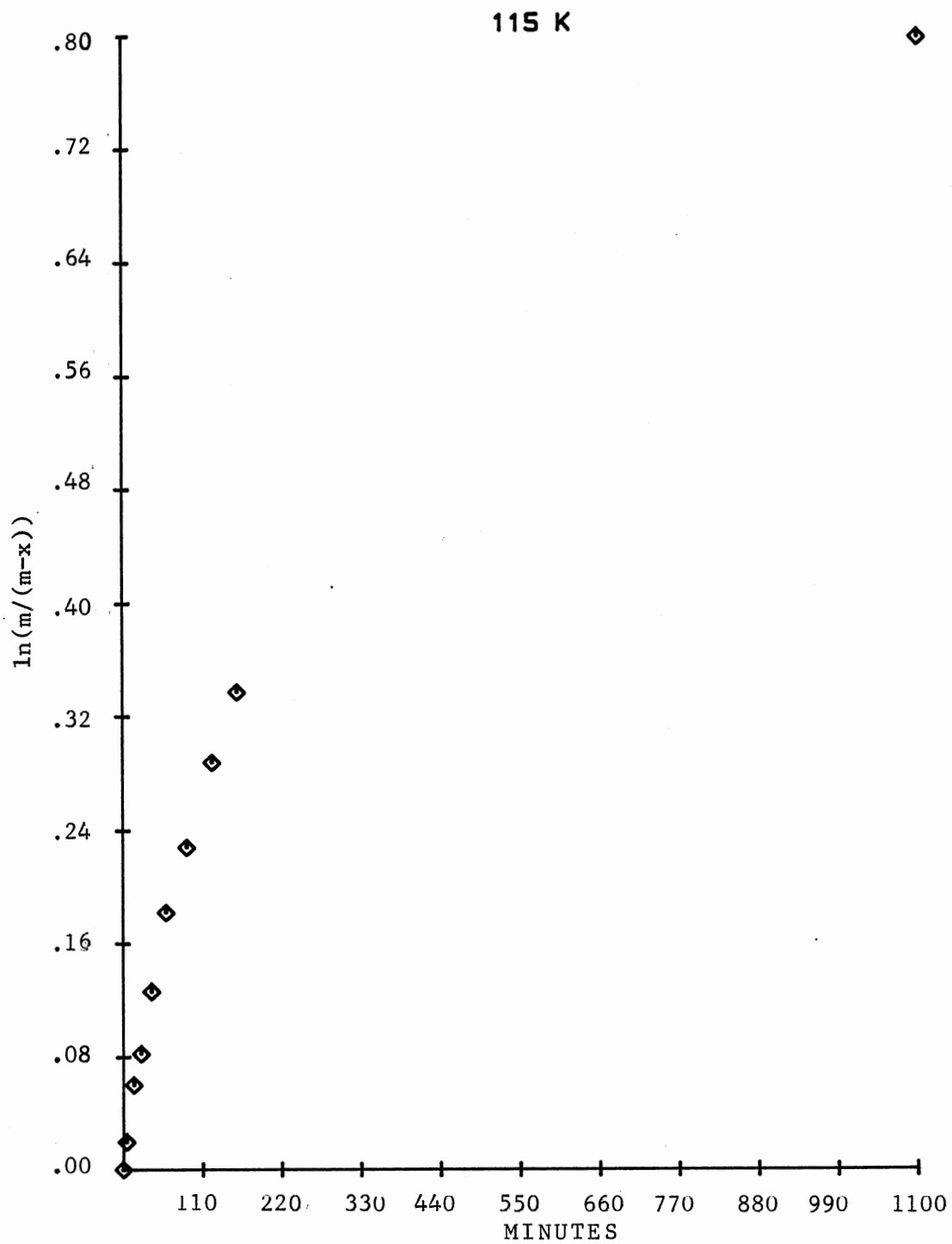


Figure 34. Integrated rate from 115 K data.

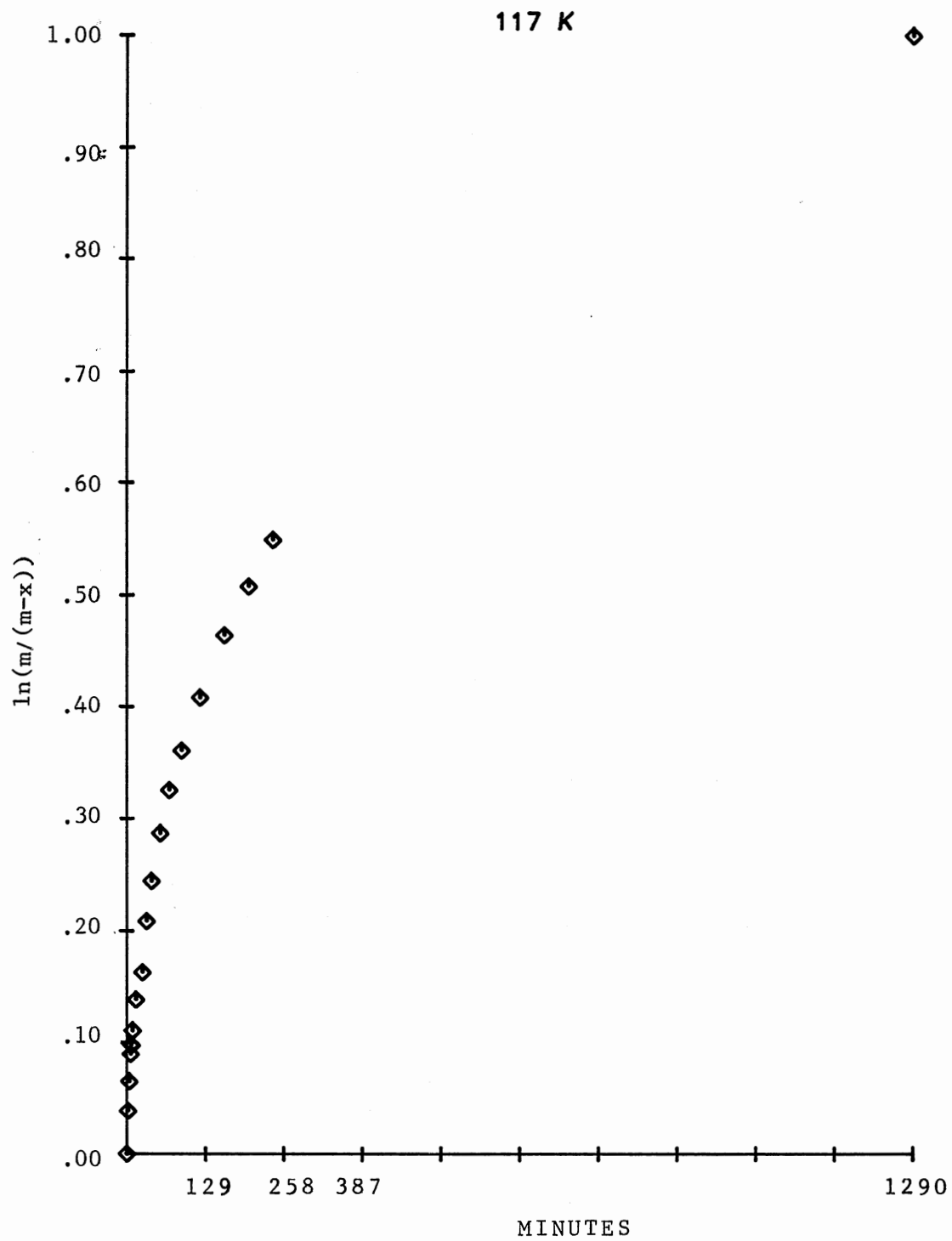


Figure 35. Integral of rate from 117 K data.

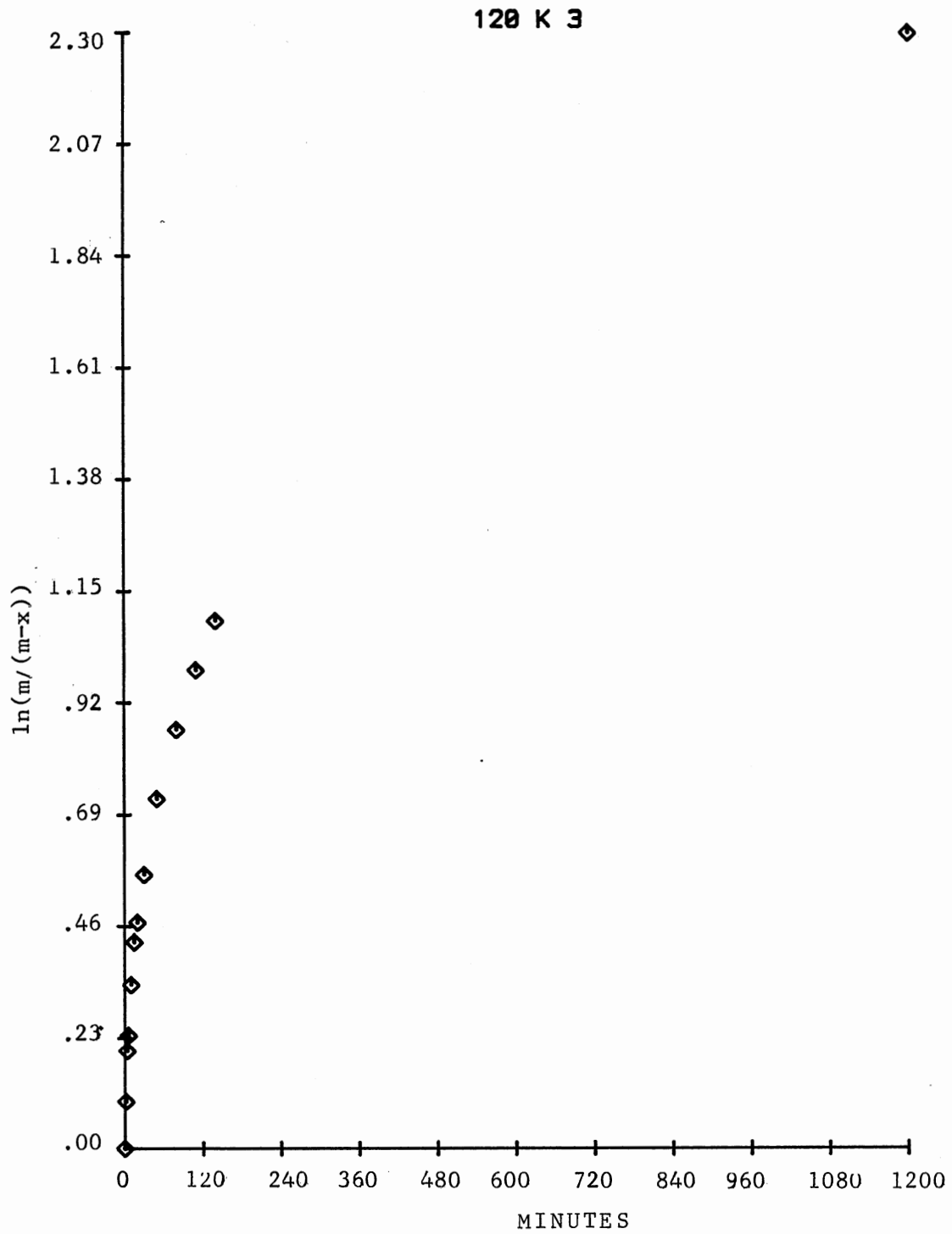


Figure 36. Integral of rate from March 120 K data.

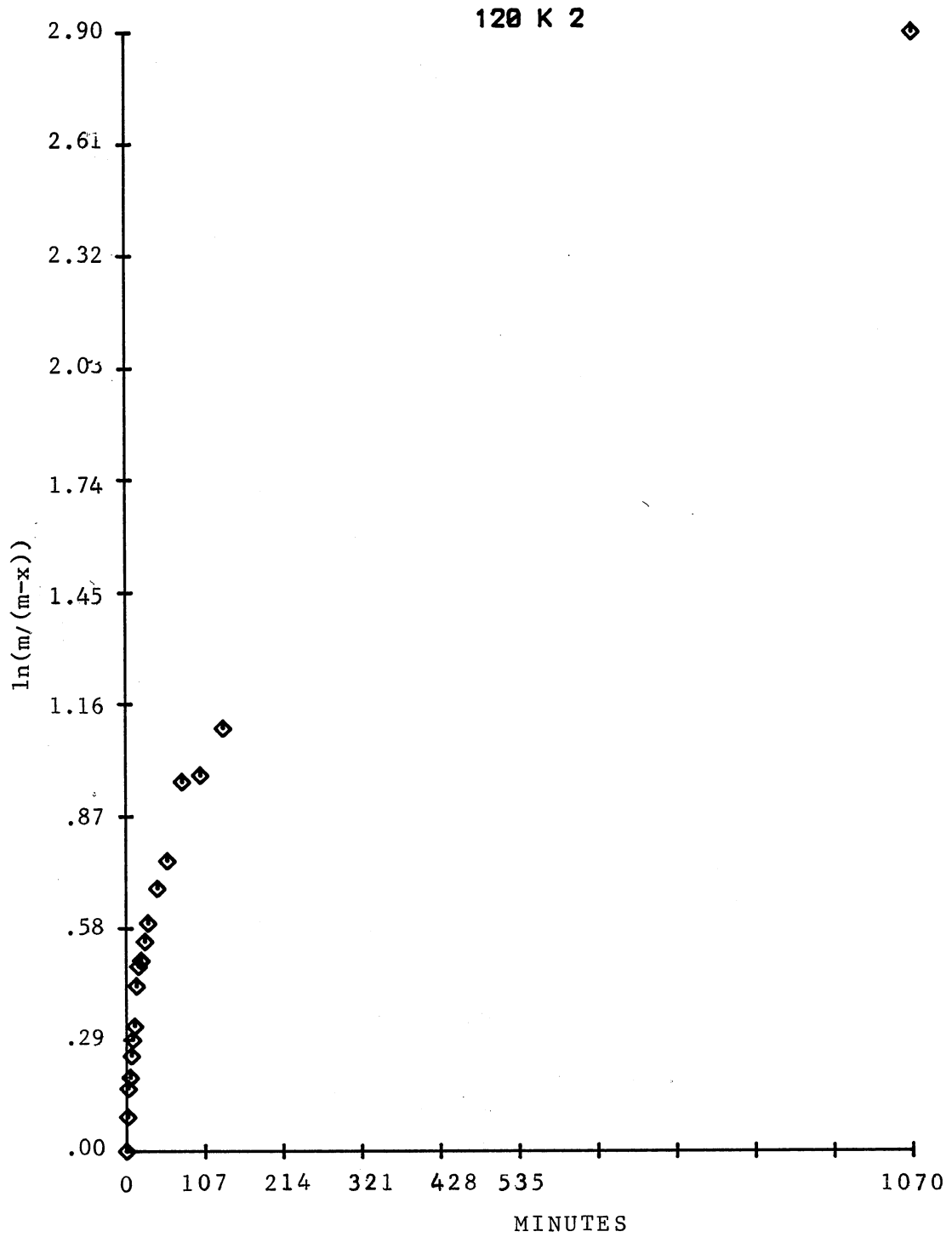


Figure 37. Integral of rate from February 120 K data.

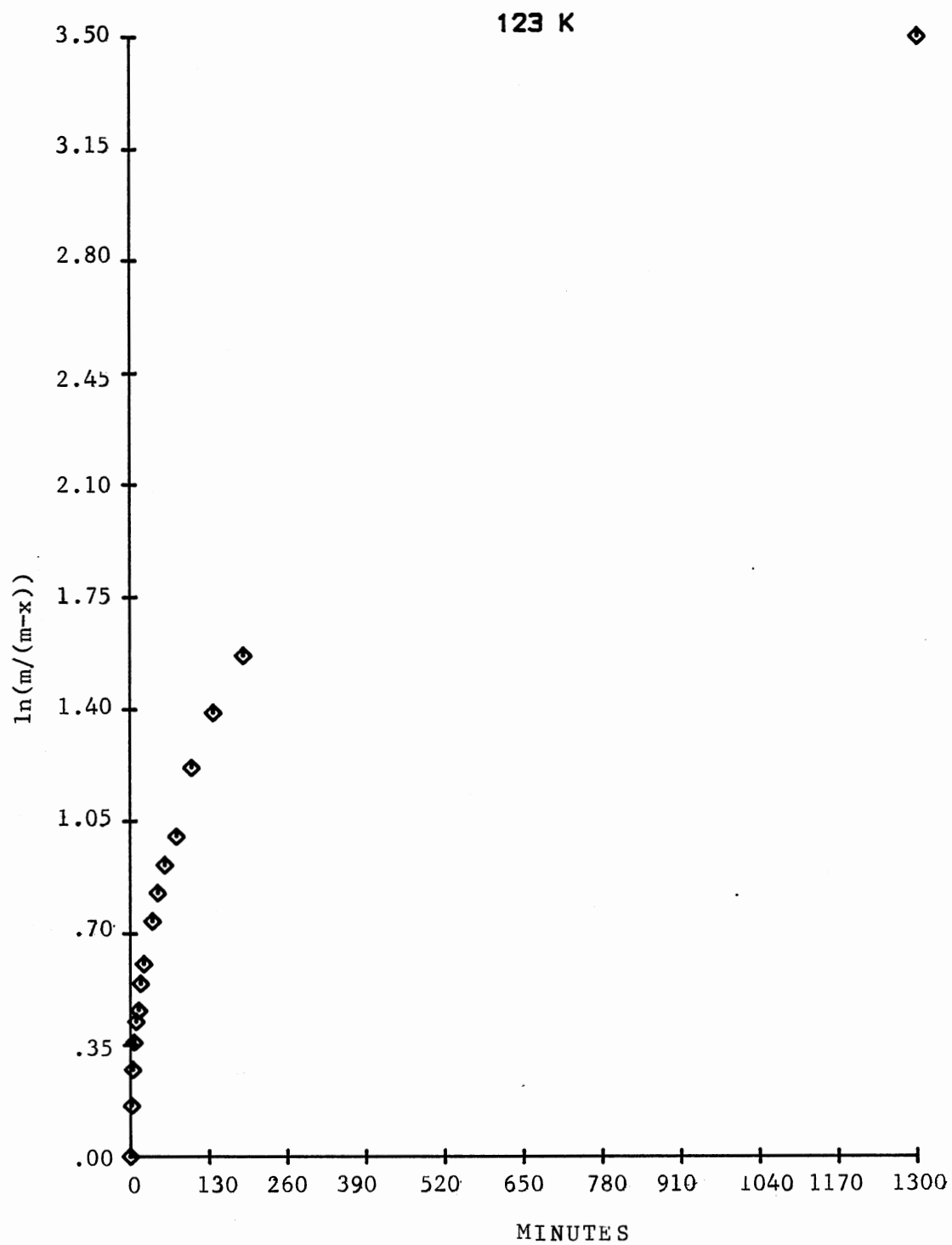


Figure 38. Integral of rate from 123 K data.

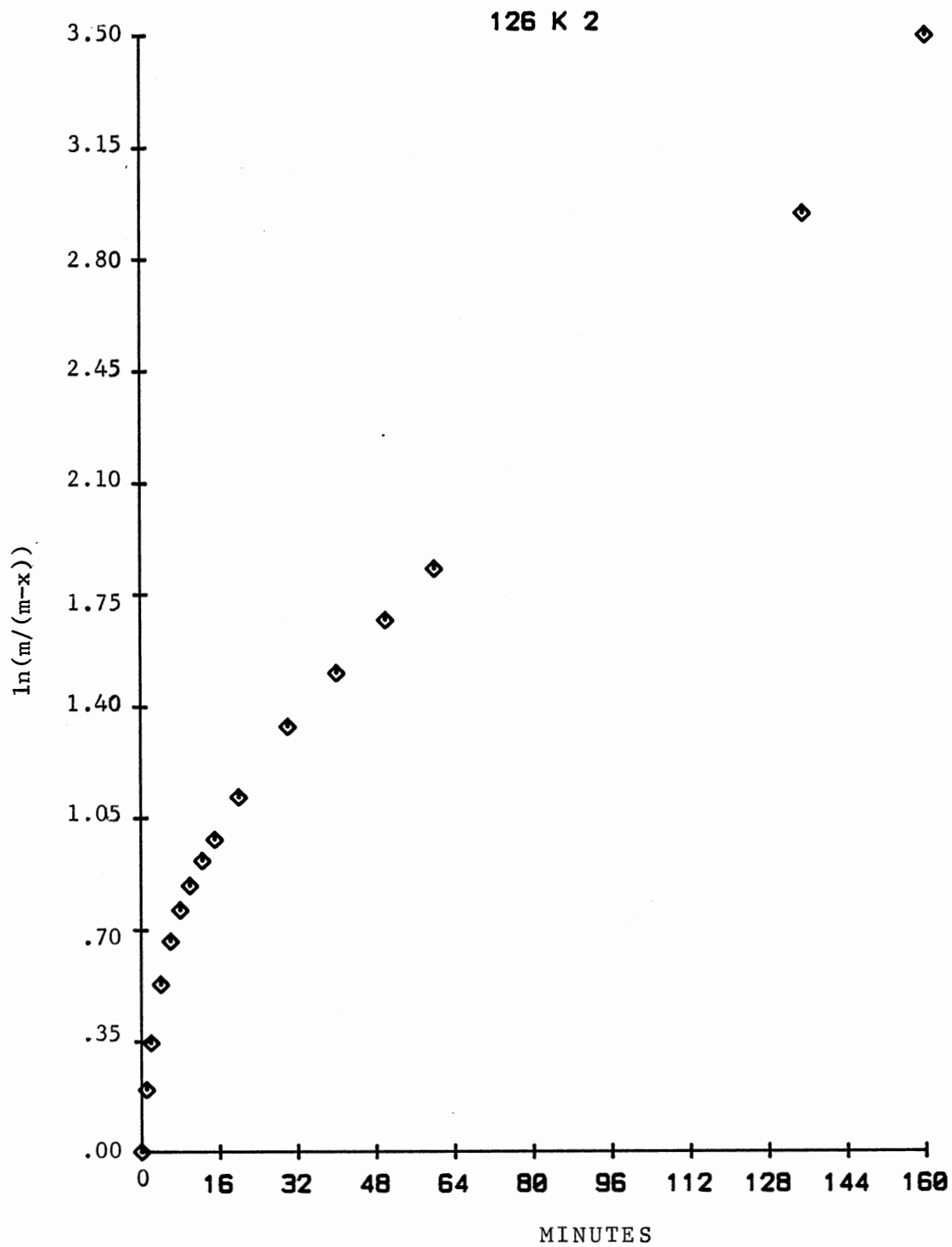


Figure 39. Integrated rate from February 126 K data.

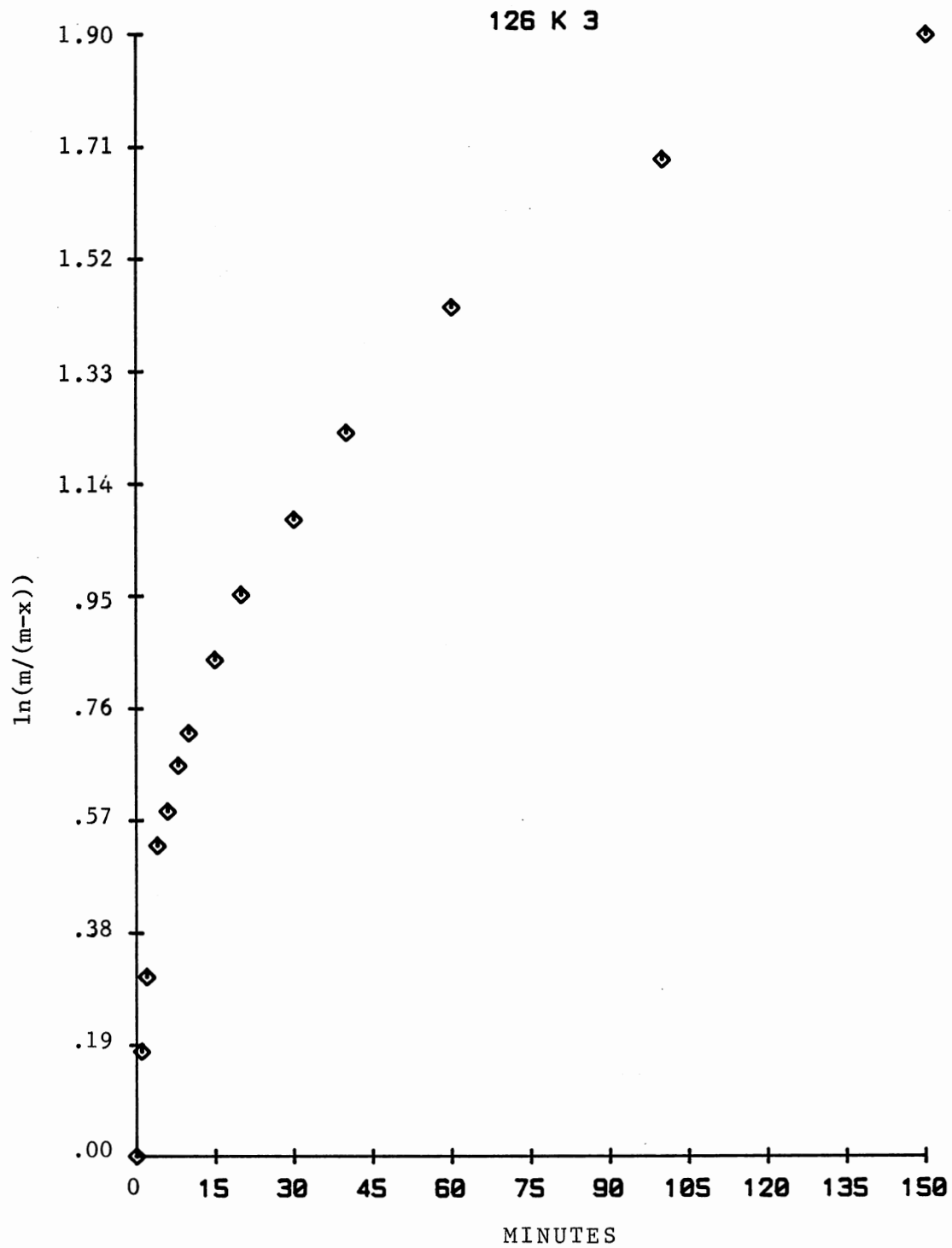


Figure 40. Integrated rate from March 126 K data.

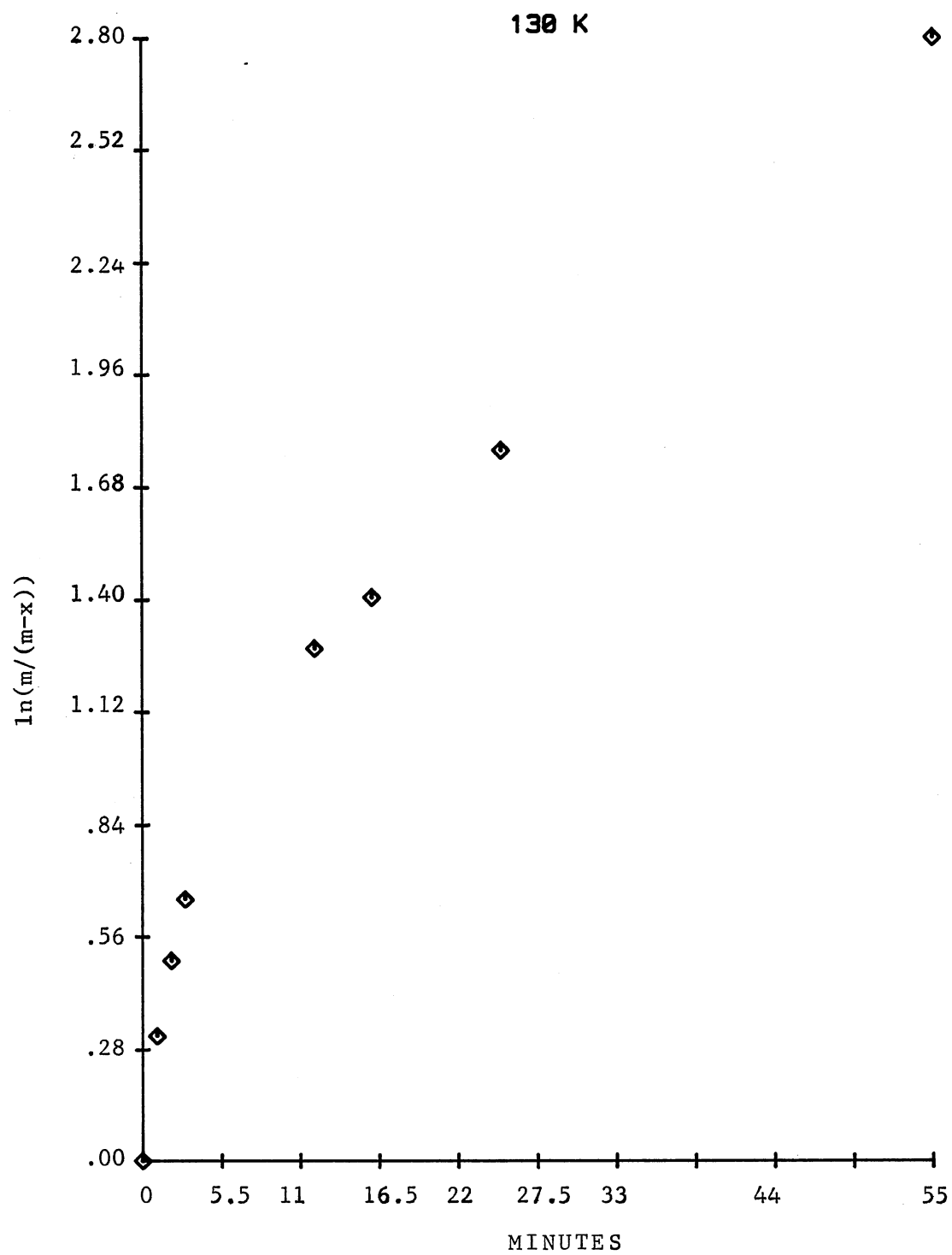


Figure 41. Integral of rate of 130 K data.

isotopic scrambling is dominated initially by the recombination part of reaction 3.1 so that the initial decay of the mobile proton concentration can be approximated by first-order kinetics:

$$[H^+] = [H^+]_0 \exp(-kt) \quad (3.11)$$

Keeping (3.10) in mind, the integrated form to which to compare the data is

$$\int_0^t [H^+] dt = C' [H^+]_0 (1 - \exp(-kt)) \quad (3.12)$$

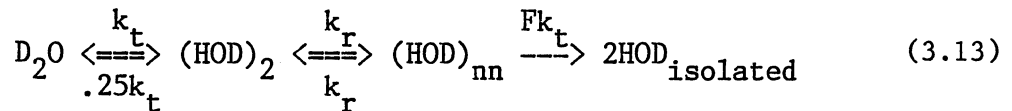
where C' is a composite of constants including k ; but this k along with the earlier k_H involves the basic proton hopping step which is only very weakly activated if at all. Observations of the hopping step from measurements on carrier mobilities have yielded values of less than 1 kcal/mole; in fact the most common values given are slightly negative (6). The temperature dependence will be found in $[H^+]_0$ as governed by a pseudoequilibrium in (3.2) if all other experimental conditions are the same. During the time period that the data series was gathered the irradiation times were always for two hours at 90 K and the cell was never opened to the atmosphere. In addition the constant temperature runs were staggered with respect to the overall time period of the series: the actual sequence being 113-123-115-120-126-117-130-126 and 120 K.

Appendix B contains a listing of the program used to fit data of the form $\ln(m/(m-x))$ to the function $C(1-\exp(-kt))$. The iterative nonlinear least-squares strategy of Marquardt (86) was used to vary C and, if desired, k for the best fit to the chosen number of points. The lowest temperature plots, 120-113 K, could be fit reasonably well to form of (3.12) over most of their time ranges and all of those yielded values for k close to an average of 0.0047. At temperatures 120 K and

above the single exponential could not reproduce both the rapid initial rates and the long term rate behavior. In keeping with the initial rate approximations made above only the first half-lives of the 130-113 K data sets were fit to (3.12) while holding k fixed at 0.0047 for all and varying the constant $C = C'[H^+]_0$ for the best fit. Table IV summarizes the results of the fits and Figures 42-50 contain smooth curves calculated with the fitted parameter along marked points derived from the data as in Figures 33-41. Finally, Figure 51 shows an Arrhenius plot made to determine the activation energy for the release of mobile protons from shallow traps.

High Temperature Data Fitting

The treatment of the high temperature data was similar to the previous analysis by Collier, Ritzhaupt and Devlin (59), who analysed data gathered at high temperatures ($T > 140$ K) by assuming that $[L]_{\text{mobile}}$ and $[H^+]$ quickly attain constant thermal equilibrium values at a given temperature. In this case the model of Figure 32 becomes



if the defect concentrations are combined with the rate constants to become k_t for proton transfer and k_r for water molecule rotation caused by L-defect passage. Also the minor species $(HOD)_{pc}$ was ignored and a constant factor F was introduced as in the earlier analysis. When fitting the data, the total observed uncoupled HOD was compared to the sum of the calculated $(HOD)_{nn}$ and the calculated HOD. Differential equations representing the model

TABLE IV

Best Pseudo-First Order Kinetic Parameters for
the First Half-lives of the 113-130 K Data

Date	T(K)	k	C	s.dev.
1/28/85	113	0.0047	0.3761	0.01256
2/11/85	115	0.0047	0.7131	0.01449
2/26/85	117	0.0047	0.9734	0.06860
2/15/85	120	0.0047	6.0079	0.06699
3/18/85	120	0.0047	6.1386	0.07780
2/ 5/85	123	0.0047	7.0828	0.11995
3/ 8/85	126	0.0047	21.48	0.1472
2/19/85	126	0.0047	26.63	0.1035
2/28/85	130	0.0047	50.975	0.1001

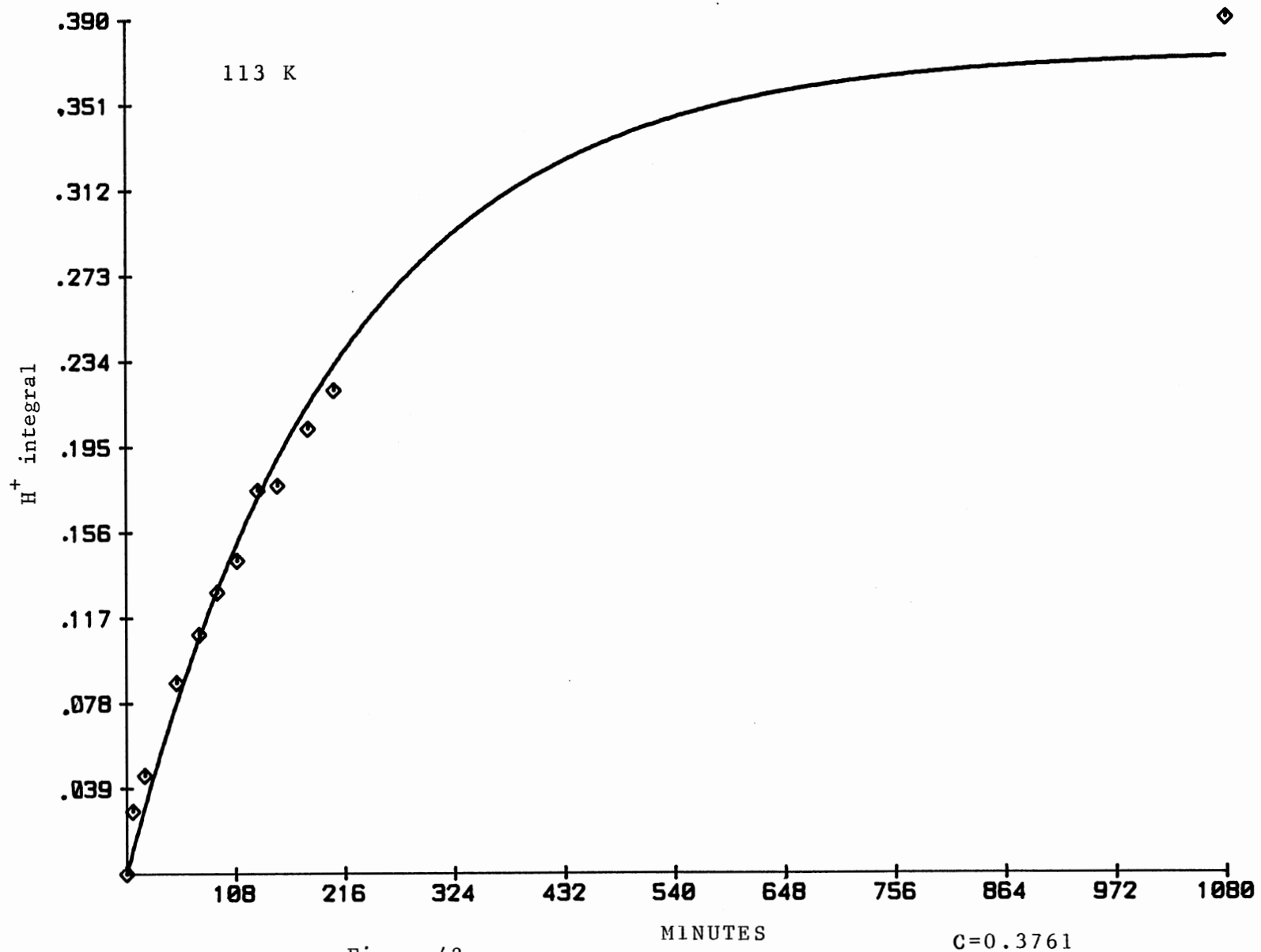


Figure 42.

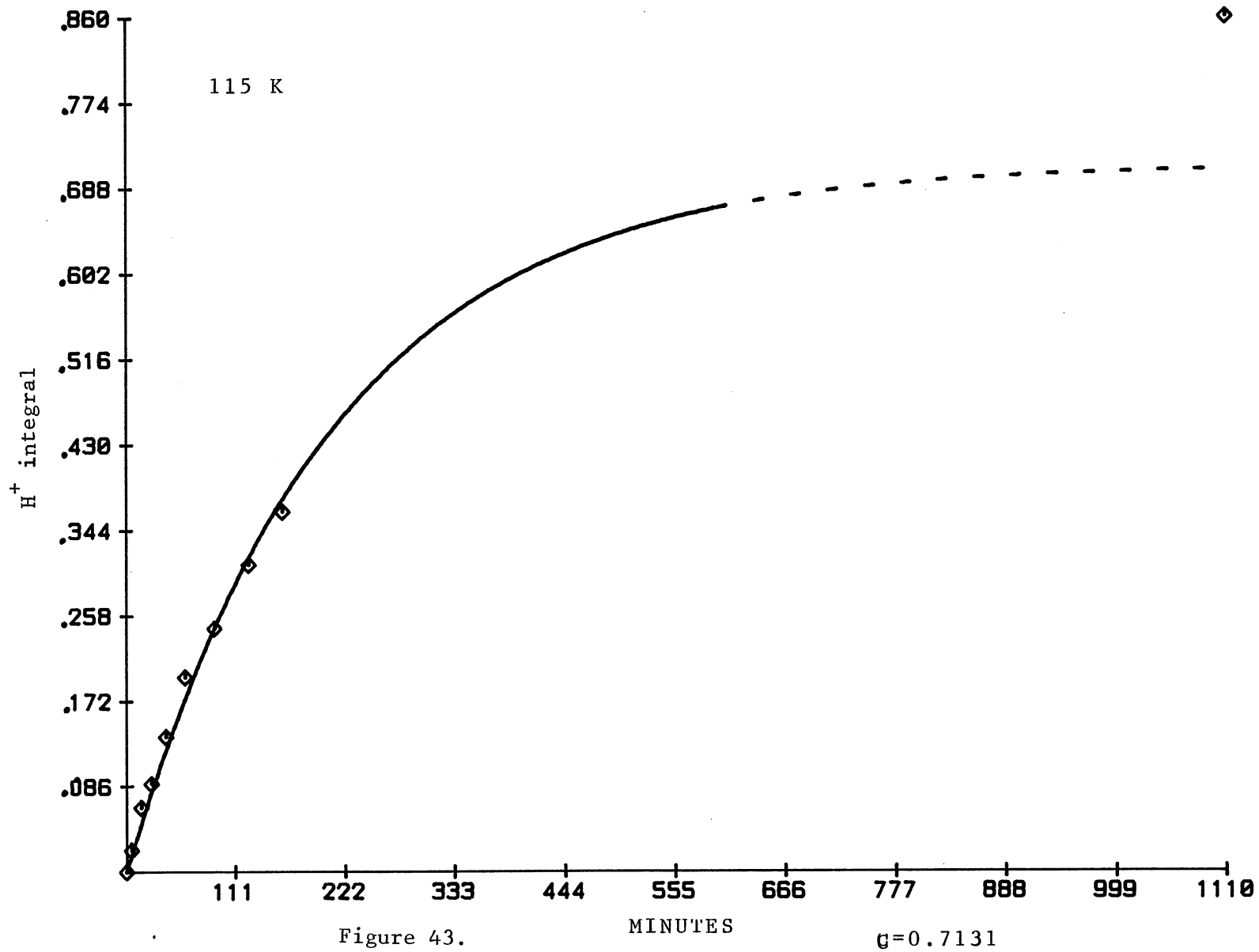


Figure 43.

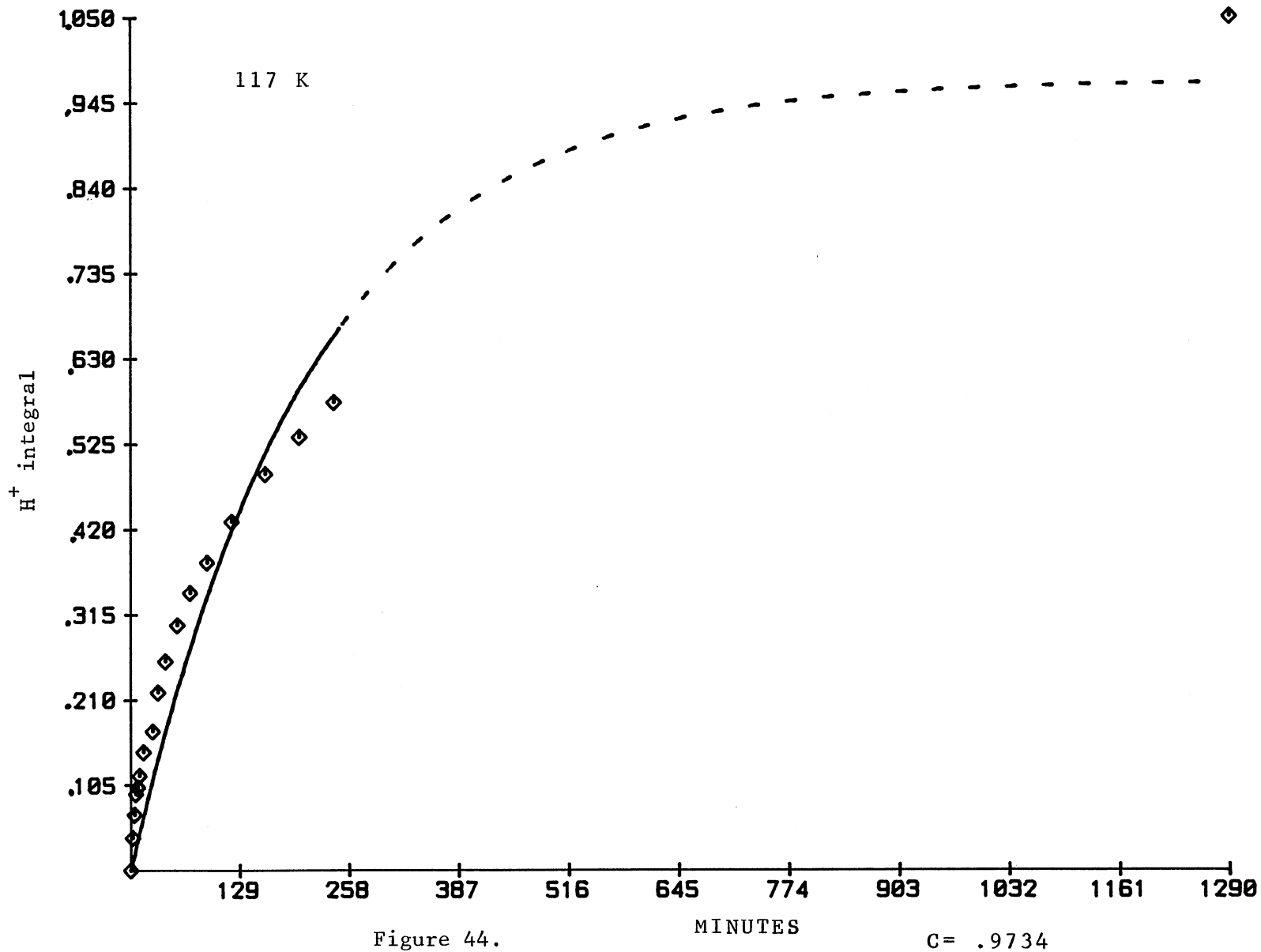


Figure 44.

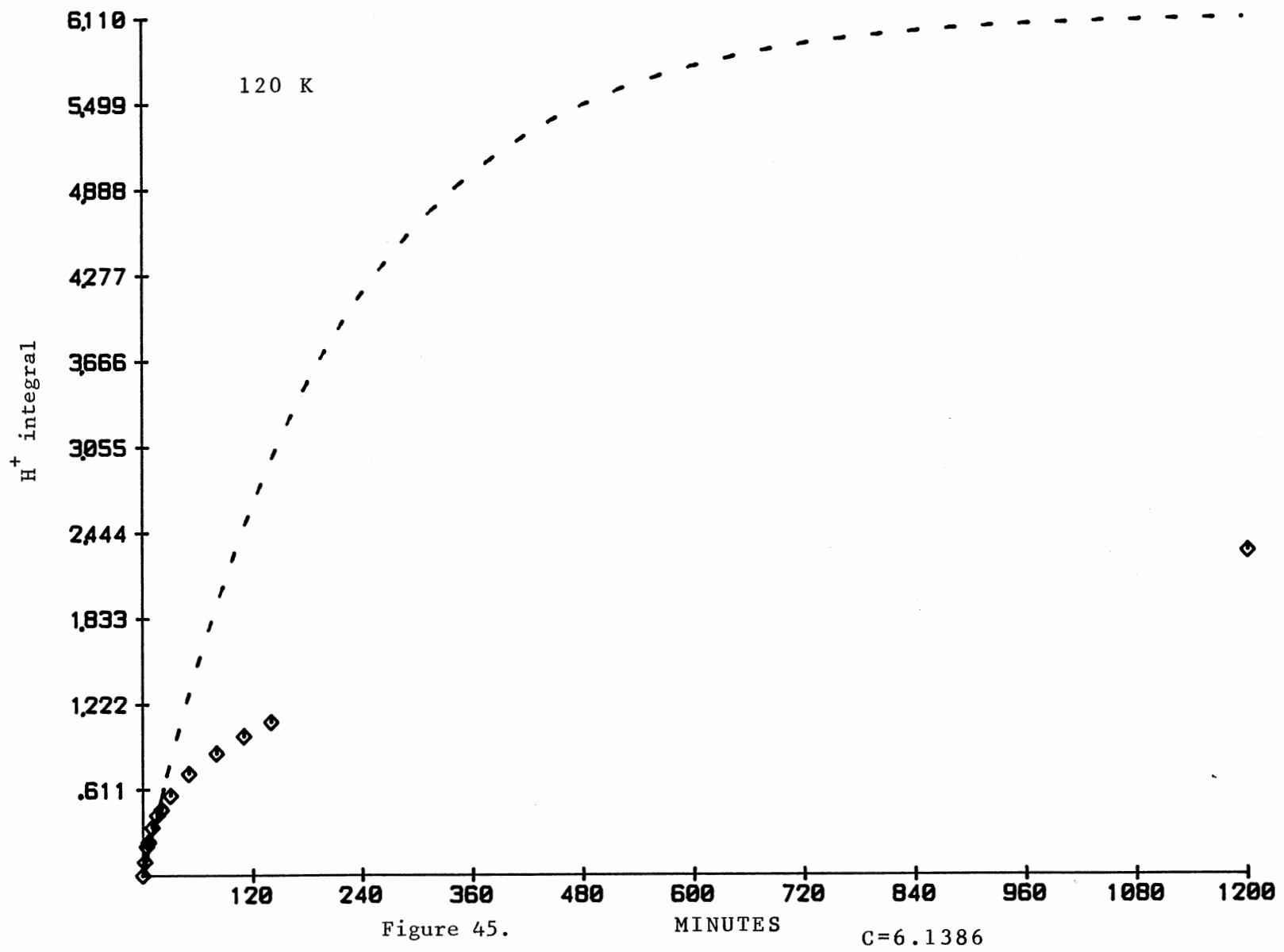


Figure 45.

C=6.1386

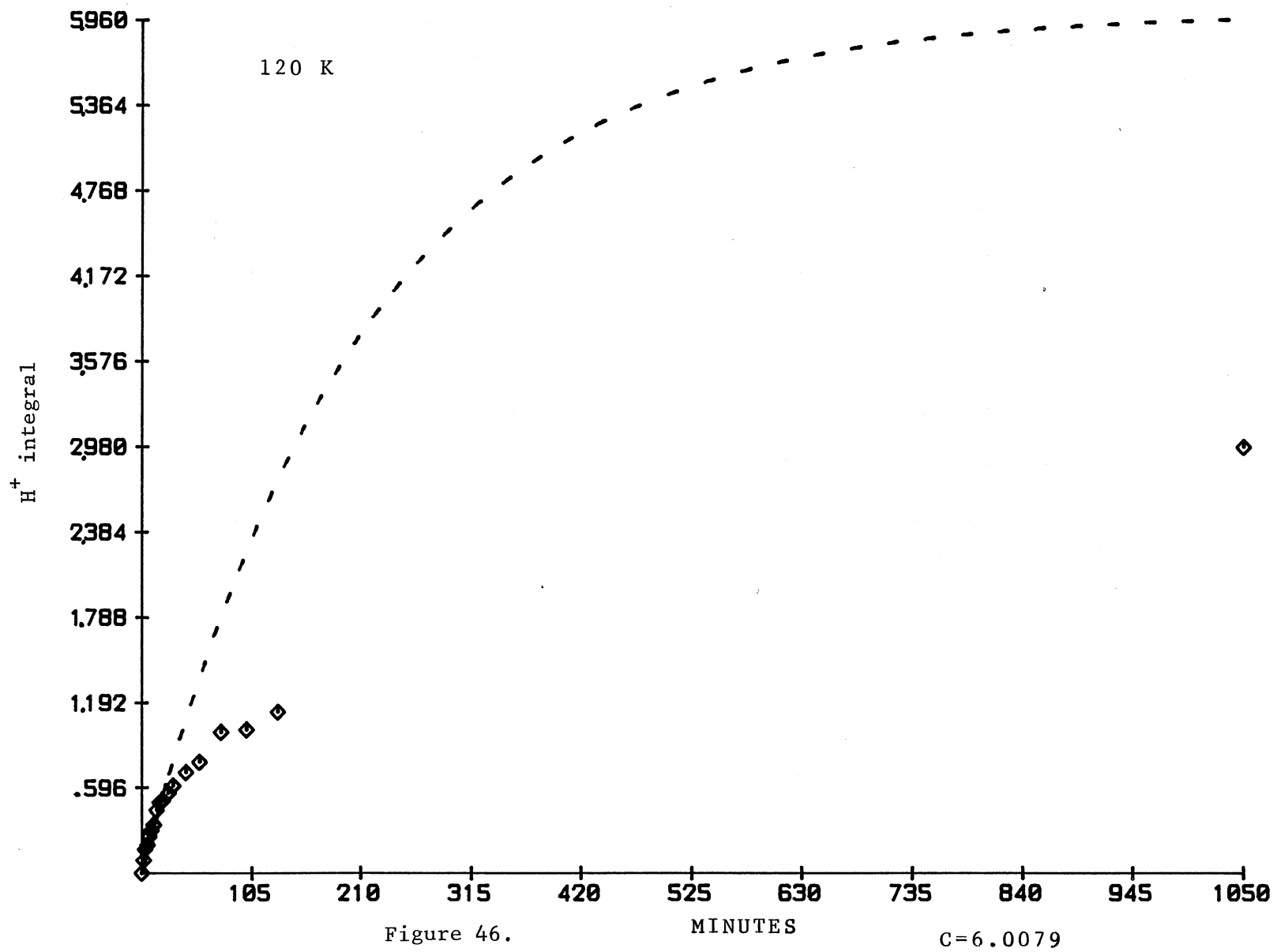


Figure 46.

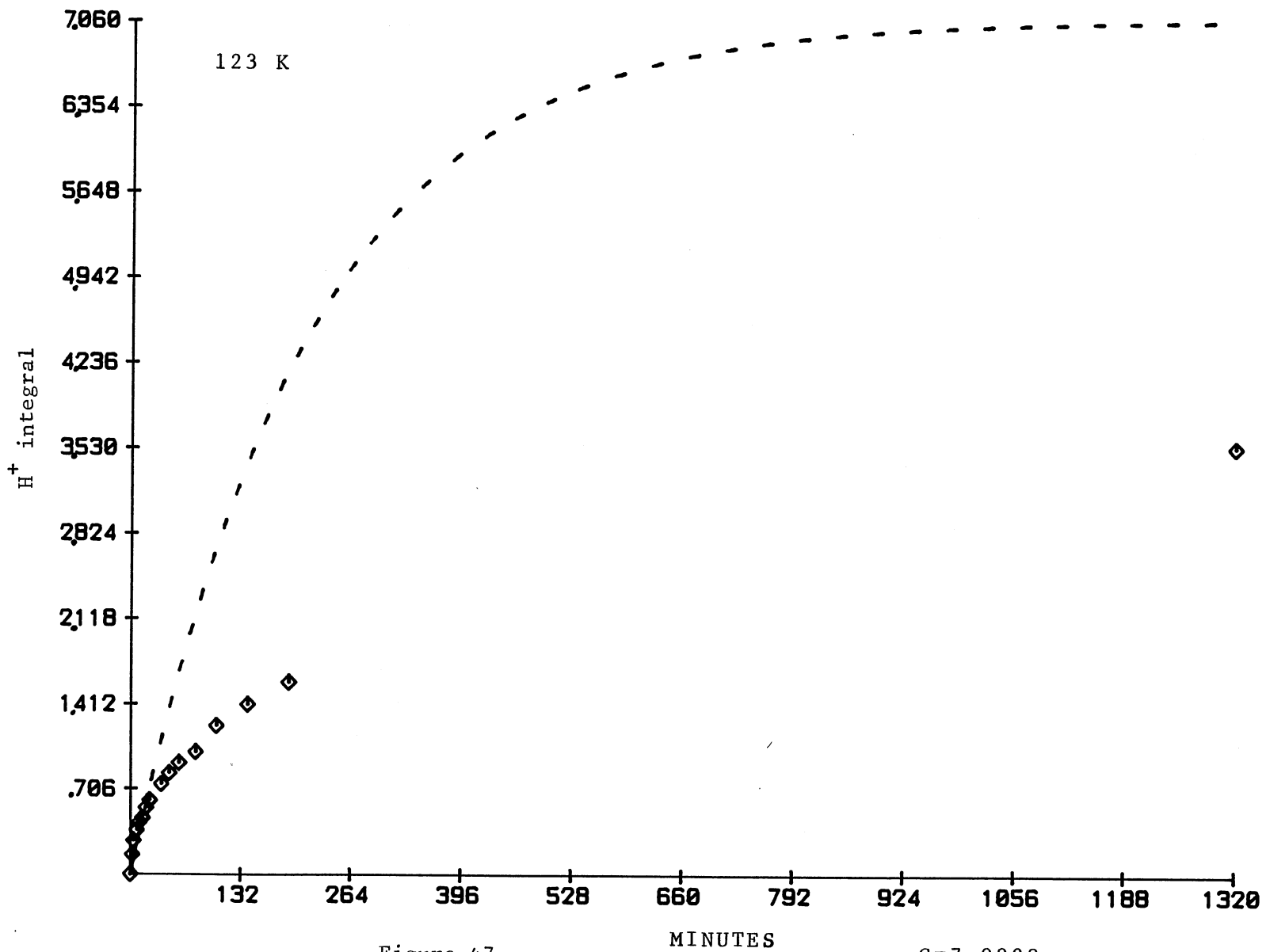


Figure 47.

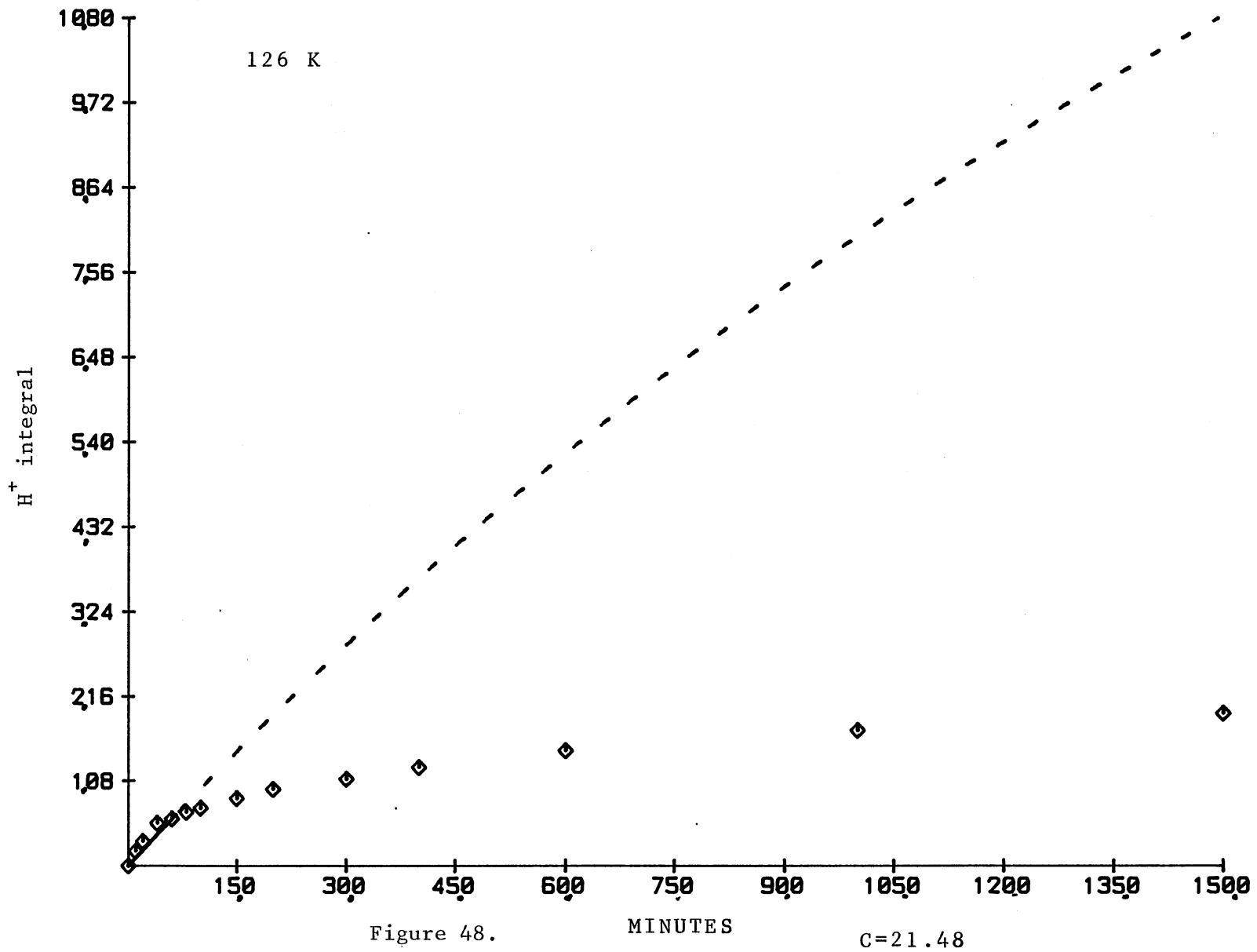


Figure 48.

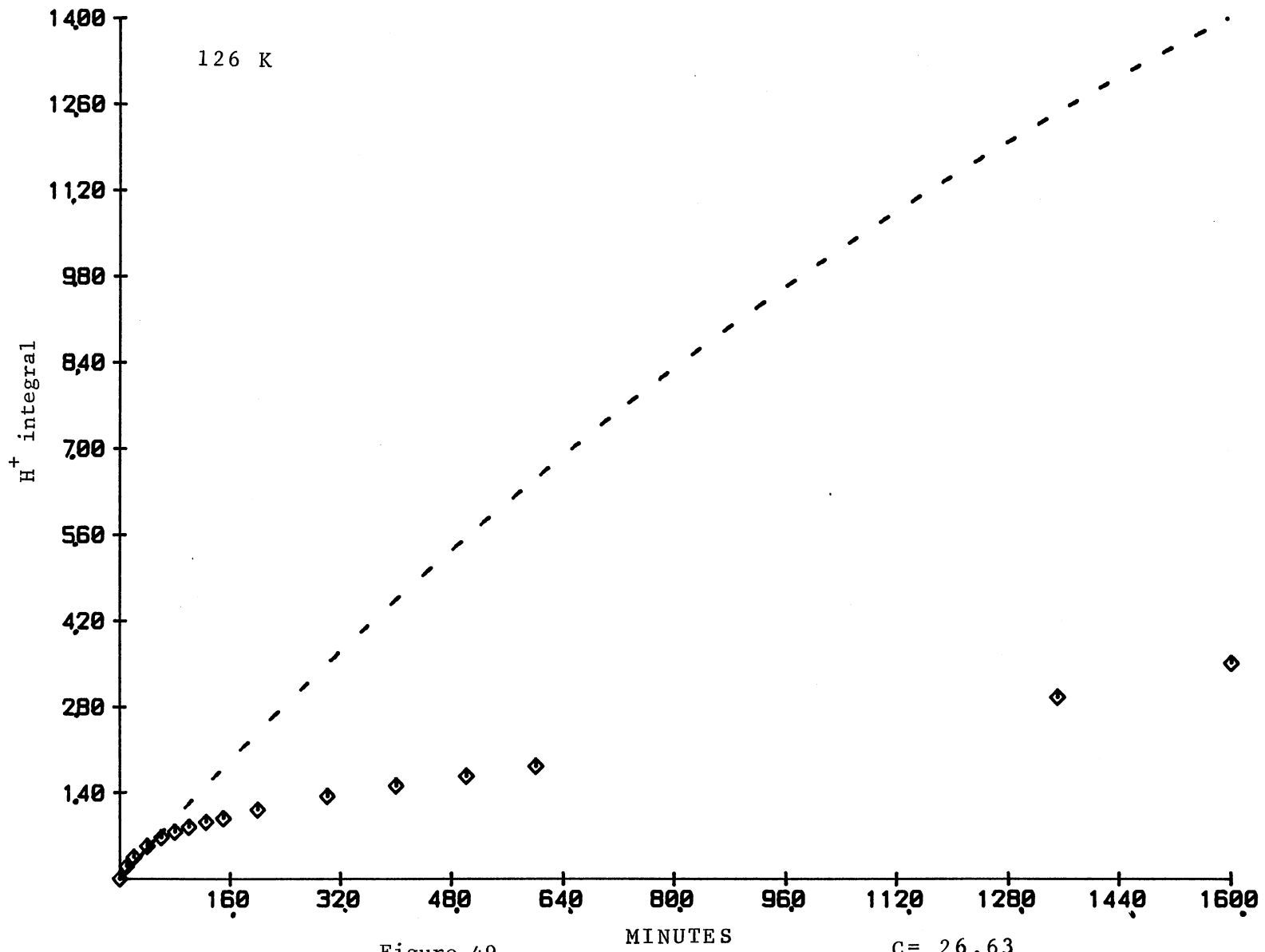
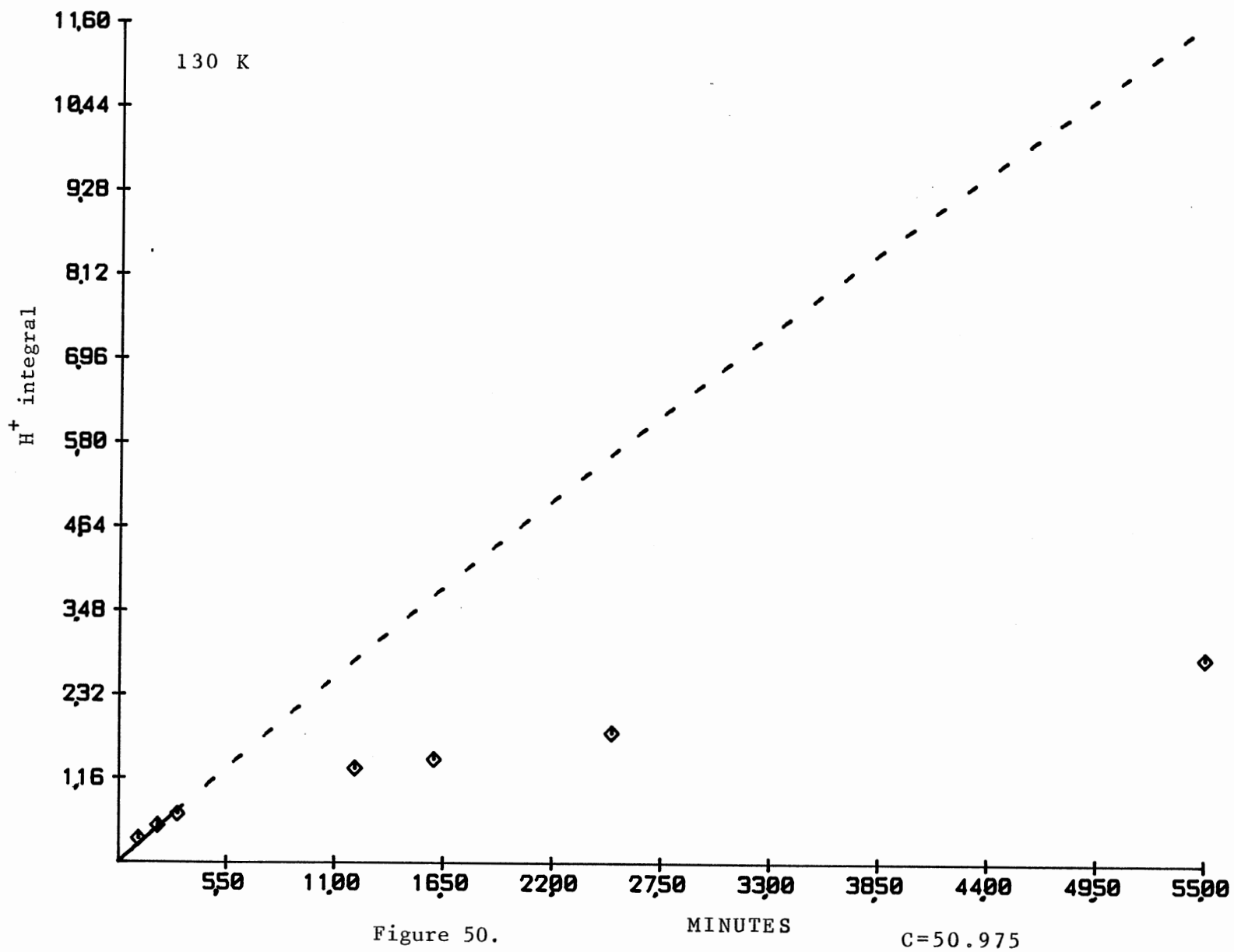


Figure 49.



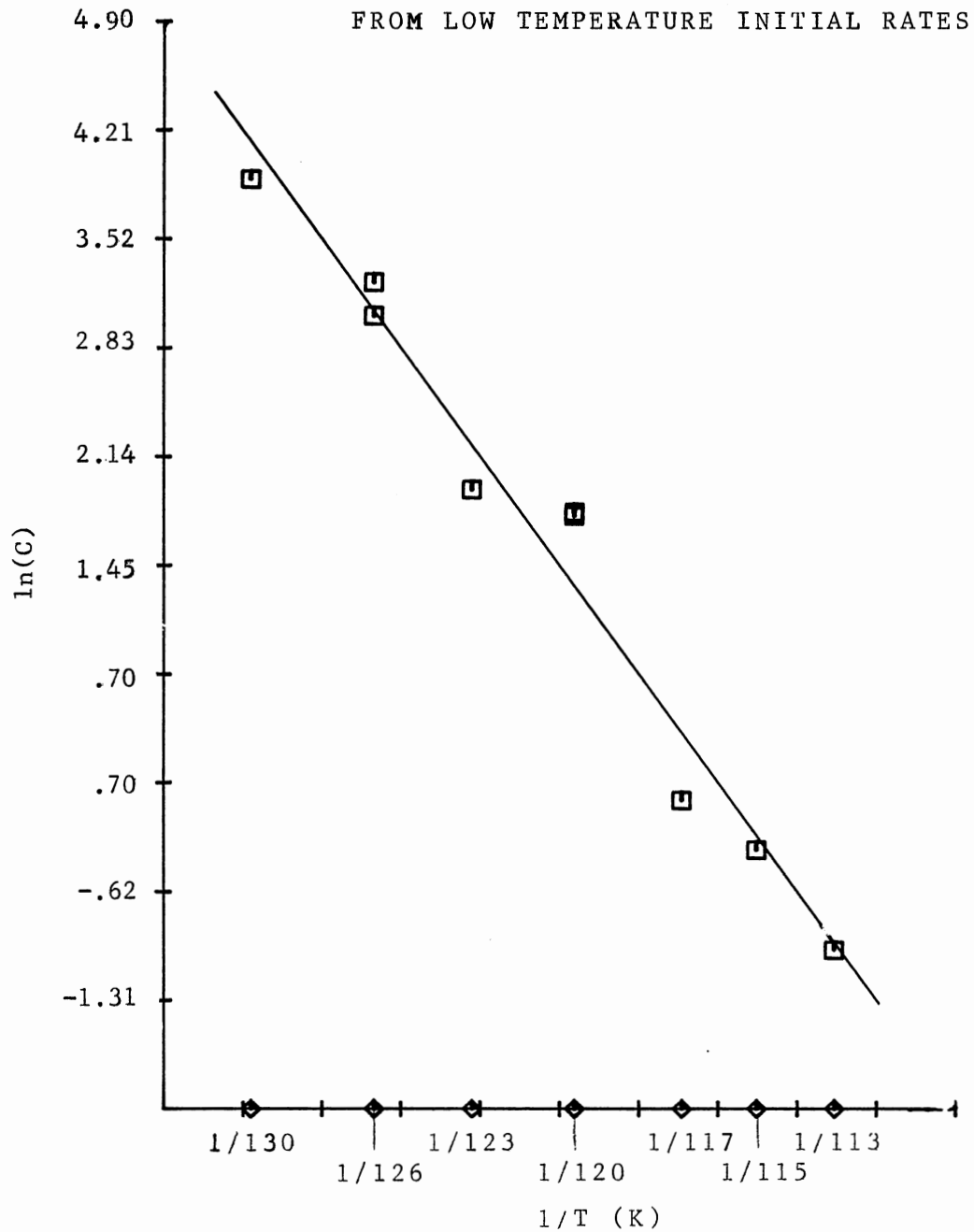


Figure 51. Arrhenius plot for release from shallow traps. The slope corresponds to 8.76 kcal/mole and has a correlation coefficient of 0.983.

$$\frac{d[D_2O]}{dt} = k_t (-[D_2O] + .25[(HOD)_2])$$

$$\frac{d[(HOD)_2]}{dt} = - \frac{d[D_2O]}{dt} - k_r ([(HOD)_2] - [(HOD)_{nn}])$$

$$\frac{d[(HOD)_{nn}]}{dt} = k_r ([(HOD)_2] - [(HOD)_{nn}]) - Fk_t [(HOD)_{nn}]$$

$$\frac{d[2HOD]}{dt} = Fk_t [(HOD)_{nn}]$$

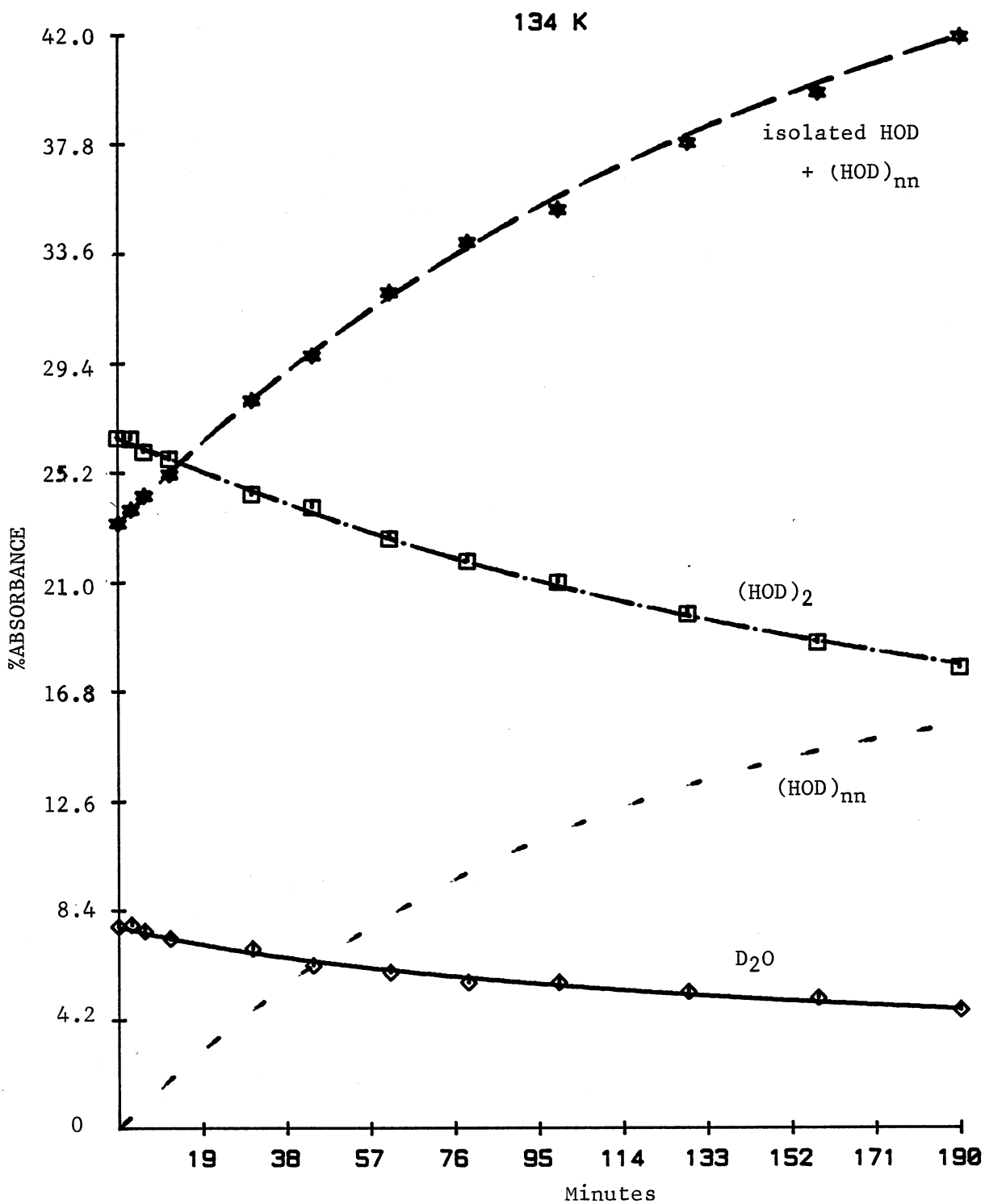
were coded into an iterative nonlinear least-squares fitting program and the parameters, k_t , k_r , F , $[(HOD)_{nn}]_0$ and the molar absorptivities of D_2O and $(HOD)_2$ relative to isolated HOD, were adjusted to obtain the best fit. The program is described and listed in Appendix C. Calculated parameters are summarized in Table V and plots of the calculated absorbance changes vs. time along with the actual data points are shown in Figures 52-59.

That model provided a good fit to the high temperature data and a linear Arrhenius plot from the k_r 's and hence the activation energy for $k_L[L]$ as shown in Figure 60. Because the mobile proton concentrations had been intentionally modified by the 90 K irradiations and because samples were annealed at different temperatures in the 113-130 K range, an Arrhenius plot made from the k_t 's would not have good correlation.

TABLE V

Best Constants From Higher Temperature Analysis

Date	T(K)	Kr	Kt	F	$[(\text{HOD})_{\text{nn}}]_0$	s.dev.	$e_{\text{D}_2\text{O}}$	$e_{(\text{HOD})_2}$
2/ 9/85	160	18.05	1.900	0.5998	0.000296	0.764	1.15	1.22
2/16/85	150	0.4421	1.225	0.4674	8.7121	1.24	0.74	1.28
3/ 8/85	145	0.1383	0.1222	0.6383	5.136	1.29	1.11	1.56
2/19/85	145	0.1170	0.09253	0.7664	1.7192	0.939	1.29	1.31
2/27/85	140	0.05245	0.2628	0.08514	11.8255	0.590	1.79	1.07
3/19/85	140	0.03903	0.1175	0.2794	0.00009	0.541	1.27	1.36
2/12/85	137	0.01873	0.1986	0.04462	8.2529	0.622	1.44	1.17
2/ 5/85	134	0.004028	0.03483	0.04653	0.000002	0.225	1.25	1.27



$$k_t = 0.03483 \quad k_r = 0.004028$$

Figure 52.

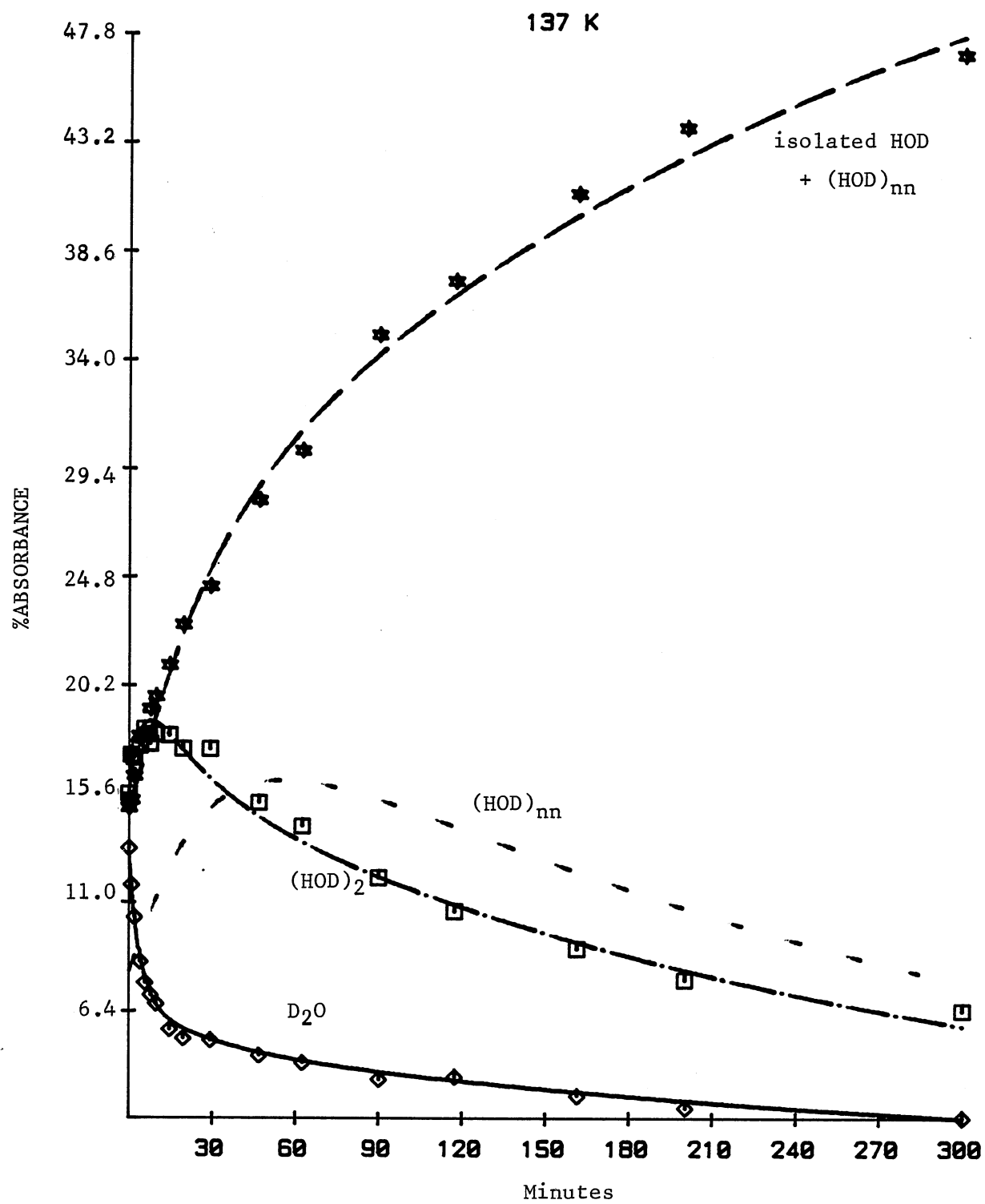


Figure 53.

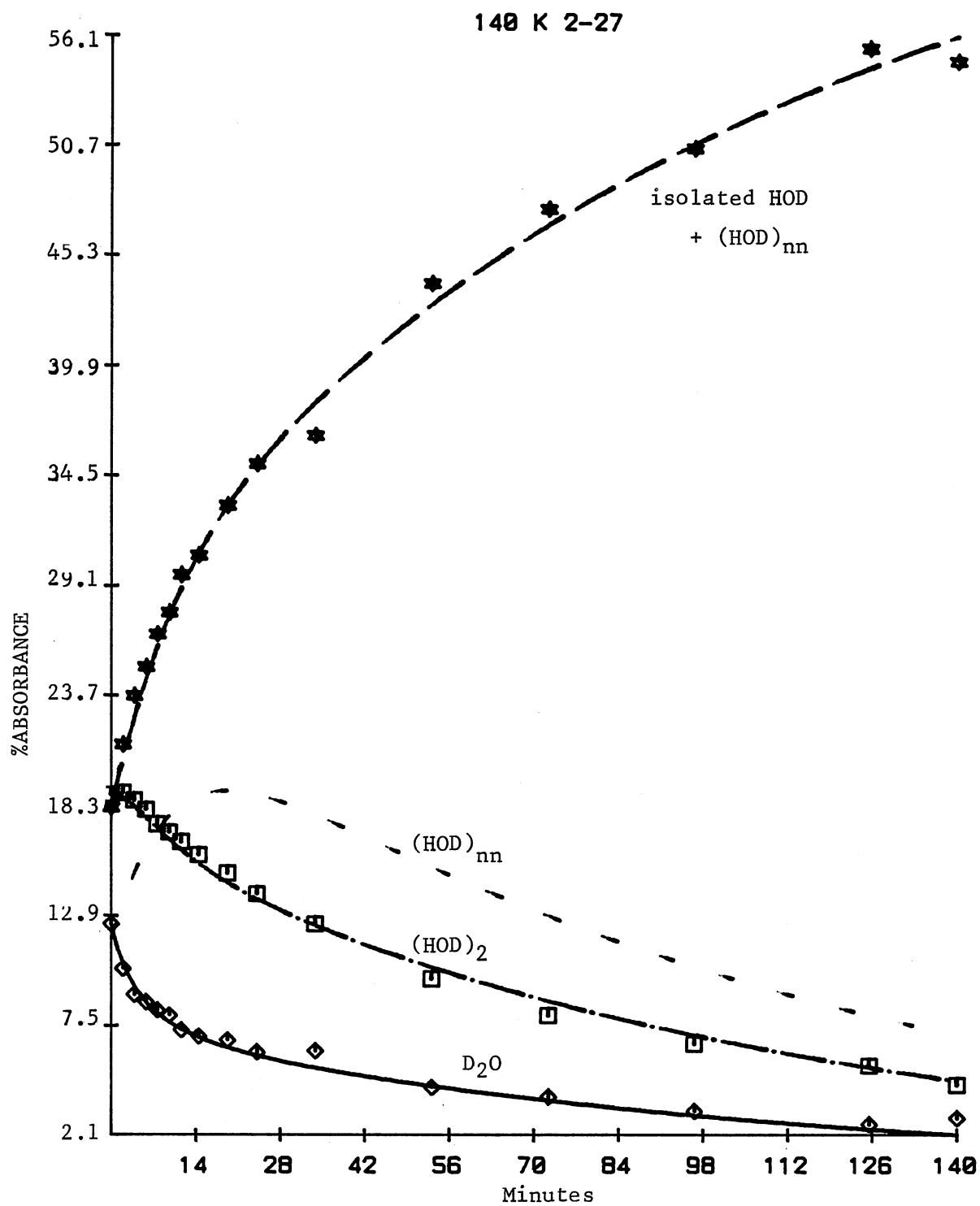


Figure 54.

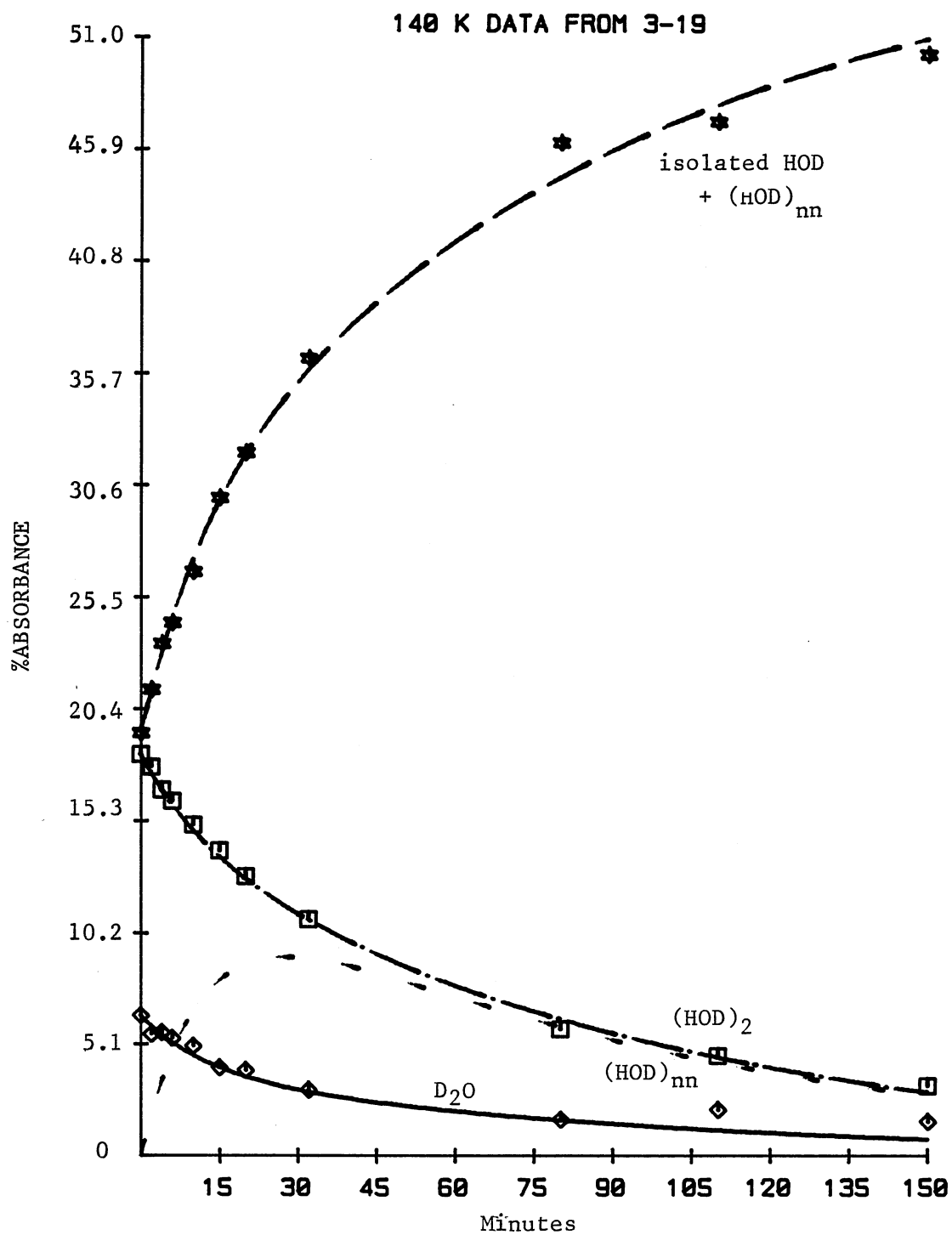


Figure 55.

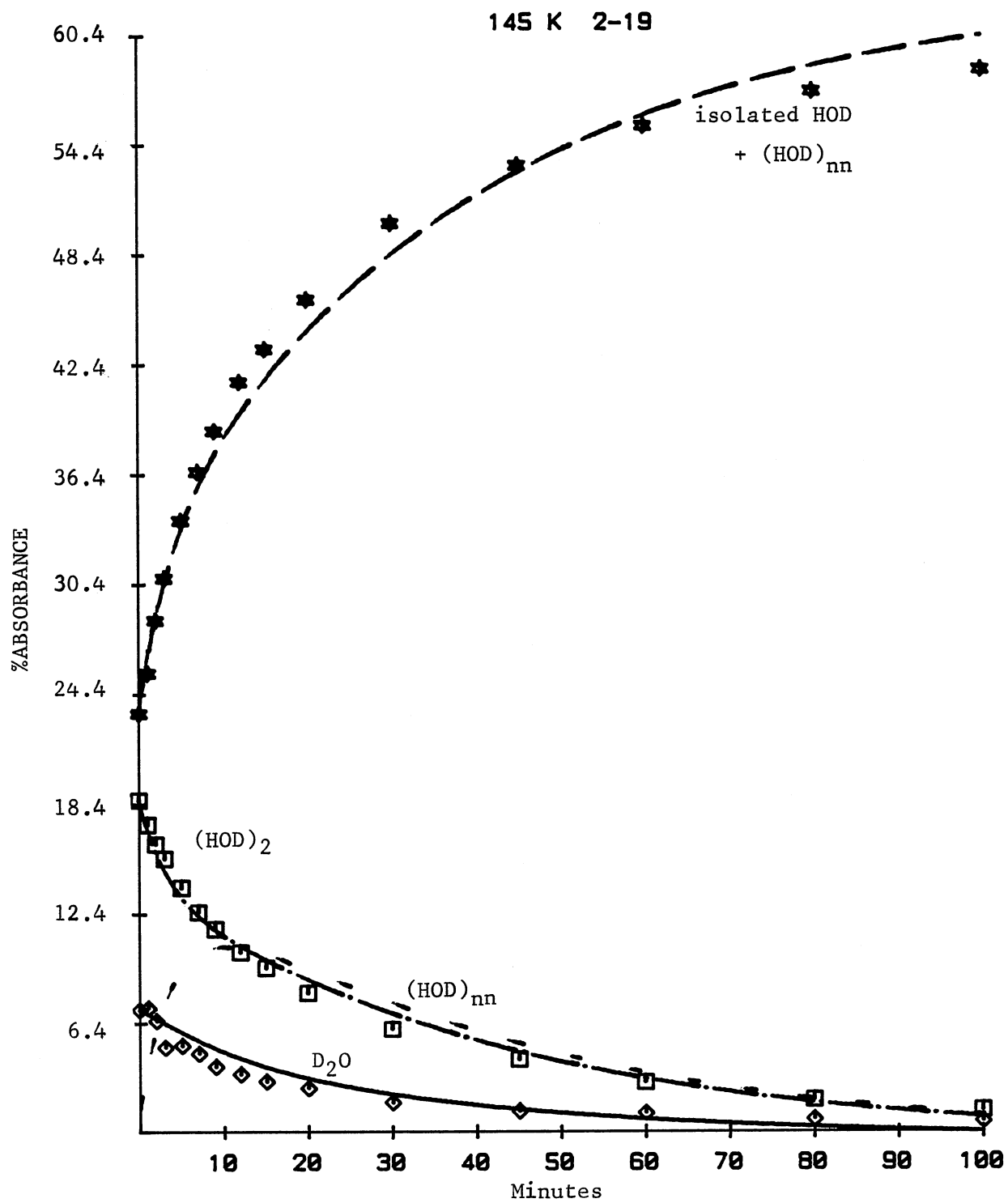


Figure 56.

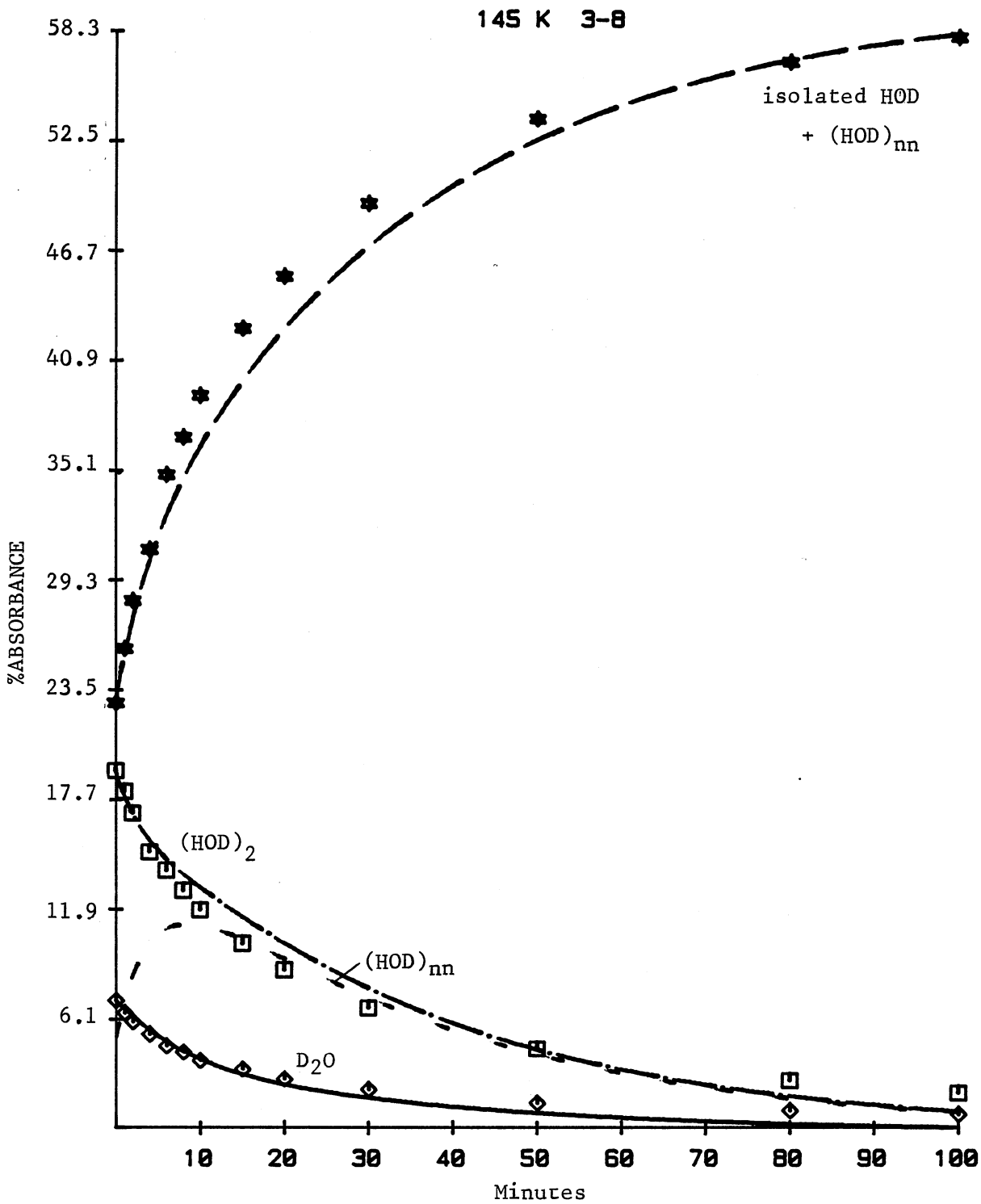


Figure 57.

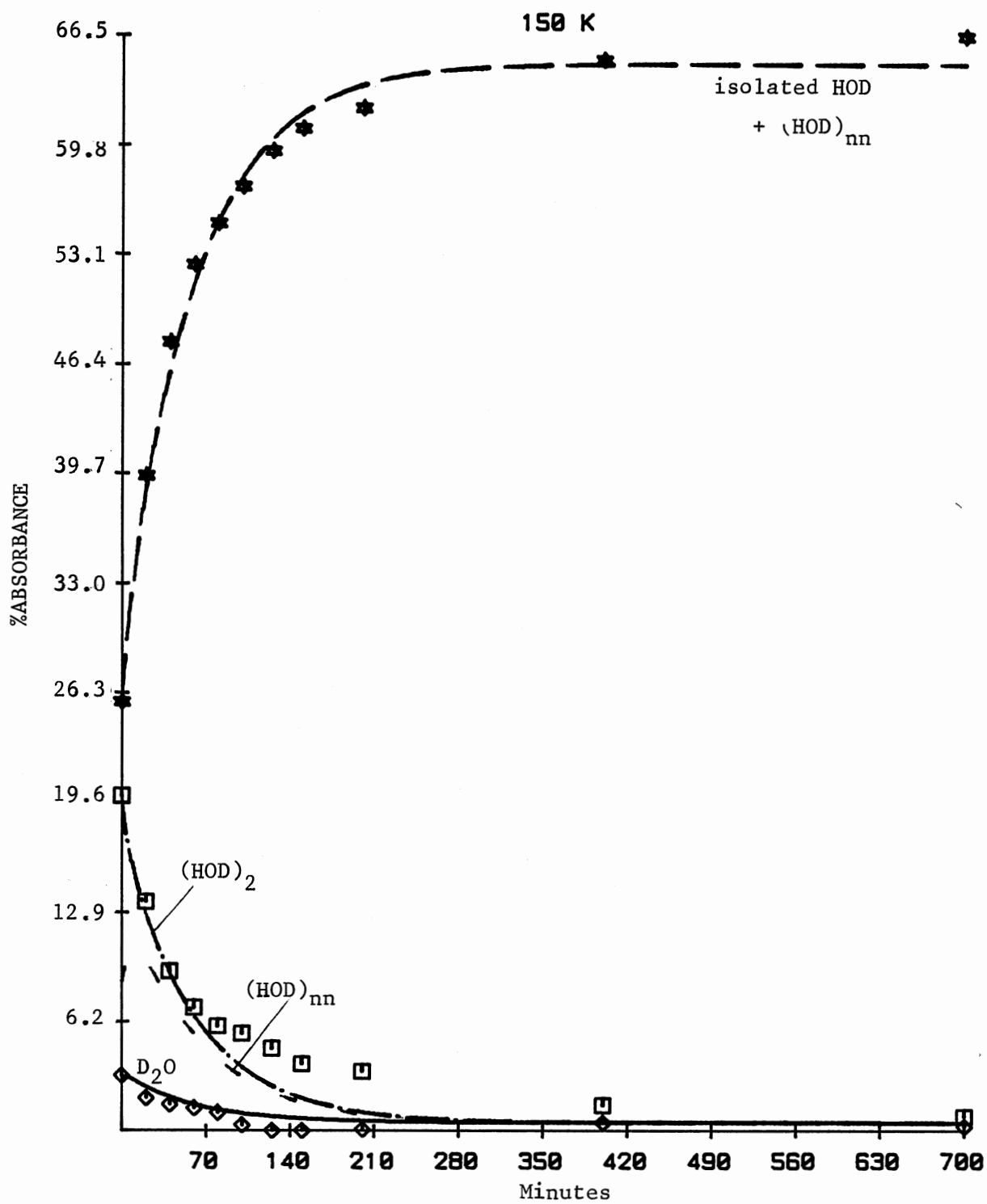


Figure 58.

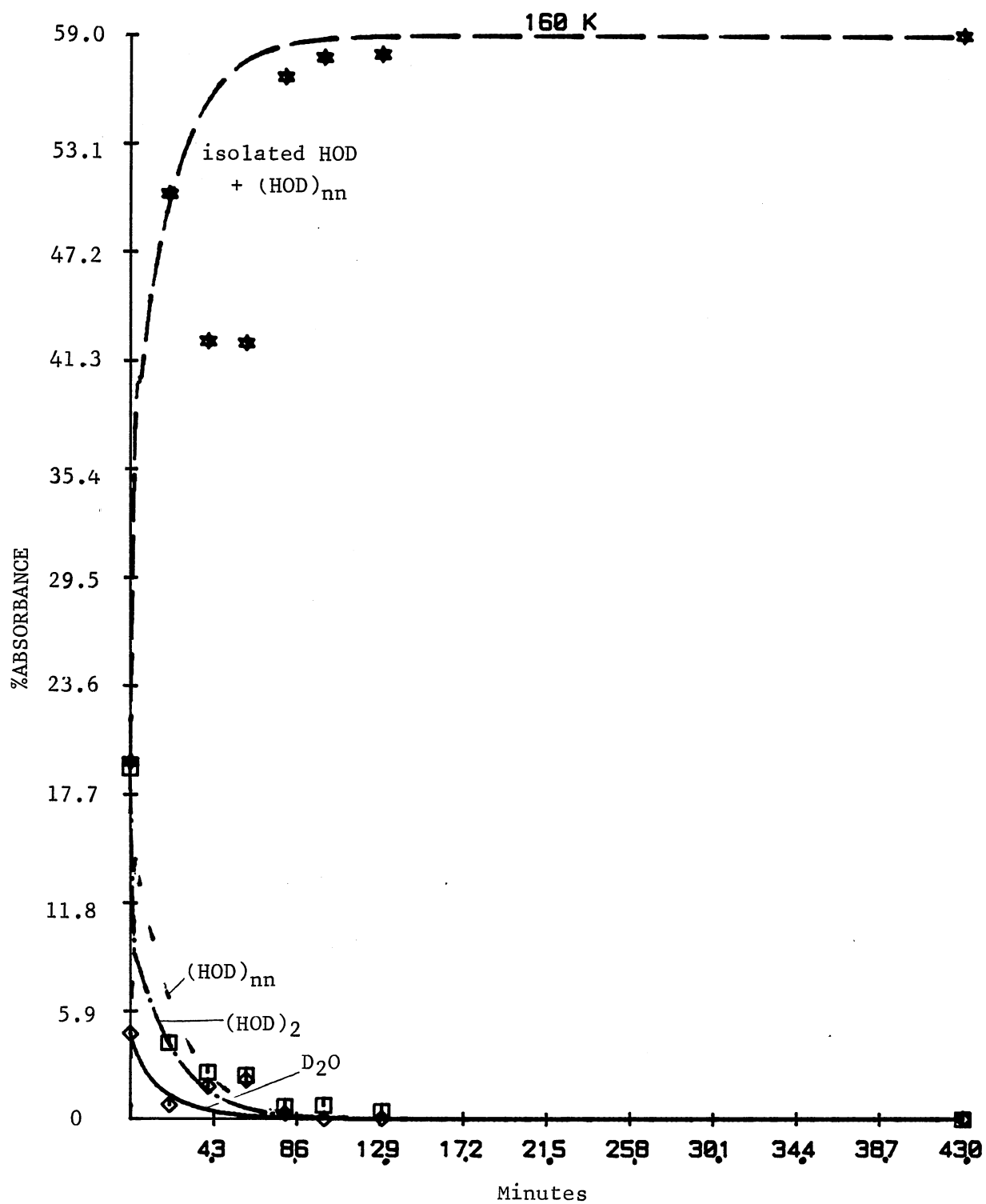


Figure 59.

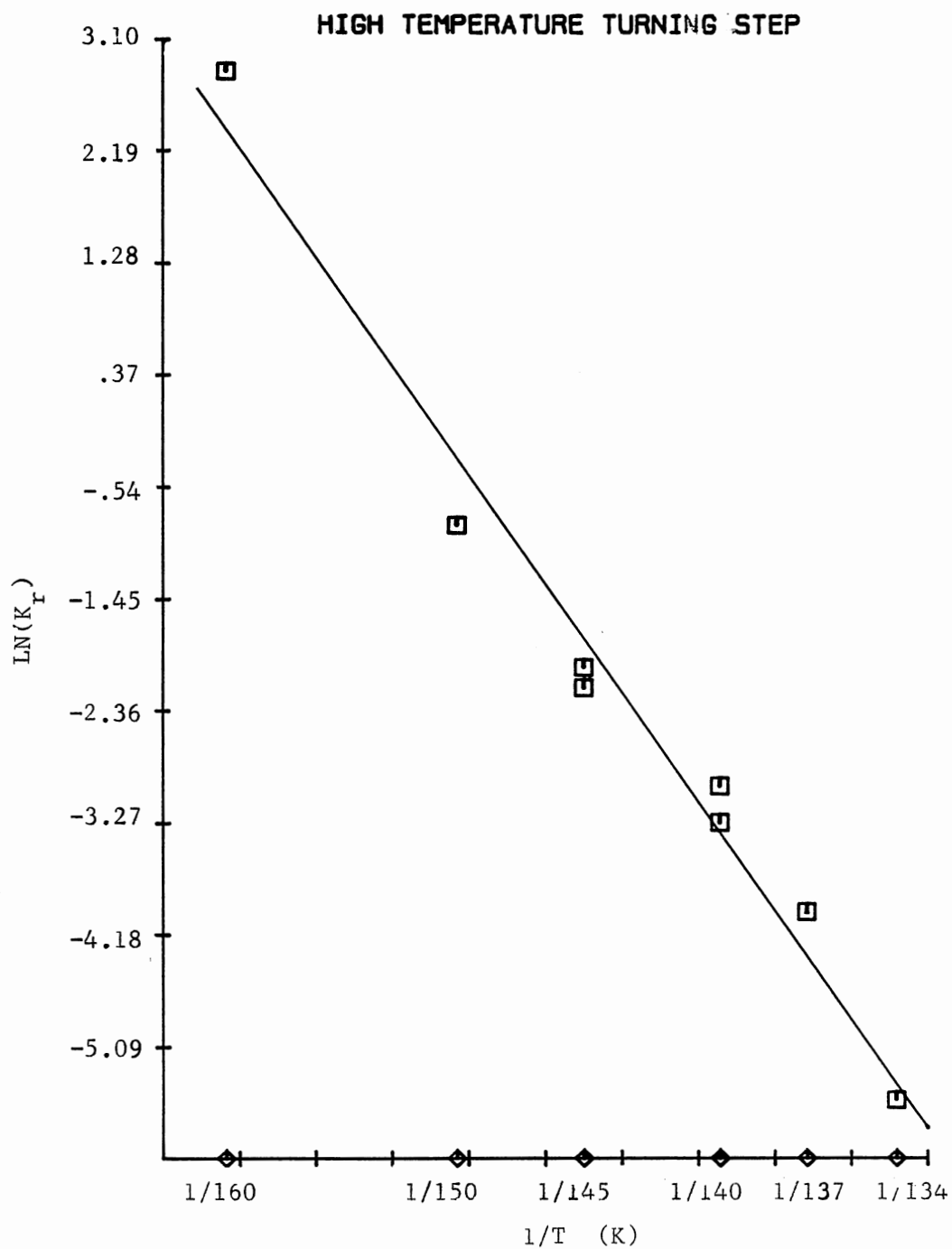


Figure 60. Arrhenius plot for L-defect activity. The slope corresponds to 12.8 kcal/mole and has a correlation coefficient of 0.988.

CHAPTER IV

DISCUSSION AND SUMMARY

Discussion

One goal of this study was to seek the photoionization of low temperature ice using energies less than those of electron beam radiolysis. Photons at wavelengths longer than about 190 nm were found to be ineffective at ionizing ice, in apparent contradiction to the liquid water work of Goodall, et. al. (77,78), who observed the effects of ionization following intense laser pulses at wavelengths around 1 micron, where OH stretching overtones absorb. It cannot be said for certain why liquid water undergoes single photon dissociative ionization and ice does not, especially considering the similarity of the absorption spectra at the wavelengths involved, but perhaps the much lower thermal energy in 90 K ice does not support separation of an ion pair by more than some geminant recombination distance. Or perhaps the total lack of orientational mobility in ice at temperatures less than 110 K causes the effect not to be observed, though separation without orientational mobility should be possible, as in the hopping steps shown in Figure 12.

Dissociative photoionization in ice was indeed observed at higher photon energies: 184.9 nm light was effective but 253.7 nm was not. At this energy the proton may be ejected from a water molecule site and thereby not require thermal energy or orientational mobility to separate

the ions. The uv photoionization was found to occur down to the lowest temperature obtainable, 12 K. The evidence of photoionization was the observation of the conversion of D_2O to neighbor-coupled HOD. There can be no doubt that the conversion is caused by mobile protons in light of the basic mechanism which must be involved and also the fact that similar results could be induced using a known source of mobile protons in ice--photolysis of a frozen solution of o-nitrobenzaldehyde, which Konstantinov et. al. (84) observed to convert pH indicator molecules frozen in ice to their acid colors upon warming after uv photolysis at 77 K. Further, Petrenko et. al. (80) found increased electrical conductivity during uv illumination of nitrobenzaldehyde containing ice samples, which is a direct consequence of an increased mobile proton concentration.

Another goal was to study the shallow trapping of mobile protons which had been generated in ice at temperatures low enough that normal thermal processes were negligible. At about 90 K or lower these protons were always quickly trapped before causing much isotopic exchange. Previous experiments (76) demonstrated the shallow trapping effect in electron-beam-ionized ice, but that sort of radiolysis is known to cause many structural defects in a crystal, perhaps generating proton traps much faster than mobile protons, though Warman's results suggest otherwise (75). That the shallow traps are truly intrinsic to ice, and so are present in any ice sample, is strongly suggested by the demonstration of trapping in ice that has been subjected only to mercury lamp illumination. The intrinsic nature of the traps cannot be stated with absolute certainty from this study, because these wavelengths are known to produce slight concentrations of other species besides the

ions, such as H, OH and H_2O_2 (50). If however the traps were being produced by the uv photolysis, then they would be produced at the same time as the mobile protons and so a proton liberated during the first part of the irradiation would have many more opportunities to visit D_2O sites before meeting with one of the still dilute shallow traps. To verify that the trap concentration was not increasing dramatically during the course of the photolysis, experiments were performed in which spectra were taken at intervals during the irradiation period. The results did show that the slight progress of the D_2O to coupled HOD reaction was linear with irradiation time, further strengthening the suggestion that the shallow traps for mobile protons are truly intrinsic to ice.

The kinetics of the release of mobile protons from the shallow traps was examined in terms of a model in which mobile protons rapidly attain a pseudoequilibrium with trapped protons and the proton concentration is gradually diminished by combination with deep traps. The deep traps may in fact be a number of different species: the term used in the data treatment sections was OH^- but another possibility for uv irradiated ice would be solvated electrons, and for naphthol-doped ice the ground state naphtholate ion. But in any case, the charge balance of the sample is maintained and the kinetics are the same whether all of the deep traps are given the same label or not, assuming the deep traps all have similar depths. The goal to evaluate the depth of the shallow traps also required the assumption that there was only one shallow trap depth rather than a variety of traps having a spread of depths. Good linear correlation of the Arrhenius plot (Figure 51) over the entire temperature range supports that assumption. The

activation energy for release from shallow traps was determined to be 8.76 kcal/mole, which is only slightly lower than the activation energy determined for the thermal generation of mobile protons in cubic ice for the temperature range 135–150 K, i.e. 9.5 kcal/mole (59), and considerably higher than Kunst and Warman's estimate of 4.2 kcal/mole for the release of mobile protons from shallow traps in hexagonal ice ionized by a pulsed electron beam at much higher temperatures (75). It cannot be said now whether the difference between Kunst and Warman's value and the value of 8.76 determined here is due to the vast temperature difference, to the different ionization sources, to the different nature and treatment of the data, or perhaps even due to unequal defect energies and populations in cubic versus hexagonal ice, though a very large difference from I_c to I_h is unlikely considering that the energy difference is only 0.012 kcal/mole (32) and the other similarities. When comparing the present value to Kunst and Warman's it must be held in mind that they concluded that the basic proton hopping step had an activation energy of -5.1 kcal/mole whereas this analysis utilised the traditional concept that the step is much more weakly activated. Actually, in their experiments (which were from near the melting point of ice to roughly 40 degrees below) the initial conductivity yield from an ionization pulse was independent of the temperature but the initial amount of optical absorption assigned to solvated electrons in ice was activated by 5.1 kcal/mole. That optical absorption at 680 nm was assumed to be directly proportional to the initial mobile proton yield at all temperatures. Conductivity is proportional to the product of carrier concentration and mobility so the proton mobility was deduced to be activated by -5.1 kcal/mole. The

activation energy of 5.1 kcal/mole for the production of mobile protons by electron beams implies a very small yield at 90 K and a vanishing small yield at 10 K. Electron beam radiolysis of the ice at 90 K was, however, shown to generate an appreciable amount of mobile protons (76).

There is no data available on the electron beam radiolysis of ice containing isolated D_2O at temperatures below 90 K, but the effects have been observed in the oxirane clathrate hydrate at 75 K and at 30 K (87). Being at least 80% H_2O , the clathrate hydrates have many similar properties as ice including the hop-turn conduction and isotopic scrambling mechanism and also including unique spectral contributions due to D_2O , $(HOD)_2$ and isolated HOD in the otherwise H_2O cage structure (87).

A previous study by Collier et. al. (39,59) determined activation energies for the purely thermal generation of mobile protons in cubic ice as well as for mobile Bjerrum L-defects. Of the two, the L-defect activation energy was probably less accurately determined because the quality of rate data for the step $(HOD)_2 \rightarrow 2HOD$ depends on how well the amount of $(HOD)_2$ is determined, and in the purely thermal study of D_2O scrambling in H_2O ice, $(HOD)_2$ is always in low concentration relative to the other deuterated species. In this work the ultimate condition of a sample which had been irradiated and annealed at $T \leq 130$ K was for the D_2O to $(HOD)_2$ hopping step to be in equilibrium; that is with four times as much $(HOD)_2$ as D_2O . $(HOD)_2$ was then the major deuterated species. Warming such a sample to the temperature range where L-defects become active provided a superior look at the kinetics of the decoupling step. The model applied to the data was equivalent to Collier's, though arrived at by different means. The

major difference was his close attention to the probably unequal hopping rates of deuterons versus protons and his wrapping this dependence up into the constant F which was assigned the value of 0.736842 and assumed to be independent of temperature. The number was derived from Kunst and Warman's transient conductivity measurements on H_2O and D_2O ices

(75). From the truncated statistical treatment used here the factor F would be $\frac{5}{8}$; but, by recognizing the inexactness of the treatment, F was allowed to vary to obtain the best fits to the data. The best value for F was typically 0.6 or 0.7 but some fits resulted in much smaller values, possibly a consequence of systematic error in separating the spectra into the components. Another difference in the models was that he assigned arbitrary values to the initial amounts of the not uniquely observable nearly neighbor HOD, which was denoted as $(HOD)_{nn}$.

Having no reason to assign any particular value, that parameter was also allowed to vary in the present study. The calculated absorbance curves fit the data points very well and the Arrhenius plot from the rate constants of the turning step was linear. Calculated was an activation energy of 12.8 kcal/mole, which agrees very well with Collier's result of 12.0 ± 0.5 kcal/mole and also with energies determined by electrical conductivity experiments, such as the value 13.1 kcal/mole determined by Camp et. al. (70) for polycrystalline ice. The apparent availability of immobile L-defects for proton trapping at $T < 130$ K supports the partitioning of this energy into a part for L-defect formation and a part for mobilization, which have been estimated at 7.8 and 5.5 kcal/mole, respectively, as reviewed by Hobbs (6).

Summary

The goals of this study included finding ways to liberate mobile protons in ice at low temperatures by means less damaging to the crystal than electron bombardment, and to study the kinetics of the thermal release of those protons from the shallow traps which they quickly associate with at low temperatures. The fundamental probe of proton motion was the infrared spectroscopic observation of the isotopic scrambling steps of D_2O isolated in thin films of otherwise H_2O ices. Many of these samples were made by co-condensation of separate vapor streams at about 130 K where purely thermal isotopic exchange was negligible.

It had been supposed that by pumping overtones of the OH stretching mode protons could be mobilized, but in pure ice it was found that photons with wavelengths longer than about 200 nm were totally ineffective at causing ionization of ice. Using 184.9 nm at 90 K, protons were clearly liberated then quickly trapped, and were subsequently caused to be released by warming the sample to 110 K or higher. The amount of photogeneration of mobile protons in uv irradiated pure ice was however too small to allow kinetic studies of their release from shallow traps over a significant temperature range. Some samples were doped with molecules which would undergo uv photolysis while in ice to provide much increased concentrations of liberated protons, all of which were always quickly trapped at temperatures less than 110 K, after causing only a slight amount of isotopic exchange.

When these samples were warmed to over 110 K but to less than 130 K, only proton hopping occurred because the L-defect motions necessary for the completion of isotopic scrambling were absent. The kinetics of

the D_2O to neighbor-coupled HOD conversion were studied in nine samples at temperatures ranging from 113 to 130 K. Infrared spectra from those samples were separated into components due to D_2O , neighbor-coupled HOD and fully isolated HOD. A model was developed to explain the observed kinetics. Consistent with the notion that a finite concentration of protons had been shallowly trapped, it was found to be necessary to include equations for a rapid pseudo-equilibrium of mobile protons with shallow traps as well as an equation for the eventual deep trapping of the protons. The time dependent rate of the D_2O to $(HOD)_2$ step was representative of the amount of mobile protons available at that time and the initial portion of the rate was indicative of the extent of the release from shallow traps at the particular temperature. The temperature dependence of the initial rates corresponded to an activation energy of 8.76 kcal/mole for the release of mobile protons from shallow traps.

Having samples with most of the D_2O converted to $(HOD)_2$ provided a clean look at the higher temperature orientational L-defect motion, which is necessary to decouple the $(HOD)_2$ to form isolated HOD. Kinetic spectra were obtained over the temperature range 134 to 160 K and reduced to relative concentration changes of deuterated species and the activation energy for this water molecule turning step determined.

REFERENCES

- (1) U. Chowdhry, J. R. Barkley, A. D. English and A. W. Sleight, Mater. Res. Bull., **17**, 917 (1982).
- (2) J. Favrot, J. M. Leclercq, R. Roberge, C. Sandorfy and D. Vocelle, Chem. Phys. Lett., **53**, 433 (1978).
- (3) A. Warshel, Photochem. and Photobiol., **30**, 285 (1979).
- (4) Gary Ritzhaupt and J. Paul Devlin, Chem. Phys. Lett., **65**, 592 (1979).
- (5) Gary Ritzhaupt and J. Paul Devlin, Chem. Phys. Lett., **72**, 6807 (1980).
- (6) Peter V. Hobbs, Ice Physics; Oxford University: London, 1974.
- (7) N. H. Fletcher, The Chemical Physics of Ice; Cambridge University Press: London, 1970.
- (8) N. H. Fletcher, Rept. Prog. Phys., **34**, 913 (1971).
- (9) K. Lonsdale, Proc. Roy. Soc. Lond. A, **247**, 424 (1958).
- (10) Von R. Brille und A. Tippe, Acta Cryst., **23**, 343 (1967).
- (11) G. Dantl, Z. Phys., **166**, 115 (1962).
- (12) J. D. Bernal and R. H. Fowler, J. Chem. Phys., **1**, 515 (1933).
- (13) Linus Pauling, J. Amer. Chem. Soc., **57**, 2680 (1935).
- (14) P. Flubacher, A. J. Leadbetter and J. A. Morrison, J. Chem. Phys., **33**, 1751 (1960).
- (15) E. F. Burton and W. F. Oliver, Proc. Roy. Soc. Lond. A, **153**, 166 (1935).
- (16) John F. Nagle, J. Math. Phys., **7**, 1484 (1966).
- (17) S. W. Peterson and H. A. Levy, Acta Cryst., **10**, 70 (1957).
- (18) J. Chamberlain, Ph.D. Thesis, University of New England, 1971.
- (19) Y. Tajima, T. Matsuo and H. Suga, Nature, **299**, 810 (1982).

- (20) M. Ueda, T. Matsuo and H. Suga, J. Phys. Chem. Solids, **43**, 1165 (1982).
- (21) A. J. Leadbetter, R. C. Ward, J. W. Clark, P. A. Tucker, T. Matsuo and H. Suga, J. Chem. Phys., **82**, 424 (1985).
- (22) M. G. Sceats and S. A. Rice, In Water - A Comprehensive Treatise, Vol. 7, F. Franks, Ed.; Plenum: New York, 1982; p 87.
- (23) R. H. Beaumont, H. Chihara and J. A. Morrison, J. Chem. Phys., **34**, 1456 (1961).
- (24) A. H. Narten, C. G. Venkatesh and S. A. Rice, J. Chem. Phys., **64**, 1106 (1976).
- (25) Y. Paul Handa, O. Mishima and E. Whalley, J. Chem. Phys., **84**, 2766 (1986).
- (26) Erwin Mayer, J. Phys. Chem., **89**, 3474 (1985).
- (27) J. E. Bertie and E. Whalley, J. Chem. Phys., **40**, 1637 (1964).
- (28) W. Hagen, A. G. G. M. Tielens and J. M. Greenberg, Chem. Phys., **56**, 367 (1981).
- (29) G. Honjo and K. Shimaoka, Acta Cryst., **10**, 710 (1957).
- (30) M. Blackman and N. D. Lisgarten, Adv. Phys., **7**, 189 (1958).
- (31) M. Sugisaki, H. Suga and S. Seki, Bull. Chem. Soc. Japan, **41**, 2591 (1968).
- (32) Y. Paul Handa, D. D. Klug and E. Whalley, J. Chem. Phys., **84**, 7009 (1986).
- (33) S. R. Gough and D. W. Davidson, J. Chem. Phys., **52**, 5442 (1970).
- (34) J. E. Bertie and S. M. Jacobs, J. Chem. Phys., **67**, 2445 (1977).
- (35) J. E. Bertie and E. Whalley, J. Chem. Phys., **46**, 1271 (1967).
- (36) J. E. Bertie, H. J. Labbe' and E. Whalley, J. Chem. Phys., **50**, 4501 (1969).
- (37) E. Whalley, Can. J. Chem., **55**, 3429 (1977).
- (38) S. A. Rice, M. S. Bergren, A. C. Belch and G. Nelson, J. Phys. Chem., **87**, 4295 (1983).
- (39) W. B. Collier, Ph.D. Thesis, Oklahoma State Universtiy, August 1984.

- (40) C. Haas and D. F. Hornig, J. Chem. Phys., **32**, 1763 (1960).
- (41) Gary Ritzhaupt and J. Paul Devlin, J. Chem. Phys., **67**, 4779 (1977).
- (42) Gary Ritzhaupt, C. Thornton and J. P. Devlin, Chem. Phys. Lett., **59**, 420 (1978).
- (43) Gary Ritzhaupt, W. B. Collier, C. Thornton and J. P. Devlin, Chem. Phys. Lett., **70**, 294 (1980)
- (44) J. P. Devlin, P. J. Wooldridge and Gary Ritzhaupt, J. Chem. Phys., **84**, 6095 (1986).
- (45) D. Kroh and A. Ron, Chem. Phys. Lett., **36**, 527 (1975).
- (46) M. G. Sceats and S. A. Rice, J. Chem. Phys., **71**, 973 (1979).
- (47) W. M. Irvine and J. B. Pollack, Icarus, **8**, 335 (1968).
- (48) E. J. Cassel, Proc. Roy. Soc. Lond. A, **153**, 534 (1935).
- (49) R. Onaka and T. Takahashi, J. Phys. Soc. Japan, **24**, 548 (1968).
- (50) J. A. Ghormley and C. J. Honchanadel, J. Phys. Chem., **75**, 40 (1971).
- (51) T. I. Quickenden, R. A. J. Litjens, C. G. Freeman and S. M. Trotman, Chem. Phys. Lett., **114**, 164 (1985).
- (52) T. I. Quickenden, S. M. Trotman and D. F. Sangster, J. Chem. Phys., **77**, 3790 (1982).
- (53) C. G. Freeman, T. I. Quickenden, R. A. J. Litjens and D. F. Sangster, J. Chem. Phys., **81**, 5252 (1984).
- (54) I. A. Taub and K. Eiben, J. Chem. Phys., **49**, 2499 (1968).
- (55) H. C. Box, K. T. Lilga, E. E. Budzinski and R. Derr, J. Chem. Phys., **50**, 5422 (1969).
- (56) J. M. Flournoy, L. H. Baum and S. Siegel, J. Chem. Phys., **36**, 2229 (1962).
- (57) S. Siegel, J. M. Flournoy and L. H. Baum, J. Chem. Phys., **34**, 1782 (1961).
- (58) C. Jaccard, Ann. New York Acad. Sci., **125**, 390 (1965).
- (59) W. B. Collier, Gary Ritzhaupt and J. P. Devlin, J. Phys. Chem., **88**, 363 (1984).
- (60) Neils Bjerrum, Science, **115**, 385 (1952).

- (61) Steve Scheiner and J. F. Nagle, J. Phys. Chem., 87, 4267 (1983).
- (62) H. Granicher, Z. Kristallog., 110, 432 (1958).
- (63) H. Granicher, Phys. Kondes. Materie, 1, 1 (1963).
- (64) L. Onsager and M. Dupuis, In Electrolytes, B. Pesce, Ed.; Pergamon: New York, 1962; p27.
- (65) V. F. Petrenko and I. A. Rhyzhkin, Phys. Stat. Sol., 121, 421 (1984).
- (66) A. von Hippel, D. B. Knoll and W. B. Westphal, J. Chem. Phys., 54, 134 (1971).
- (67) V. F. Petrenko, R. W. Whitworth and J. W. Glen, Philosophical Magazine B, 47, 259 (1983).
- (68) M. Durand, M. Deleplanque and A. Kahane, Solid State Comm., 5, 759 (1967).
- (69) C. Jaccard, Helv. Phys. Acta, 32, 89 (1959).
- (70) P. R. Camp, W. Kiszenick and D. Arnold In Physics of Ice, N. Riehl, B. Bullemer and H. Engelhardt, Eds.; Plenum: New York, 1969; p 450.
- (71) J. C. Decroly, H. Granicher and C. Jaccard, Helv. Phys. Acta, 30, 465 (1957).
- (72) B. E. Conway, J. O'M. Bockris and H. Linton, J. Chem. Phys., 24, 834 (1956).
- (73) M. Hubmann, Z. Physik, B32, 127 (1979).
- (74) B. Bullemer, H. Engelhardt and N. Riehl In Physics of Ice, N. Riehl, B. Bullemer and H. Engelhardt, Eds.; Plenum: New York, 1969; p 416.
- (75) M. Kunst and J. M. Warman, J. Phys. Chem., 87, 4093 (1983).
- (76) J. P. Devlin and H. H. Richardson, J. Chem. Phys., 81, 3250 (1984).
- (77) B. Knight, D. M. Goodall and R. C. Greenhow, J. Chem. Soc. Faraday Trans. 2, 75, 841 (1979).
- (78) W. C. Natzle, C. B. Moore, D. M. Goodall, W. Frisch and J. F. Holzwarth, J. Phys. Chem., 85, 2882 (1981).
- (79) A. Weller In Progress in Reaction Kinetics, Vol. 1, G. Porter Ed.; Pergamon: New York, 1961; p 200.

- (80) V. F. Petrenko, T. Ebinuma and N. Maeno, phys. stat. solidi, **93**, 695 (1986).
- (81) E. Pines and D. Huppert, Chem. Phys. Lett., **116**, 295 (1985).
- (82) L. R. Koller, Ultraviolet Radiation; Wiley: New York, 1965; pp 51-53.
- (83) R. Hilsch und R. W. Pohl, Z. Physik, **59**, 812 (1930).
- (84) A. A. Konstantinov, O. P. Kaminskaya and V. A. Grigor'ev, Dolk. Akad. Nauk SSSR, **264**, 488 (1982).
- (85) M. K. Antoon, J. H. Koenig and J. L. Koenig, Appl. spec., **31**, 518 (1977).
- (86) D. W. Marquardt, J. Soc. Ind. Appl. Math., **11**, 431 (1963).
- (87) H. H. Richardson, P. J. Wooldridge and J. P. Devlin, J. Phys. Chem., **89**, 3552 (1985).

APPENDICES

APPENDIX A

DETERMINATION OF D_2O AND $(HOD)_2$ ABSORPTIVITIES RELATIVE TO ISOLATED HOD

The Relations

The mass balance of the isotopic scrambling steps requires that the concentrations follow the relation below, with the total amount of deuterated species at any time being equal to the amount after enough time has passed to scramble the D_2O completely into only isolated HOD.

$$[D_2O] + [(HOD)_2] + 2[HOD] = 2[HOD]_{\infty}$$

Applying Beer's law yields

$$\frac{A_{D_2O}}{e_{D_2O}} + \frac{A_{(HOD)_2}}{e_{(HOD)_2}} + \frac{A_{2HOD}}{e_{2HOD}} = \frac{A_{2HOD_{\infty}}}{e_{2HOD}}$$

where A_{D_2O} is the measured absorbance of D_2O which is equal to the molar absorptivity times the concentration, i.e. $e_{D_2O}[D_2O]$. The mass balance relation provides only information to determine the relative absorptivities, so e_{2HOD} was arbitrarily set to 2.0. Also let $a_1=1/e_{D_2O}$ and $a_2=1/e_{(HOD)_2}$ so that

$$a_1 A_{D_2O} + a_2 A_{(HOD)_2} + 0.5 A_{2HOD} = 0.5 A_{2HOD_{\infty}}$$

changing notation

$$a_1 X_1 + a_2 X_2 + Y = a_0 \quad \text{at each time.}$$

The Least Squares Treatment

Applying the method of least squares, sum over the N observations

$$\sum a_1 X_{1_i} + \sum a_2 X_{2_i} + \sum Y_i = \sum a_0$$

and divide by N to get

$$a_1 \bar{X}_1 + a_2 \bar{X}_2 + \bar{Y} = a_0$$

Minimize the sum of squared residuals,

$$\sum w_i [(\bar{Y} - Y_i) - a_1 (X_{1_i} - \bar{X}_1) - a_2 (X_{2_i} - \bar{X}_2)]^2$$

with respect to a_1 and a_2 by setting their partial derivatives equal to zero. After multiplying out and separating the terms, a_1 and a_2 can be found by solving the 2 by 2 matrix using Cramer's rule. If desired, a_0 can be calculated after the other a 's have been determined. The weights, w_i , could equal unity or $1/Y$ or whatever else it is felt represents the errors incurred in the spectral decompositions.

The Program

The above analysis was encoded into the program listed below and the data were run through it. The results were given in Chapter II, Table III.

```

1020 rem program to determine the relative molar absorbtivities
1030 :
1040 rem read in the data set
1050 :
1060 input "Sname of data set";in$
1070 open 2,8,2,"0:"+in$+",s,r"
1080 input#2,in$:printin$:print
1090 input#2,in$:np=val(in$):printnp"points":print
1100 input#2,in$:input#2,in$:input#2,in$
1110 dim y(np),x1(np),x2(np),w(np)
1120 print
1130 print "t","d2o","(hod)2","hod","2hod"
1140 print
1150 for i=1 to np
1160 : input#2,in$:printin$,

```

```

1170 : input#2,in$:x1(i)=val(in$):printin$,
1180 : input#2,in$:x2(i)=val(in$):printin$,
1190 : input#2,in$:y(i)=val(in$)/2:printin$,y(i)
1200 next i
1210 print
1220 close2
1230 :
1240 ya = 0 : rem average y value
1250 xa = 0 : rem average x1
1260 xb = 0 : rem average x2
1270 for i=1 to np
1280 : ya=ya+y(i)
1290 : xa=xa+x1(i)
1300 : xb=xb+x2(i)
1310 next i
1320 ya = ya/np
1330 xa = xa/np
1340 xb = xb/np
1350 :
1360 rem use statistical weighting
1370 for i=1 to np : w(i) = 1/y(i) : next i
1380 :
1390 rem build matrix of deviations
1400 :
1410 s11=0:s22=0:ss12=0
1420 t1 = 0 : t2 = 0
1430 for i=1 to np
1440 : s11=s11+w(i)*(x1(i)-xa)^2
1450 : s22=s22+w(i)*(x2(i)-xb)^2
1460 : ss12=ss12+w(i)*(x1(i)-xa)*(x2(i)-xb)
1470 : t1=t1+(ya-y(i))*(x1(i)-xa)*w(i)
1480 : t2=t2+(ya-y(i))*(x2(i)-xb)*w(i)
1490 next i
1500 :
1510 rem print out matrix for perusal
1520 :
1530 print:prints11,ss12,t1:printss12,s22,t2
1540 :
1550 d = s11*s22-ss12*ss12
1560 print
1570 print"d = "d
1580 a1 = (s22*t1-ss12*t2)/d
1590 a2 = (s11*t2-ss12*t1)/d
1600 print
1610 print"a1 ="a1,"a2 ="a2
1620 print
1630 print"by taking epsilon for hod = 1, and using weighting
w(i)=1/[2hod(i)]
1640 print
1650 print" eps d2o ="int(1000/a1+.5)/1000
1660 print
1670 print" eps (hod)2 ="int(1000/a2+.5)/1000
1680 :
1690 rem calculate the variance of the fit

```



```

1700 :
1710 xs = 0
1720 a0 = ya+a1*xa+a2*xb
1730 print:print"hod absorbance at long time ="a0*2
1740 print
1750 for i=1 to np
1760 : xs=xs+((y(i)-a0+a1*x1(i)+a2*x2(i)))^2
1770 next i
1780 xs = xs / (np-2-1)
1790 print"rmsd ="int(1000*sqr(xs)+.5)/10000
1800 print:close4
1810 end

```

A few of the runs:

150K data of 2/16/85

```

11 points
t          d2o          (hod)2          hod          2hod
0           2.87          20.15          25.91          12.955
2           1.5           13.66          39.81          19.905
4           1.11          9.37           48.08          24.04
6           .86           7.17           52.82          26.41
8           .59           5.99           55.33          27.665
10          0           5.54           57.63          28.815
12.5        0           4.6            59.79          29.895
15          0           3.64           61.17          30.585
20          0           3.19           62.47          31.235
40          0           1.09           65.4           32.7
70          0           .43            66.89          33.445
.513719683          3.10532114          3.30216057
3.10532114          19.5917479          20.6807562
d = .421647115
a1 = 1.12584166          a2 = .87713747

```

taking epsilon for hod = 1, and using weighting $w(i)=1/[2hod(i)]$

eps d2o = .888

eps (hod)2 = 1.14

hod absorbance at long time = 67.4705963

rmsd = .0182

data of 2/27/85 140k kinetics

```

16 points
t          d2o          (hod)2          hod          2hod
0           12.48          18.9           18.24          9.12
2           10.31          19.01          21.34          10.67
4           9.03           18.64          23.73          11.865
6           8.66           18.17          25.15          12.575
8           8.25           17.45          26.77          13.385

```

10	8	17.05	27.86	13.93
12	7.25	16.58	29.7	14.85
15	6.95	15.93	30.66	15.33
20	6.75	15.02	33.12	16.56
25	6.16	14	35.16	17.58
35	6.24	12.51	36.57	18.285
55	4.42	9.84	44.06	22.03
75	3.96	8.03	47.7	23.85
100	3.23	6.61	50.7	25.35
130	2.59	5.53	55.66	27.83
145	2.9	4.56	55.01	27.505
8.16114391		12.2426343	15.6872086	
12.2426343		21.8725277	26.3170081	

d = 28.6227508
a1 = .731215454 a2 = .793918516

taking epsilon for hod = 1, and using weighting $w(i)=1/[2\text{hod}(i)]$

eps d2o = 1.368

eps (hod)2 = 1.26

hod absorbance at long time = 66.5032429

rmsd = .0302

134k data of 2/6/85

12 points

t	d2o	(hod)2	hod	2hod
0	7.84	26.7	23.42	11.71
3	7.9	26.27	23.95	11.975
6	7.66	26.18	24.48	12.24
12	7.38	25.9	25.3	12.65
31	6.98	24.57	28.17	14.085
45	6.32	24.05	29.9	14.95
63	6.07	22.85	32.32	16.16
81	5.68	21.97	34.27	17.135
102	5.67	21.16	35.54	17.77
132	5.32	19.92	38.12	19.06
162	5.08	18.82	40.06	20.03
195	4.61	17.84	42.25	21.125
.969640093		2.49289555	2.72058745	
2.49289555		6.66819143	7.19507832	

d = .251217556
a1 = .815306226 a2 = .774213689

taking epsilon for hod = 1, and using weighting $w(i)=1/[2\text{hod}(i)]$

eps d2o = 1.227

eps (hod)2 = 1.292

hod absorbance at long time = 77.5216878

rmsd = 4.1e-03

data of 2/28/85 130k

9 points

t	d2o	(hod)2	hod	2hod
0	19.79	8.28	13.43	6.715
1	15.95	11.32	13.69	6.845
2	14.19	12.72	14.14	7.07
3	12.98	14.24	13.73	6.865
12	9.59	16.53	14.85	7.425
16	9.12	16.82	15.15	7.575
25	8.08	17.59	15.46	7.73
55	6.58	17.92	16.8	8.4
1320	3.34	10.05	32.9	16.45
	24.6989236	-12.6426153	7.37683288	
	-12.6426153	12.5245787	.690224099	

d = 149.50789
a1 = .676338631 a2 = .737822283

taking epsilon for hod = 1, and using weighting $w(i)=1/[2hod(i)]$

eps d2o = 1.479

eps (hod)2 = 1.355

hod absorbance at long time = 52.2280925

rmsd = 7.9e-03

126k data of 2/19/85

17 points

t	d2o	(hod)2	hod	2hod
-1	31.68	0	18.38	9.19
0	26.68	4.88	17.99	8.995
1	23.06	8.31	17.73	8.865
2	20.71	10.5	17.78	8.89
4	18.27	12.69	17.97	8.985
6	16.77	14.14	18.07	9.035
8	15.81	14.93	18.27	9.135
10	15.11	15.57	18.35	9.175
12.5	14.45	16.17	18.4	9.2
15	13.92	16.77	18.32	9.16
20	12.97	17.36	18.74	9.37
30	11.65	18.47	18.96	9.48
40	10.83	19.26	19.04	9.52
50	10.15	19.59	19.51	9.755
60	9.59	20.01	19.66	9.83
135	7.42	21.17	21.24	10.62
160	6.97	21.35	21.62	10.81
	77.060447	-67.7787244	4.32125394	
	-67.7787244	59.9363144	-3.51454545	

d = 24.7636957
a1 = .839480005 a2 = .890684373

taking epsilon for hod = 1, and using weighting $w(i)=1/[2\text{hod}(i)]$

eps d2o = 1.191

eps (hod)2 = 1.123

hod absorbance at long time = 71.41923
rmsd = 5.2e-03

120k data of 3/18/85
14 points

t	d2o	(hod)2	hod	2hod
-1	28.92	0	16.36	8.18
0	24.79	4.01	15.45	7.725
2	23.02	5.78	15.65	7.825
4	21.28	7.08	15.78	7.89
6	20.79	8.17	15.43	7.715
10	19.3	9.41	15.47	7.735
15	18.16	10.35	15.57	7.785
20	17.67	11	15.61	7.805
30	16.55	12.16	15.53	7.765
50	14.99	13.69	15.59	7.795
80	13.76	15.01	15.58	7.79
110	12.84	15.45	16.21	8.105
140	12.15	16.38	15.86	7.93
1200	7.67	18.98	19.12	9.56
	48.8815806	-45.8783671	1.76118334	
	-45.8783671	43.3384974	-1.40660849	
	d = 13.6296831			
	a1 = .865327474	a2 = .883584006		

taking epsilon for hod = 1, and using weighting $w(i)=1/[2\text{hod}(i)]$

eps d2o = 1.156

eps (hod)2 = 1.132

hod absorbance at long time = 65.696353
rmsd = .017

113k data of 1/28/85
12 points

t	d2o	(hod)2	hod	2hod
0	29.61	4.34	15.67	7.835
6	28.97	4.93	15.57	7.785
18	28.61	5.46	15.67	7.835
50	27.71	6.63	15.4	7.7
72	27.26	6.98	15.56	7.78
90	26.87	7.35	15.57	7.785
110	26.58	7.84	15.31	7.655
130	25.96	8.02	15.7	7.85
150	25.92	8.36	15.41	7.705

180	25.43	8.75	15.39	7.695
205	25.11	8.95	15.42	7.71
1080	22.27	12.45	15.47	7.735
5.60979869		-6.05665481	-.0815270779	
-6.05665481		6.5788725	.0937840959	
d = .223082798				
a1 = .141927774		a2 = .144917177		

taking epsilon for hod = 1, and using weighting $w(i)=1/[2\text{hod}(i)]$

eps d2o = 7.046

eps (hod)2 = 6.9

hod absorbance at long time = 25.2634512

rmsd = 5.8e-03

At the highest temperatures the scatter in the points caused large variations in the determined absorptivity values. At the lowest temperatures only the ratio $e_{D_2O}/e_{(HOD)_2}$ has significance because the ratios to isolated HOD could not be determined when that component remained constant. An indication of the errors in the low temperature determinations relative to HOD can be seen by comparing the computed final HOD absorbance to the measured one: for example at 113 K, 25.3 was calculated but 66.6 was observed. The higher temperature observed final HOD absorbances all agreed very well with the calculated values.

APPENDIX B

PARAMETER FITTING PROGRAM FOR THE 113 K TO 130 K DATA

In Chapter III the lower temperature rate data was transformed to a form which was representative of the integral of the mobile proton concentration. The Pascal program listed here reads from disk the transformed data and least-squares fits one or both parameters of integrated first order kinetics to that data.

```
PROGRAM HInt (datadata);
(* Program to do least squares fit of rate constants using Marquadt strategy.
Usage:
  Rename (or copy) the datafile (created with editor) to 'datadata'
  Input parameter guesses from keyboard, program will prompt and write
  results to screen.
Description of variables:
npts      - number of data points
npar      - number of parameters to vary
best[1]   - A
best[2]   - k
time[i]   - time of the ith observation
data[i]   - ln(m/(m-x))
delk      - array of variations in parameters to form partial derivs.
chisqr    - chi squared from previos iteration
chisqr1   - new chi squared
alpha     - matrix of partials
beta      - array used in parameter adjustments
trial     - trial guesses for parameters
calc[i,k] - calculated
deriv[i,k]- partial derivitives
           k=0 : no variations, just calculate value at point [trial]
           k=1..npar : calculate, partial w/r to the kth parameter
array     - modified alpha matrix inverted to adjust parameters
lambda    - diagonal weight used to modify alpha
temp      - tempory storage
deter     - determinate returned from Matinv
mainiter  - number of iterations main has gone thru
i,j,k,l,n - general use integers      *)
```

```

LABEL 1;
CONST  maxpar = 2;  maxpts = 20;
TYPE  pararray = Array[0..maxpar] of Real;
      ararray = Array[1..maxpar,1..maxpar] of Real;
      dvarray = Array[0..maxpts,0..maxpar] of Real;
      xarray = Array[0..maxpts] of Real;
      dtarray = Array[0..maxpts] of Real;
VAR    datadata : Text;
      trial, best, delk, beta : pararray;
      array, alpha : ararray;
      time : xarray;
      data : dtarray;
      calc, deriv : dvarray;
      chisqr, chisqrl, lambda, temp, deter, delkk, dellam, m : Real;
      i, j, k, l, n, mainiter, npts, npar, jstart, ti : Integer;
      done : Boolean;

```

```

Procedure Matinv(Var arry: ararray; n: Integer; Var d: Real);
  (* this inverts a Real, square matrix  by gauss-jorden elimination
  <<< see Appendix C >>>
End; (* Matinv *)

```

```

Function Fct(k: pararray; time: real): Real;
  (* this is the fitting function *)
Begin
  Fct:= k[1]*(1.0-exp(-k[2]*time))
End;

```

```

BEGIN (* Beginning of mainline *)
  Reset (datadata);
  Write('# of parameters to vary (<',maxpar+1:1,')- '); Readln(npar);
  Write('number of points- '); Readln(datadata,npts); Write(npts:4);
  Writeln('there are',npts:1,' in file');
  Write('use how many? '); Readln(npts);
  npts:= npts-1;
  Write(' x and y at each i');
  For i:=0 To npts Do Begin
    Readln(datadata,time[i],data[i]);
    Writeln(i:2,time[i]:6:1,data[i]:10:6)
  End;
  Writeln('Enter initial guesses');
  Write('  A - '); Readln(best[1]);
  Write('  k - '); Readln(best[2]);
  delk[0]:= 0.0; trial[0]:= 0.0; best[0]:= 0.0;
  Write('initial lambda - '); Readln(lambda);
  Write('delta in lambda - '); Readln(dellam);
  Write('del in k s = '); Readln(delkk);
  For j:=1 To npar Do delk[j]:= delkk;
  mainiter:= 0;  jstart:= 0; done:= false;  best[0]:= 0;

```

```

(* Begin building alpha and beta matrices of partial derivatives *)

1:for j:=1 To npar Do Begin
  beta[j]:= 0.0;
  For k:=1 To npar Do    alpha[j,k]:= 0.0;
End;
For j:=jstart To npar Do Begin
  trial:= best;
  if trial[j]<>0.0 then
    trial[j]:= trial[j]*(1.0+delk[j])
  else trial[j]:= 1.0e-50;
  If j=jstart then
    Writeln(time[0]:6:1,data[0]:10:6);
  For i:=1 To npts Do Begin
    calc[i,j]:= Fct(trial, time[i]);
    (* Write out results of on first iter. *)
    If mainiter=0 Then Writeln(time[i]:6:1,calc[i,j]:10:6,data[i]:12:6);
  End;
End;
(* form the derivatives *)
For j:=1 To npar Do
  For i:=1 To npts Do
    deriv[i,j]:= (calc[i,j]-calc[i,0])/(2.0*delk[j]*trial[j]);
(* build the matrices *)
For i:=1 To npts Do
  For j:=1 To npar Do Begin
    beta[j]:= beta[j]+(data[i]-calc[i,0])*deriv[i,j];
    For k:=1 To j Do alpha[j,k]:= alpha[j,k]+deriv[i,k]*deriv[i,j];
  End;
For j:=1 To npar Do For k:=1 To j Do alpha[k,j]:= alpha[j,k];

(* evaluate chi squared *)
If mainiter=0 Then Begin
  chisqr:= 0.0;
  For i:=1 To npts do
    chisqr:= chisqr+Sqr(data[i]-calc[i,0]);
  Writeln('chisqr = ',chisqr);
  chisqrl:= chisqr; End
Else chisqr:= chisqrl;

(* modify matrix and iterate on lambda *)
done:= false; jstart:= 0;
Repeat
  For j:=1 To npar Do Begin
    For k:=1 To npar Do arry[j,k]:= alpha[j,k]/Sqrt(alpha[j,j]*alpha[k,k]);
    arry[j,j]:= 1.0 + lambda
  End;

  Matinv(arry,npar,deter);
  If deter=0.0 Then Writeln('singular arry matrix');

(* adjust the parameters *)
  trial:= best;
  For j:=1 To npar Do For k:=1 To npar do

```



```

trial[j]:= trial[j]+beta[k]*arry[j,k]/Sqrt(alpha[j,j]*alpha[k,k]);

(* for this model require that all parameters be positive and within four
orders of magnitude of previous value *)

For j:=1 To npar Do Begin
  If trial[j]<=0.0 Then trial[j]:= -trial[j]/10000.0 + 1.0e-50;
  If trial[j]>best[j]*10000 Then trial[j]:= best[j]*10000;
  If trial[j]<best[j]/10000 Then trial[j]:= best[j]/10000;
  Write(trial[j]:13:9)
End;  Writeln;

(* If chi squared increased Then increase lambda and try re-invert arry *)
chisqr:= 0.0;
For i:=1 To npts Do Begin
  calc[i,0]:= Fct(trial, time[i]);
  Writeln(time[i]:6:1,calc[i,0]:10:6,data[i]:12:6);
  chisqr:= chisqr + Sqr(data[i]-calc[i,0]);
End;
Writeln('new chisqr =',chisqr,'          lambda = ',lambda:8,'  mainiter =
',mainiter:1);
If chisqr<=chisqr Then
  Begin
    lambda:= lambda/dellam;
    done:= true
  End
Else lambda:= lambda*dellam;
Until done;

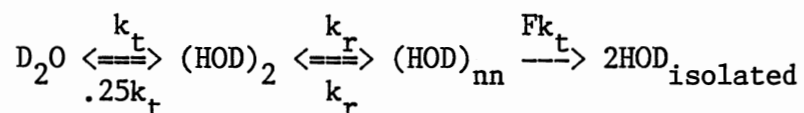
(* print out results of iteration *)
mainiter:= mainiter + 1;
Writeln('results of iteration #',mainiter:2);
best:= trial;
(* evaluate uncertianties *)
For j:=1 To npar Do
  Begin
    Writeln(best[j]:14,' +/-',Sqrt(arry[j,j]/alpha[j,j]):7);
  End;
jstart:= 1;  done:= false;
GoTo 1
END.

```

APPENDIX C

RATE CONSTANT FITTING PROGRAM FOR THE 134 K TO 160 K DATA

The method used was to read in the observed absorbances for D_2O , $(HOD)_2$, and HOD, and to fit the concentration changes to the differential equations representing the model



A program "datafit" was written in Pascal to perform an iterative nonlinear least-squares fit of the parameters involved in the high temperature model to the data. Marquardt's (86) strategy was used for parameter adjustments and a fourth-order Runge-Kutta method was used to integrate the differential equations. The integrations were done admitting relative errors of 10^{-9} or less per step. The steps were the times between the data points.

For the initial values from which to integrate the equations, $[D_2O]$ and $[(HOD)_2]$ were taken to be the time zero observed values, that is the initial absorbance values divided by the molar absorptivities. The observed initial amount of HOD was split between $[(HOD)_{nn}]_0$ and $[HOD]_0$ with the amount of the split being a varied parameter. This was done because the spectra of $(HOD)_{nn}$ and HOD were considered to be identical. The factor F was also allowed to vary to obtain the best fit to the data.

The integrity of the individual routines (Matinv, Rk4 and Runge) were verified with short driver programs solving known matrices and differential equations. The listing on the next pages was ported through the word processor with no characters changed for the purposes of margin setting and pagination.

```
Program datafit(input,output,indata);
```

```
(* program to do least squares fit of rate constants to differential rate equations using marquadt strategy and runge-kutta integration.
```

```
usage:
```

```
  rename (or copy) the datafile (created with store) to 'indata'  
  input parameter guesses from keyboard, program will prompt and write results.
```

```
description of variables:
```

```
best[5] - d2o molar absorbivity relative to epshod = 1.0  
best[6] - for (hod)2  
npts    - number of data points  
ndiff   - number of differential equations in model  
g       - global work array to pass local arrays between procedures  
x[i]    - time of the ith observation  
data[i,1] - d2o peak hieght at ith time  
data[i,2] - (hod)2  
data[i,3] - hod  
npar    - number of parameters to vary  
y0      - array of initial values for differential equations  
y       - final values of patrticular integration step  
yprime  - the form of the differential equations  
best[1] - current best hopping rate constant  
best[2] - rotation rate constant  
best[4] - f .. h vs d relative frequency  
best[3] - initial (hod)nn conc.  
delk    - array of variations in parameters to form partial derivs.  
chisqr  - chi squared from previos iteration  
chisqr1 - new chi squared  
alpha   - matrix of partials  
beta    - array used in parameter adjustments  
trial   - trial guesses for parameters  
calc[i,1,k] - calculated d2o concentrations returned from runge  
           2 - (hod)2  
           3 - (hod)nn  
           4 - hod  
deriv[i,j,k] - partial derivitives  
              k=0 : no variations, just calculate value at point [trial]  
              k=1..npar : calculate, partial w/r to the kth parameter  
array      - modified alpha matrix inverted to adjust parameters
```

```

lambda    - diagonal weight used to modify alpha
temp      - tempory storage
deter     - determinate returned from matinv
xo,xf     - initial and final x values in integration step
h         - step size for runge-kutta integration
ho,tol    - step and tolerence used in runge
mainiter  - number of iterations main has gone thru
i,j,k,l,n,m - general use integers      *)

```

```
label 1;
```

```
const ndiff = 4; maxpar = 7; maxpts = 30;
```

```

type      garray = array[0..ndiff] of real;
          trarray = array[0..maxpar] of real;
          bsarray = array[0..maxpar] of real;
          yparray = array[0..ndiff] of real;
          y0array = array[0..ndiff] of real;
          yarray  = array[0..ndiff] of real;
          ararray = array[1..maxpar,1..maxpar] of real;
          dvarray = array[0..maxpts,0..3,0..maxpar] of real;
          caarray = array[0..maxpts,0..3,0..maxpar] of real;
          alarray = array[1..maxpar,1..maxpar] of real;
          bearray = array[1..maxpar] of real;
          xarray  = array[0..maxpts] of real;
          dlarray = array[0..maxpar] of real;
          dtarray = array[0..maxpts,1..3] of real;

```

```
var      indata : file of real;
```

```

g      : garray ; y0 : y0array;   yprime : yparray;
arry: ararray;  x  : xarray ;     data  : dtarray;
y      : yarray ; delk: dlarray;   alpha : alarray ;
beta: bearray ; trial: trarray;    calc  : caarray;
deriv: dvarray; best: bsarray;

```

```

xo,xf,h,ho,tol,chisqr,chisqr1,chisqr2,lambda,temp,deter,mass,newmass,
dlk: real;

```

```
i,j,k,l,n,m,mainiter,npts,npar,jstart :integer;
```

```

procedure matinv(var arry: ararray; n: integer; var d: real);

(* this inverts a real, square matrix  by gauss-jorden elimination

  arry is the matrix ( n x n ), up to 10x10 with current iparray
  n is the order of arry
  and d is the determinate of arry

  arry is replaced by arry(-1)  *)

label 1;

type iparray = array[1..10,1..3] of integer;

var  ipv : iparray;
     toler,amax,swap,pivot,t :real;
     i,j,k,l,11,irow,icolum,jrow,jcolum,nsdap :integer;

begin
  d := 1.0;      toler := 1.0e-35;
  for j:=1 to n do  ipv[j,3] := 0;

(* main loop, eliminate one row at a time *)

  for i:=1 to n do begin

(* search remaining matrix for maximum element (pivot);
   test for a singular matrix *)

  amax := 0.0;
  for j:=1 to n do begin
    if ipv[j,3] <> 1 then begin
      for k:=1 to n do begin
        if ipv[k,3] <>1 then begin
          if abs(arry[j,k])>amax then begin
            irow := j;
            icolum := k;
            amax := abs(arry[j,k])
          end; (* if abs... *)
        end; (* if ipv[k... *)
      end; (* k loop *)
    end; (* if ipv[j... *)
  end; (* j loop *)
  if amax < toler then goto 1 ;
  ipv[icolum,3] := 1;      ipv[i,1] := irow;      ipv[i,2] := icolum;

  (* intechange rows (if necessary) to put pivot element on diagonal *)

  if irow <> icolum then begin
    for l:=1 to n do begin
      swap := arry[irow,l];
      arry[irow,l] := arry[icolum,l];
      arry[icolum,l] := swap
    end; (* l loop *)
  end;

```

```

end; (* if irow... *)

(* update determinate and normalize pivot row *)

pivot := array[icolum,icolum]; d := d*pivot; array[icolum,icolum] := 1.0;
for l:=1 to n do array[icolum,l] := array[icolum,l]/pivot ;

(* eliminate icolum retaining inverse elements *)

for ll := 1 to n do begin
  if ll <> icolum then begin
    t := array[ll,icolum];
    array[ll,icolum] := 0.0;
    for l:=1 to n do array[ll,l] := array[ll,l]-array[icolum,l]*t;
  end; (* if ll.. *)
end; (* ll loop *)

end; (* i loop *)

(* interchange columns and modify determinate *)

nswap := 0;
for i:=1 to n do begin
  l := n-i+1;
  if ipv[1,l] <> ipv[1,1] then begin
    jrow := ipv[1,l];
    jcolum := ipv[1,1];
    nswap := nswap + 1;
    for k := 1 to n do begin
      swap := array[k,jrow];
      array[k,jrow] := array[k,jcolum];
      array[k,jcolum] := swap
    end; (* k loop *)
  end; (* if ipv... *)
end; (* i loop *)

if (nswap mod 2)=1 then d := -d;
l: if amax<toler then d := 0.0

end; (* matinv *)

```

```

procedure fct(b:trarray; g:garray; var yprime:yarray);

  (* actual differential equations are encoded here
     b are trial parameters passed in *)

var f1,f2,f3,f4,rate1,rate2,rate3,rate4,rate5 : real;

begin
  f1 := g[1];          f2 := g[2];          f3 := g[3];          f4 := g[4];

  rate1 := b[1]*f1;
  rate2 := b[1]*f2/4.0;
  rate3 := b[2]*f2;
  rate4 := b[2]*f3;
  rate5 := b[1]*b[4]*f3;

  yprime[1] := rate2 - rate1;
  yprime[2] := rate1 - rate2 - rate3 + rate4;
  yprime[3] := rate3 - rate4 - rate5;
  yprime[4] := rate5

end; (* fct *)

procedure rk4(xo,h:real; kk:integer; y0:y0array; var y:yarray);

  (* perform one runge-kutta step from xx to xx+h on system of ndiff equations*)

const ndiff = 4;

var yy:array[0..ndiff] of real;          rk:array[0..ndiff] of real;
    xx:real ; ii,jj : integer;

begin
  xx := xo;          y := y0;
  for jj:=1 to kk do begin
    g := y;          fct (trial,g,yprime);
    for ii:=1 to ndiff do begin
      yy[ii] := y[ii]+h*yprime[ii]/2.0;
      rk[ii] := yprime[ii]
    end;
    xx := xx + h/2.0;
    g := yy;          fct (trial,g,yprime);
    for ii:=1 to ndiff do begin
      yy[ii] := y[ii]+h*yprime[ii]/2.0;
      rk[ii] := rk[ii]+2.0*yprime[ii]
    end;
    g := yy;          fct (trial,g,yprime);
    for ii:=1 to ndiff do begin
      yy[ii] := y[ii]+h*yprime[ii];
      rk[ii] := rk[ii]+2.0*yprime[ii]
    end;
    xx := xx + h/2.0;
    g := yy;          fct (trial,g,yprime);
    for ii:=1 to ndiff do begin

```

```

        rk[ii] := h*(rk[ii]+yprime[ii]);
        y[ii] := y[ii] + rk[ii]/6.0
    end;
end; (* jj loop *)
end; (* of rk4 *)

procedure runge(trial:trarray; tol,xo,xf,ho:real; var y0:y0array);

(* this solves a system of differential equations with initial values using an
   iterative forth order runge-kutta algorithm..rk4, with actual eqns. in fct *)

const ndiff = 4 ;itermax = 20;(*maximum number of binary step size reductions*)

var yhold : array[0..ndiff] of real;
    hh,sum:real ; kj,ij,iter:integer;

(* sum is sum of relative changes in solutions vector
   yhold is temporary storage for y *)

begin
    kj := 1; hh := 0.0;
    rk4 (xo,ho,kj,y0,y);
    iter := 0;
    repeat
        kj := 2*kj;
        hh := ho/kj;
        rk4 (xo,hh,kj,y0,y);
        sum := 0.0;
        for ij:=1 to ndiff do sum := sum+abs((yhold[ij]-y[ij])/y[ij]);
        yhold := y;
        iter := iter + 1
    until ((sum<tol) or (iter>itermax));
    if iter>itermax then writeln('failed to find stable solution in ',itermax:2,'
tries');
        xo := xo + ho ;      y0 := y;
    end;

    (* beginning of mainline *)

begin
    (* read in the data *)
    reset (indata); (* open file and reset pointer to first position *)
    write('number of parameters to vary - ');readln(npar);
    write('number of points - ');
    npts := round(indata^);
    writeln(npts:4);
    npts := npts - 1;
    writeln('input time d2o (hod)2 hod at each i');
    for i:=0 to npts do begin
        write(i:2,' ');
        get(indata);x[i]:=indata^;
        get(indata);data[i,1]:=indata^;
    end;
end;

```



```

    get(indata);data[i,2]:=indata^;
    get(indata);data[i,3]:=indata^;
    writeln(x[i]:6:2,data[i,1]:8:2,data[i,2]:8:2,data[i,3]:8:3);
end;
writeln;
write('      kt - '); readln(best[1]);
write('      kr - '); readln(best[2]);
write('[(hod)mn]0 - '); readln(best[3]);
write('      f - '); readln(best[4]);
write('      epsd2o - '); readln(best[5]);
write('      epschod- '); readln(best[6]);
write('tol for diff eqns. - '); readln(tol);
write('delta in parameters for forming partials - '); readln(dlk);
delk[0] := 0.0; trial[0] := 0.0; best[0] := 0.0;
for j:=1 to npar do delk[j]:= dlk;
mainiter := 0; jstart := 0; lambda := 0.0001;

(* begin building alpha and beta matrices of partial derivatives *)

1:for j:=1 to npar do begin
    beta[j] := 0.0;
    for k:=1 to npar do alpha[j,k] := 0.0;
end;
writeln(x[0]:6:1,data[0,1]:8:3,data[0,2]:8:3,data[0,3]:8:3,best[3]:8:3);

for j:=jstart to npar do begin
    trial := best;
    trial[j]:= trial[j]*(1.0+delk[j]);
    y0[1] := data[0,1]/trial[5];
    y0[2] := data[0,2]/trial[6];
    y0[3] := trial[3]/2.0;
    y0[4] := data[0,3]/2.0 - y0[3];

    for i:=1 to npts do begin
        xo := x[i-1]; xf := x[i];
        ho := xf - xo ;
        runge(trial,tol,xo,xf,ho,y0);

        (* write out results of runge *)

        if mainiter=0 then
writeln(x[i]:6:1,y0[1]*trial[5]:8:3,y0[2]*trial[6]:8:3,(y0[3]+y0[4])*2.0:8:3,y0[3]
*2.0:8:3);

        calc[i,1,j] := y0[1]*trial[5];
        calc[i,2,j] := y0[2]*trial[6];
        calc[i,3,j] := (y0[3]+y0[4])*2.0
    end; (* i loop *)
end; (* j loop *)

```

```

(* form the derivitives *)

for j:=1 to npar do
  for i:=1 to npts do
    for l:=1 to 3 do deriv[i,1,j] :=
(calcul[i,1,j]-calcul[i,1,0])/(2.0*delk[j]*trial[j]);

  if mainiter=0 then begin
    for j:=1 to npar do
      for i:=1 to npts do begin
        writeln(j:3,i:10);
        for l:=1 to 3 do write(deriv[i,1,j]:10:6); writeln;
      end;
    end;

(* build the matrices *)

for i:=1 to npts do begin
  for j:=1 to npar do
    for l:=1 to 3 do begin
      beta[j] := beta[j]+(data[i,1]-calcul[i,1,0])*deriv[i,1,j];
      for k:=1 to j do alpha[j,k] := alpha[j,k]+deriv[i,1,k]*deriv[i,1,j];
    end;
  end;
  for j:=1 to npar do    for k:=1 to j do    alpha[k,j] := alpha[j,k];

for j:=1 to npar do begin
  for k:=1 to npar do write(alpha[j,k]:11:7);
  writeln(beta[j]:11:7);
end;

(* evaluate chi squared *)

if mainiter=0 then begin
  chisqr := 0.0;
  for i:=1 to npts do
    for l:=1 to 3 do chisqr := chisqr+sqr(data[i,1]-calcul[i,1,0]);
  writeln('chisqr = ',chisqr) ;
  chisqrl := chisqr ; end
else  chisqr := chisqrl ;

  (* modify matrix *)
  repeat
    lambda := lambda * 10.0;    chisqr2 := chisqrl;
    for j:=1 to npar do begin
      for k:=1 to npar do array[j,k] := alpha[j,k]/sqrt(alpha[j,j]*alpha[k,k]);
      array[j,j] := 1.0 + lambda
    end;

    matinv(array,npar,deter);

    if deter=0.0 then writeln('singular array matrix');

    for j:=1 to npar do begin

```

```

    for k:=1 to npar do write(array[j,k]:11:7); writeln
end;

(* adjust the parameters *)

trial := best;
for j:=1 to npar do for k:=1 to npar do trial[j] :=
trial[j]+beta[k]*array[j,k]/sqrt(alpha[j,j]*alpha[k,k]);

(* for this model require that all parameters be positive *)

for j:=1 to npar do write(trial[j]:11:7); writeln;

for j:=1 to npar do begin
  if trial[j]<=0.0 then trial[j] := -trial[j]/1000.0 + 1.0e-30;
end;

for j:=1 to npar do write(trial[j]:11:7); writeln;

(* if chi squared increased then increase lambda and try re-invert array *)

y0[1] := data[0,1]/trial[5] ;
y0[2] := data[0,2]/trial[6];
y0[3] := trial[3]/2.0 ;
y0[4] := data[0,3]/2.0-y0[3];
chisqr1 := 0.0 ;
for i:=1 to npts do begin
  xo:=x[i-1]; xf:=x[i]; ho:=xf-xo;
  runge(trial,tol,xo,xf,ho,y0);

writeln(x[i]:6:1,y0[1]*trial[5]:8:3,y0[2]*trial[6]:8:3,(y0[3]+y0[4])*2.0:8:3,y0[3]
*2.0:8:3);

  calc[i,1,0] := y0[1]*trial[5]; calc[i,2,0] := y0[2]*trial[6];
  calc[i,3,0] := (y0[3]+y0[4])*2.0;

  for l:=1 to 3 do chisqr1 := chisqr1 + sqr(data[i,l]-calc[i,l,0])
end;
writeln('new chisqr =',chisqr1,'          log lambda
=',round(ln(lambda)/ln(10.0)):3)
until ( (chisqr1<chisqr) and (chisqr1>=chisqr2) ) ;

lambda := lambda/10.0 ; chisqr1 := chisqr2;
for j:=1 to npar do begin
  for k:=1 to npar do array[j,k]:=alpha[j,k]/sqrt(alpha[j,j]*alpha[k,k]);
  array[j,j] := 1.0 + lambda;
end;
matinv(array,npar,deter);
trial := best;
for j:=1 to npar do for k:=1 to npar do
trial[j]:=trial[j]+beta[k]*array[j,k]/sqrt(alpha[j,j]*alpha[k,k]);
for j:=1 to npar do if trial[j]<=0.0 then trial[j]:=-trial[j]-1.0e-30;

```

```
(* print out results of iteration *)  
  
mainiter := mainiter + 1;  
writeln('results of iteration #',mainiter:3);  
best := trial;  
for j:=1 to npar do write(trial[j]:12:7);  
writeln;  
writeln('rmsd =',sqrt(chisqr1/(npts-npar-1)));  
jstart := 1; lambda := 0.0001;  
goto 1  
end.
```

VITA

Paul Joseph Wooldridge

Candidate for the Degree of

Doctor of Philosophy

Thesis: FT-IR SPECTROSCOPIC STUDY OF PROTON TRANSPORT AND TRAPPING IN
CUBIC ICE

Major Field: Chemistry

Biographical:

Personal Data: Born in Cyril, Oklahoma, October 26, 1961, one of
eight children of Sylvester E. and Myrtle T. Wooldridge.

Education: Graduated from Fletcher High School, Fletcher, Oklahoma,
in May 1979; recieved Bachelor of Science Degree from Cameron
University, Lawton, Oklahoma, with a major in Chemistry in May,
1983; completed requirements for the Doctor of Philosophy Degree
at Oklahoma State University in December, 1987.

Professional Experience: Graduate Teaching Assistant, Oklahoma State
University, 1983-84; Graduate Research Assistant 1985-87; Member
of American Chemical Society.